Theses and Dissertations   1. Thesis and Dissertation Collection, all items

2008-09

High-order non-reflecting boundary conditions for the linearized Euler equations

Dea, John R.

Monterey, California. Naval Postgraduate School

http://hdl.handle.net/10945/47446

NAVAL POSTGRADUATE SCHOOL
Monterey, California

Dissertation

HIGH-ORDER NON-REFLECTING BOUNDARY CONDITIONS FOR THE LINEARIZED EULER EQUATIONS

by

John R. Dea

September 2008

Dissertation Supervisors: Beny Neta

                                        Francis X. Giraldo

THIS PAGE INTENTIONALLY LEFT BLANK

REPORT DOCUMENTATION PAGE		Form Approved OMB No. 0704-0188

1. AGENCY USE ONLY (*Leave blank*)	2. REPORT DATE September 2008	3. REPORT TYPE AND DATES COVERED Dissertation—Sept 06–Sept 08

4. TITLE AND SUBTITLE High-Order Non-Reflecting Boundary Conditions for the Linearized Euler Equations	5. FUNDING NUMBERS
6. AUTHORS Dea, John R	

7. PERFORMING ORGANIZATION NAME(S) AND ADDRESS(ES) Naval Postgraduate School Monterey CA 93943-5000	8. PERFORMING ORGANIZATION REPORT NUMBER

9. SPONSORING/MONITORING AGENCY NAME(S) AND ADDRESS(ES)	10. SPONSORING/MONITORING AGENCY REPORT NUMBER

11. SUPPLEMENTARY NOTES The views expressed in this dissertation are those of the author and do not reflect the official policy or position of the Department of Defense or the U.S. Government.

12a. DISTRIBUTION/AVAILABILITY STATEMENT Approved for public release; distribution is unlimited.	12b. DISTRIBUTION CODE

13. ABSTRACT(*maximum 200 words*)

   We wish to solve fluid flow problems in only a portion of a large or infinite domain. By restricting our area of interest, we effectively create a boundary where none exists physically, dividing our computational domain from the rest of the physical domain. The challenge we must overcome, then, is defining this boundary in such a way that it behaves computationally as if there were no physical boundary. Such a boundary definition is often called a *non-reflecting* boundary, as its primary function is to permit wave phenomena to pass through the open boundary without reflection. In this dissertation we develop several non-reflecting boundary conditions for the linearized Euler equations of inviscid gas dynamics. These boundary conditions are derived from the Higdon, Givoli-Neta, and Hagstrom-Warburton boundary schemes for scalar equations, and they are adapted here for a system of first-order partial differential equations. Using finite difference methods, we apply the various boundary schemes to the gas dynamic equations in two dimensions, in an open domain with and without the influence of gravity or Coriolis forces. These new methods provide significantly greater accuracy than the classic Sommerfeld radiation condition with only a modest increase to the computation time.

14. SUBJECT TERMS open boundary conditions, auxiliary variables, wave propagation, Euler equations, gravity, infinite domains, non-reflecting, finite differences	15. NUMBER OF PAGES 202
	16. PRICE CODE

17. SECURITY CLASSIFICATION OF REPORT Unclassified	18. SECURITY CLASSIFICATION OF THIS PAGE Unclassified	19. SECURITY CLASSIFICATION OF ABSTRACT Unclassified	20. LIMITATION OF ABSTRACT UU

THIS PAGE INTENTIONALLY LEFT BLANK

HIGH-ORDER NON-REFLECTING BOUNDARY CONDITIONS FOR THE LINEARIZED EULER EQUATIONS

John R. Dea
Major, United States Air Force
B.S. Computer Science, Baylor University, Waco, TX, 1993
M.S. Mathematics, Creighton University, Omaha, NE, 1998

Submitted in partial fulfillment of the
requirements for the degree of

DOCTOR OF PHILOSOPHY IN APPLIED MATHEMATICS

from the

NAVAL POSTGRADUATE SCHOOL
September 2008

Author:

John R. Dea

Approved by:

Beny Neta	Francis X. Giraldo
Professor of Appl. Math.	Assoc. Prof. of Appl. Math.
Dissertation Supervisor	Dissertation Supervisor
Clyde Scandrett	Garth Hobson
Professor of Appl. Math.	Professor of Mech. Eng.

Saša Gaberšek
Naval Research Laboratory

Approved by:

Carlos Borges, Chair, Department of Applied Mathematics

Approved by:

Doug Moses, Vice Provost for Academic Affairs

THIS PAGE INTENTIONALLY LEFT BLANK

ABSTRACT

We wish to solve fluid flow problems in only a portion of a large or infinite domain. By restricting our area of interest, we effectively create a boundary where none exists physically, dividing our computational domain from the rest of the physical domain. The challenge we must overcome, then, is defining this boundary in such a way that it behaves computationally as if there were no physical boundary. Such a boundary definition is often called a *non-reflecting* boundary, as its primary function is to permit wave phenomena to pass through the open boundary without reflection. In this dissertation we develop several non-reflecting boundary conditions for the linearized Euler equations of inviscid gas dynamics. These boundary conditions are derived from the Higdon, Givoli-Neta, and Hagstrom-Warburton boundary schemes for scalar equations, and they are adapted here for a system of first-order partial differential equations. Using finite difference methods, we apply the various boundary schemes to the gas dynamic equations in two dimensions, in an open domain with and without the influence of gravity or Coriolis forces. These new methods provide significantly greater accuracy than the classic Sommerfeld radiation condition with only a modest increase to the computation time.

THIS PAGE INTENTIONALLY LEFT BLANK

TABLE OF CONTENTS

LIST OF FIGURES

THIS PAGE INTENTIONALLY LEFT BLANK

LIST OF TABLES

THIS PAGE INTENTIONALLY LEFT BLANK

ACKNOWLEDGMENTS

Even though my name is the only one next to the word "author," this dissertation was most definitely *not* an a capella performance. I had invaluable advice, encouragement and moral support from many people throughout this effort. First, of course, I wish to thank my advisors, Drs. Beny Neta and Frank Giraldo, for teaching me the basics from which this research was launched, for their timely advice whenever I seemed to hit a brick wall, for keeping me from trying to do more than could actually be done in the time the Air Force has allotted me, and for guiding me through the process of getting published; in short, for teaching me to be a mathematician, rather than a math student. Thanks as well to the other members of my dissertation committee: Drs. Clyde Scandrett, Garth Hobson, and Sasa Gabersek. Although I did not work as closely with them as with my advisors, each one of them provided valuable insight and feedback which made this dissertation stronger and made me a better mathematician. I also greatly appreciate the technical insight and comments of Dr. Dan Givoli of the Technion (Israel Institute of Technology) Department of Aerospace Engineering. His expertise and experience saved me from a long and fruitless effort to "fix" something that was in fact already correct. I also appreciate the insight of Dr. Pante Stănică here at NPS for his discovery concerning the polynomial sequence discussed on p. 108. I am of course deeply indebted to the Air Force for this opportunity to further my education. I look forward to applying these past three years to training my fellow officers, continuing further mathematical research, and making the Air Force stronger. Many thanks also to my lovely wife for her patience, support and encouragement. They say there are no challenges, only opportunities, and I am eternally grateful to her for encouraging me as I faced the seemingly-insurmountable opportunities of this effort. I also want to give a heartfelt thanks to the Del Monte Brass for the stress relief; thanks for letting me join the great music. Finally, I thank God for all the blessings that came with this assignment, professional and personal.

THIS PAGE INTENTIONALLY LEFT BLANK

I.   INTRODUCTION

Many problems in computational fluid dynamics occur within a limited portion of a very large or infinite domain. Difficulties immediately arise when one attempts to define the boundary condition for such a system. Such boundary conditions are necessary for the problem to be well-posed, but the physical system under consideration has no boundary to model. One needs to define an artificial boundary whose behavior models the open edge of the physical system. Such a boundary definition is often called a *non-reflecting* boundary condition (NRBC), as its primary function is to permit wave phenomena to pass through the open boundary without reflection.

NRBC development has been an ongoing research area since the 1960s. As with any computational endeavor, there are trade-offs involved. An ideal NRBC would be fast, accurate, stable, and easy to implement: *fast*, meaning that the computation of boundary values is small or negligible relative to the interior domain; *accurate*, meaning that there is little to no spurious reflection induced by the boundary condition; *stable*, meaning that the boundary computations do not cause the solution to degrade catastrophically over time; and *easy to implement*, meaning that the user can incorporate the NRBC computations into an operational model with minimal modification to existing code. Realistically, one must settle for two or three of these attributes, at best. Consequently, the search for better NRBC methods continues. In addition, researchers continue to apply existing NRBC methods to new domains and wave propagation equations.

In this dissertation we develop several NRBCs for the linearized Euler equations of inviscid gas dynamics. These boundary conditions are derived from the Higdon, Givoli-Neta, and Hagstrom-Warburton boundary schemes for scalar equations, adapted here for a system of first-order partial differential equations. Using finite difference methods, we apply the various boundary schemes to the gas dynamic equations in two dimensions, in an open domain with and without the influence of

gravity or Coriolis forces. These new methods provide significantly greater accuracy than the classic Sommerfeld radiation condition with only a modest increase to the computational cost.

Our motivation for developing these NRBCs is to support the work of Giraldo and Restelli in their efforts to develop the next generation of mesoscale atmospheric modeling tools [32]. In their current form, the models rely on large absorbing layers surrounding the computational domain. In order to be effective, these "sponge layers" can be as thick as the original domain [31], resulting in a total domain which is nearly quadrupled in size. If we can replace these large sponge layers with accurate NRBCs, then the modeling tools will requires less memory and computational overhead, significantly increasing their efficiency.

The rest of the dissertation is outlined as follows. We begin in Chapter II by deriving the equations under consideration, the linearized Euler equations of inviscid gas dynamics. In Chapter III we provide an overview of existing NRBCs and provide specific details about the Higdon, Givoli-Neta, and Hagstrom-Warburton schemes for scalar equations. We then extend these boundary conditions to the first-order 2-D linearized Euler system in Chapters IV (Higdon), V (Givoli-Neta), and VI (Hagstrom-Warburton). In all three cases, we consider the NRBC implementation in a semi-infinite or infinite channel and in an open domain, under basic conditions as well as under the influence of Coriolis forces or gravity. Numerical examples using finite differences are provided throughout. We discuss the issue of long-time stability in Chapter VII. We offer a qualitative comparison of the three NRBC techniques in Chapter VIII. We close in Chapter IX with a summary of our results and a list of areas for further research.

II.   MODELING INVISCID FLUID FLOW

In this chapter we explore the equations governing the motion of a body of fluid. These principles describe the flow of water in a channel or in the ocean, air movement over mountains, airflow and drag in aircraft design, and even the heat generated by a spacecraft re-entering the atmosphere. Although many physical phenomena depend on the viscosity of the fluid, certain large-scale flows of low-viscosity fluids (e.g., air) can be reasonably approximated by assuming the viscosity is negligible.

By neglecting viscous forces, our fluid flow equations can be derived based simply on physical conservation laws governing mass, momentum, and energy. The following section considers each conservation law in turn and derives the relevant governing equations therefrom.

We derive the Euler equations based first on internal factors. Then we consider the inhomogeneous factors which affect these equations in the context of atmospheric modeling.

A.   DERIVATION OF EQUATIONS
1.   Conservation of Mass

Mass is conserved in a closed system. If dm denotes an infinitesimal portion of the mass, then $\int dm$ denotes the total mass of the body, and conservation of mass requires

$$\frac{d}{dt}\int dm = 0 \tag{II.1}$$

Since the mass is continuous, we can bring the derivative inside the integral; thus

$$\int \frac{d}{dt}(dm) = 0 \tag{II.2}$$

Furthermore, since this statement must be true for any piece of the body's mass, the integrand must be identically zero, i.e.,

$$\frac{d}{dt}(dm) = 0 \tag{II.3}$$

or

$$\frac{d}{dt}(\rho dx dy dz) = 0 \tag{II.4}$$

Applying the product rule gives

$$(dx dy dz)\frac{d\rho}{dt} + (\rho dy dz)d\frac{dx}{dt} + (\rho dx dz)d\frac{dy}{dt} + (\rho dx dy)d\frac{dz}{dt} = 0 \tag{II.5}$$

Define the velocity vector $\vec{u} = (u, v, w)^T$, where $u = dx/dt$, $v = dy/dt$, and $w = dz/dt$, and divide all four terms by $dx dy dz$ to get

$$\frac{d\rho}{dt} + \rho\frac{du}{dx} + \rho\frac{dv}{dy} + \rho\frac{dw}{dz} = 0 \tag{II.6}$$

Applying the chain rule to each derivative gives

$$\left.\begin{array}{l} \frac{\partial\rho}{\partial t} + u\frac{\partial\rho}{\partial x} + v\frac{\partial\rho}{\partial y} + w\frac{\partial\rho}{\partial z} + \rho\left(\frac{\partial u}{\partial x}\frac{dx}{dx} + \frac{\partial u}{\partial y}\frac{dy}{dx} + \frac{\partial u}{\partial z}\frac{dz}{dx}\right) \\ + \rho\left(\frac{\partial v}{\partial x}\frac{dx}{dy} + \frac{\partial v}{\partial y}\frac{dy}{dy} + \frac{\partial v}{\partial z}\frac{dz}{dy}\right) + \rho\left(\frac{\partial w}{\partial x}\frac{dx}{dz} + \frac{\partial w}{\partial y}\frac{dy}{dz} + \frac{\partial w}{\partial z}\frac{dz}{dz}\right) \end{array}\right\} = 0 \tag{II.7}$$

However, since x, y, and z are independent, this equation reduces to

$$\partial_t\rho + u\partial_x\rho + v\partial_y\rho + w\partial_z\rho + \rho\left(\partial_x u + \partial_y v + \partial_z w\right) = 0, \tag{II.8}$$

i.e.,

$$\partial_t\rho + \partial_x(\rho u) + \partial_y(\rho v) + \partial_z(\rho w) = 0 \tag{II.9}$$

or, in vector notation,

$$\partial_t\rho + \nabla\cdot(\rho\vec{u}) = 0, \tag{II.10}$$

where from here on, we use the following shorthand for partial derivatives:

$$\partial_t = \frac{\partial}{\partial t}, \quad \partial_{xy} = \frac{\partial^2}{\partial x\partial y}$$

This equation assumes no external sources or sinks adding or removing mass from the system. We note in passing that we have shown, from first principles, a special case of Reynold's transport theorem [3] applied to the density of a fluid.

4

2.   Conservation of Momentum

We now consider the momentum of the fluid body. To this end, we first determine what forces act upon the fluid. For the purpose of this dissertation, the fluid body is assumed to be a portion of the Earth's atmosphere.

a.   Forces Acting upon a Fluid Body

The internal forces exerted by the body on itself consist of pressure forces and viscous forces (which are neglected since we are assuming an invsicid fluid). The external inhomogeneous forces we consider are the effects of gravity and the Earth's rotation.

(1)   Force Due to Internal Pressure.   The pressure force results from pressure differences within the body (see Fig. 1) and acts to retard the motion of the fluid.
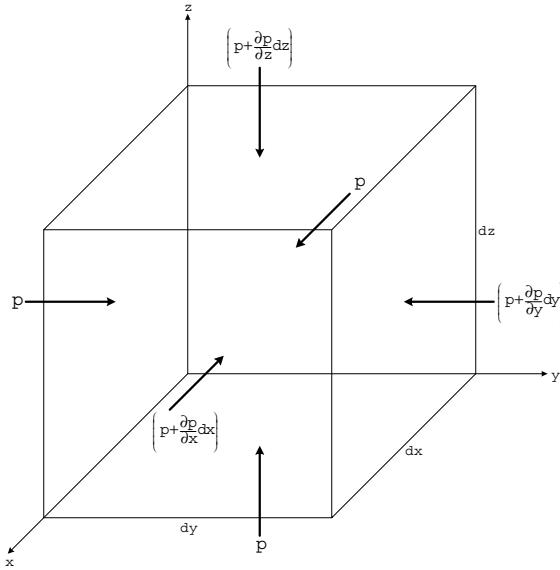
Figure 1. Pressure Differences in a Small Volume [From [113], Fig. 3, p. 15]

In a small piece of fluid volume $dV = dxdydz$, the change in pressure in the x direction is (to first order accuracy)

$$\partial_x p \ dx$$

The force exerted by this pressure difference is the product of the pressure difference and the surface area on which the pressure is exerted. Hence, the pressure force in the x direction is given by

$$dF_{pressure_x} = -\left(\partial_x p \; dx\right) dy dz = -\partial_x p \; dV \tag{II.11}$$

Similarly, the forces exerted by pressure differences in the y and z directions are given by

$$dF_{pressure_y} = -\left(\partial_y p \; dy\right) dx dz = -\partial_y p \; dV$$
$$dF_{pressure_z} = -\left(\partial_z p \; dz\right) dx dy = -\partial_z p \; dV \tag{II.12}$$

Thus, the total force due to internal pressure differences is the sum of the three components,

$$dF_{pressure} = -\left(\partial_x p \hat{i} + \partial_y p \hat{j} + \partial_z p \hat{k}\right) dV = -(\nabla p) dV, \tag{II.13}$$

and the overall force on the entire body is

$$F_{pressure} = \int dF_{pressure} = \int -(\nabla p) dV \tag{II.14}$$

(2) Force Due to Gravity. According to Vallado [112], the gravitational acceleration comes from Newton's Law of Gravitation:

$$\vec{a} = -\frac{\mu}{\|\vec{r}\|^2}\left(\frac{\vec{r}}{\|\vec{r}\|}\right), \tag{II.15}$$

where μ is the Earth's gravitational parameter (398,600.4418 km^3/s^2), and $\|\vec{r}\|$ is the radius from the center of the Earth (6378.137 km at sea level). At sea level, this gives a gravitational acceleration of approximately 9.798 m/s^2. Comparing the magnitudes of the acceleration at sea level to that at an altitude of 20 km, we find

$$\Delta a = \mu\left(\frac{1}{(r + 20\text{km})^2} - \frac{1}{r^2}\right) \approx -0.06116\frac{\text{m}}{\text{s}^2} \tag{II.16}$$

Given such a small relative difference, we can treat the gravitational acceleration as constant, so the gravitational force is simply

$$F_{gravity} = \int -g dm \hat{k} \tag{II.17}$$

6

where

$$g \approx 9.798\frac{\text{m}}{\text{s}^2} \tag{II.18}$$

(3) Force Due to Earth's Rotation. In Fig. 2, Ω represents the angular velocity of the sphere, which for Earth has a value of 2π radians per sidereal day (23 hours, 56 minutes, 4.090524 seconds [112]) or 7.292116×10^{-5} rad/s. We must consider the effects caused by the rotating reference frame. Here we follow
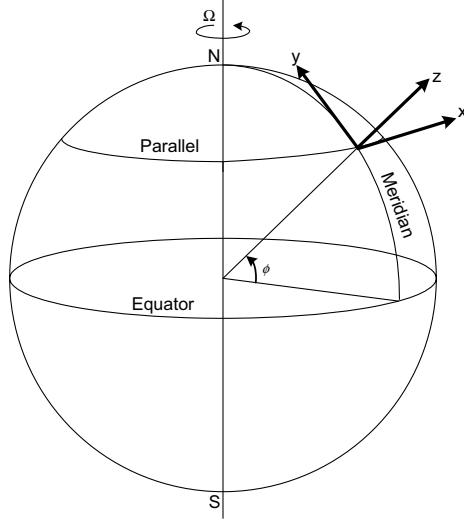
Figure 2. Rotating Sphere [From [113], Fig. 2, p. 11]

the derivation laid out by Holton [70] and Pedlosky [94]. Let $\vec{r}$ denote the position vector of an element in our rotating reference frame (see Fig. 3, where ψ is the angle between $\vec{r}$ and the angular rotation vector $\vec{\Omega}$). In a small time interval Δt, the vector rotates by an angle $\Delta\theta = |\vec{\Omega}|\Delta t$. If the time interval is small enough, the change in the vector is given by

$$\Delta\vec{r} = \vec{n}|\vec{r}|\Delta\theta\sin\psi, \tag{II.19}$$

where $\vec{n}$ is the unit vector in the direction of the cross product $\vec{\Omega} \times \vec{r}$, i.e.,

$$\vec{n} = \frac{\vec{\Omega} \times \vec{r}}{|\vec{\Omega} \times \vec{r}|} \tag{II.20}$$

7
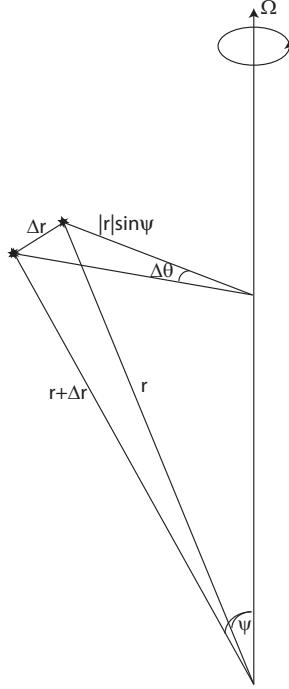
Figure 3. Vector in Rotating Reference Frame [After [94], Fig. 1.5.2, p. 15]

Thus,

$$\frac{\Delta \vec{r}}{\Delta t} = \frac{\vec{\Omega} \times \vec{r}}{|\vec{\Omega} \times \vec{r}|} |\vec{r}| \frac{\Delta \theta}{\Delta t} \sin \psi, \tag{II.21}$$

or in the limit as $\Delta t \to 0$,

$$\frac{d\vec{r}}{dt} = \frac{\vec{\Omega} \times \vec{r}}{|\vec{\Omega} \times \vec{r}|} |\vec{r}| \frac{d\theta}{dt} \sin \psi, \tag{II.22}$$

and since $\frac{d\theta}{dt} = |\vec{\Omega}|$, we get

$$\frac{d\vec{r}}{dt} = \vec{\Omega} \times \vec{r} \tag{II.23}$$

If we have $\vec{r} = x\hat{i} + y\hat{j} + z\hat{k}$ in the east-north-up coordinate frame shown in Fig. 2, then we convert from rotating to inertial reference frames by

$$\vec{u}_I = \vec{u} + \frac{d\vec{r}}{dt} = \vec{u} + \vec{\Omega} \times \vec{r}, \tag{II.24}$$

where $\vec{u}$ is the change in position within the rotating reference frame, and $\vec{u}_I$ is the same motion relative to the inertial reference frame. Differentiation of the above,

8

substituting $\vec{u}_I$ for $\vec{r}$ and noting that $\vec{\Omega}$ is constant, yields

$$
\begin{aligned}
\left(\frac{d\vec{u}_I}{dt}\right)_I &= \left(\frac{d\vec{u}_I}{dt}\right)_R + \vec{\Omega} \times \vec{u}_I \\
&= \frac{d\vec{u}}{dt} + 2\vec{\Omega} \times \vec{u} + \vec{\Omega} \times (\vec{\Omega} \times \vec{r})
\end{aligned} \tag{II.25}
$$

Based on Fig. 2, our angular momentum vector is

$$
\vec{\Omega} = |\vec{\Omega}| \cos \phi \hat{j} + |\vec{\Omega}| \sin \phi \hat{k} \tag{II.26}
$$

Using this definition and the definition of the cross product twice, we have

$$
\vec{\Omega} \times (\vec{\Omega} \times \vec{r}) = |\Omega|^2 \begin{pmatrix} x \\ z \sin \phi \cos \phi - y \sin^2 \phi \\ -z \cos^2 \phi + y \sin \phi \cos \phi \end{pmatrix}, \tag{II.27}
$$

but, since $|\Omega|^2 = 5.317496 \times 10^{-9}$, we can ignore the last term of (II.25) to get

$$
\left(\frac{d\vec{u}_I}{dt}\right)_I = \frac{d\vec{u}}{dt} + 2\vec{\Omega} \times \vec{u} \tag{II.28}
$$

Applying this formula to the momentum vector gives

$$
\left(\frac{d}{dt}(\vec{u}_I dm)\right)_I = \frac{d}{dt}(\vec{u}dm) + 2\vec{\Omega} \times (\vec{u}dm) \tag{II.29}
$$

Hence, when we consider the change in momentum, we must add to it this rotational effect. Now this rotational effect can be simplified. The atmosphere is thin compared to the radius of the Earth. Furthermore, atmospheric flows tend to be parallel to the ground (i.e., the velocity in the z direction is small). Taking the cross product of this vector and our velocity vector gives

$$
2\vec{\Omega} \times \vec{u} = 2|\vec{\Omega}|((w \cos \phi - v \sin \phi)\hat{i} + u \sin \phi \hat{j} - u \cos \phi \hat{k}) \tag{II.30}
$$

Again, assuming a thin atmosphere and thus neglecting terms in the z direction, this simplifies to

$$
2\vec{\Omega} \times \vec{u} \approx 2|\vec{\Omega}| \sin \phi(-v\hat{i} + u\hat{j}) = 2|\vec{\Omega}| \sin \phi(\hat{k} \times \vec{u}) \tag{II.31}
$$

9

If we define $f = 2|\vec{\Omega}|\sin\phi$, we can express this force as

$$\left(\frac{d}{dt}(\vec{u}dm)\right)_I = \left(\frac{d}{dt}(\vec{u}dm)\right)_R + f(\hat{k} \times (\vec{u}dm)) \qquad \text{(II.32)}$$

Since we are observing the flow from the rotating reference frame, this additional force becomes an inhomogeneous term on the right-hand-side of the momentum equation:

$$F_{Coriolis} = \int f(\vec{u} \times \hat{k})dm \qquad \text{(II.33)}$$

b.   *Summary of Forces*

Thus, the equation for conservation of momentum is

$$\frac{d}{dt}\int \vec{u}dm = -\int \nabla p dV + \int f(\vec{u} \times \hat{k})dm - \int g\hat{k}dm \qquad \text{(II.34)}$$

Here, as before, the integrand must be identically zero,

$$\frac{d}{dt}(\vec{u}dm) + \frac{\nabla p}{\rho}dm = f(\vec{u} \times \hat{k})dm - g\hat{k}dm, \qquad \text{(II.35)}$$

or, by component,

$$\begin{aligned}
\frac{d}{dt}(udm) + \frac{dm}{\rho}\partial_x p &= fvdm \\
\frac{d}{dt}(vdm) + \frac{dm}{\rho}\partial_y p &= -fudm \\
\frac{d}{dt}(wdm) + \frac{dm}{\rho}\partial_z p &= -gdm
\end{aligned} \qquad \text{(II.36)}$$

Using a derivation similar to that in Section 1, these equations can be rewritten in vector notation:

$$\partial_t(\rho\vec{u}) + \nabla \cdot (\rho\vec{u} \otimes \vec{u}) + \nabla p = f(\rho\vec{u} \times \hat{k}) - g\rho\hat{k}, \qquad \text{(II.37)}$$

where $\otimes$ denotes the tensor product. However, we can simplify the equations to

$$\begin{aligned}
\partial_t u + u\partial_x u + v\partial_y u + w\partial_z u + \frac{1}{\rho}\partial_x p &= fv \\
\partial_t v + u\partial_x v + v\partial_y v + w\partial_z v + \frac{1}{\rho}\partial_y p &= -fu \\
\partial_t w + u\partial_x w + v\partial_y w + w\partial_z w + \frac{1}{\rho}\partial_z p &= -g,
\end{aligned} \qquad \text{(II.38)}$$

or, in vector notation,

$$\frac{\partial\vec{u}}{\partial t} + (\vec{u} \cdot \nabla)\vec{u} + \frac{1}{\rho}\nabla p = f(\vec{u} \times \hat{k}) - g\hat{k} \qquad \text{(II.39)}$$

10

3. Conservation of Energy

The intrinsic energy in each piece of mass dm consists of its kinetic energy. For atmospheric modeling, there are also inhomogeneous components for thermal energy and potential energy. These quantities are defined by

$$
\begin{aligned}
dHE &= c_v T dm \\
dKE &= \frac{\|\vec{u}\|^2}{2} dm \\
dPE &= gz dm
\end{aligned}
\tag{II.40}
$$

In these equations, c_v is the specific heat at constant volume, and T is the temperature. Hence the total energy in the body is

$$
\int \left(c_v T + \frac{\|\vec{u}\|^2}{2} + gz \right) dm
$$

To change the amount of energy, apply force to the body over a distance or add/remove heat. Adding/removing heat is a complicated process involving solar radiation, thermal radiation from the Earth, heat dissipation into space, reflectivity of the Earth's surface, and other factors. Due to the complexity, factors which contribute to a change in temperature will not be considered here. Rather, we will simply consider the time derivative of our heat energy term on its own without determining the precise factors which determine it. Later in this section, we will hide the temperature component entirely, combining thermal and kinetic energy into a "total energy" term e.

For force application, the momentum equations assume a balance between the external forces and the internal pressure. However, if the two quantities are not matched, then the volume will expand/contract so that they are matched. If there is an imbalance between the forces on opposing sides of the body (hence a pressure difference), then the body will accelerate in the direction of the net force. (Imagine pulling a spring across a table. The spring will stretch according to the pulling force, and the stretched spring will move in the pulling direction.)

We can conceive of the total force as having these two components, compression and acceleration. For compression at constant temperature, as the volume decreases,

the internal pressure increases, and vice versa. Hence,

$$\frac{d}{dt}(pdV) = 0 \tag{II.41}$$

However, if the temperature is not constant, then the pressure increases proportionally to the thermal energy at the constant volume, adding the following component to our equations:

$$\frac{d}{dt}(c_v T dm) = \frac{dp}{dt}dV \tag{II.42}$$

The acceleration component is determined by Newton's Second Law. The acceleration occurs as a result of an imbalance between the force acting on one side of the body and the force acting on the opposite side, which results in the pressure differences defined in the conservation of momentum section. Using $\vec{F} = m\vec{a}$ and our definition of $dF_{pressure}$ we have

$$\vec{a} = \frac{-(\nabla p)dV}{dm} = -\frac{\nabla p}{\rho} \tag{II.43}$$

This force changes the kinetic energy of the body. The time derivative of kinetic energy is

$$\frac{d}{dt}(KE) = dm\left(\vec{u} \cdot \frac{d\vec{u}}{dt}\right) = dm(\vec{u} \cdot \vec{a}) \tag{II.44}$$

Using our formula for the acceleration, we have

$$\frac{d}{dt}(KE) = \frac{-dm}{\rho}(\vec{u} \cdot \nabla p) = -(\vec{u} \cdot \nabla p)dV \tag{II.45}$$

In the context of atmospheric modeling, this force also results in an increase in the body's potential energy as it changes position vertically, so that we have

$$\frac{d}{dt}(KE) + \frac{d}{dt}(PE) = -(\vec{u} \cdot \nabla p)dV \tag{II.46}$$

Therefore, changing the energy in the body results in increased kinetic energy, body compression, and pressure increase due to temperature

$$\frac{d}{dt}\left(\int \left(c_v T + \frac{\|\vec{u}\|^2}{2} + gz\right)dm\right) + \int \frac{d}{dt}(pdV) = -\int (\vec{u} \cdot \nabla p)dV + \int \frac{dp}{dt}dV \tag{II.47}$$

Combining the integrals and bringing the derivative inside gives

$$\int \frac{d}{dt}\left(\left(c_v T + \frac{\|\vec{u}\|^2}{2} + gz\right)dm\right) + (\vec{u}\cdot\nabla p)dV + p\frac{d}{dt}(dV) = 0, \qquad \text{(II.48)}$$

where we use the product rule to combine $\frac{d}{dt}(pdV) - \frac{dp}{dt}dV$ into $p\frac{d}{dt}(dV)$. Again, this integral must be true for any body, so the integrand must be identically zero

$$\frac{d}{dt}\left(\left(c_v T + \frac{\|\vec{u}\|^2}{2} + gz\right)dm\right) + (\vec{u}\cdot\nabla p)dV + p\frac{d}{dt}(dV) = 0 \qquad \text{(II.49)}$$

Let $e = c_v T + \frac{\|\vec{u}\|^2}{2}$ denote the total internal energy of the system (i.e., not including potential energy). Then we have

$$\frac{d}{dt}((e + gz)\rho dV) + (u\partial_x p + v\partial_y p + w\partial_z p)dV + p\frac{d}{dt}(dV) = 0 \qquad \text{(II.50)}$$

It is easy to show that this equation is equivalent to

$$\partial_t(\rho e) + \partial_x((\rho e + p)u) + \partial_y((\rho e + p)v) + \partial_z((\rho e + p)w) = -g\rho w, \quad \text{(II.51)}$$

or, in vector notation,

$$\partial_t(\rho e) + \nabla \cdot ((\rho e + p)\vec{u}) = -(g\hat{k}) \cdot (\rho\vec{u}) \qquad \text{(II.52)}$$

This equation can be placed in a simpler form, if we assume our fluid is an ideal gas. Using the ideal gas law $p = \rho RT$ [24, 58], where $R = c_p - c_v$, simple algebraic manipulation using the previous equations can reduce this energy equation to

$$\partial_t p + u\partial_x p + v\partial_y p + w\partial_z p + \gamma p\left(\partial_x u + \partial_y v + \partial_z w\right) = 0, \qquad \text{(II.53)}$$

where $\gamma = \frac{c_p}{c_v}$. In vector notation, this equation can be written as

$$\partial_t p + (\vec{u}\cdot\nabla)p + \gamma p(\nabla\cdot\vec{u}) = 0 \qquad \text{(II.54)}$$

While this equation is simple, it lacks an explicit energy term and thus fails to convey the energy conservation principle from which it was derived.

B.   SUMMARY OF NON-LINEAR EULER EQUATIONS

Using only the physical conservation principles for mass, momentum, and energy, we can derive Euler's equations for inviscid fluid motion. We have a system of five equations for six variables:

$$
\begin{aligned}
\partial_t \rho + \partial_x(\rho u) + \partial_y(\rho v) + \partial_z(\rho w) &= 0 \\
\partial_t(\rho u) + \partial_x(\rho u^2) + \partial_y(\rho u v) + \partial_z(\rho u w) + \partial_x p &= f\rho v \\
\partial_t(\rho v) + \partial_x(\rho u v) + \partial_y(\rho v^2) + \partial_z(\rho v w) + \partial_y p &= -f\rho u \quad \text{(II.55)} \\
\partial_t(\rho w) + \partial_x(\rho u w) + \partial_y(\rho v w) + \partial_z(\rho w^2) + \partial_z p &= -g\rho \\
\partial_t(\rho e) + \partial_x((\rho e + p)u) + \partial_y((\rho e + p)v) + \partial_z((\rho e + p)w) &= -g\rho w
\end{aligned}
$$

In vector notation, the equations can be written as

$$
\begin{aligned}
\partial_t \rho + \nabla \cdot (\rho \vec{u}) &= 0 \\
\partial_t(\rho \vec{u}) + \nabla \cdot (\rho \vec{u} \otimes \vec{u}) + \nabla p &= f(\rho \vec{u} \times \hat{k}) - g\rho\hat{k} \quad \text{(II.56)} \\
\partial_t(\rho e) + \nabla \cdot ((\rho e + p)\vec{u}) &= -(g\hat{k}) \cdot (\rho \vec{u})
\end{aligned}
$$

A state equation of some kind is required to close the system. For an ideal gas, we can use $p = \rho R T$ to simplify the equations to

$$
\begin{aligned}
\partial_t \rho + \partial_x(\rho u) + \partial_y(\rho v) + \partial_z(\rho w) &= 0 \\
\partial_t u + u\partial_x u + v\partial_y u + w\partial_z u + \frac{1}{\rho}\partial_x p &= fv \\
\partial_t v + u\partial_x v + v\partial_y v + w\partial_z v + \frac{1}{\rho}\partial_y p &= -fu \quad \text{(II.57)} \\
\partial_t w + u\partial_x w + v\partial_y w + w\partial_z w + \frac{1}{\rho}\partial_z p &= -g \\
\partial_t p + u\partial_x p + v\partial_y p + w\partial_z p + \gamma p \left(\partial_x u + \partial_y v + \partial_z w\right) &= 0
\end{aligned}
$$

(see Appendix A for details). For all three formulations, the terms on the right-hand-side denote forces specific to atmospheric modeling.

In the next section, we will derive the linearized form of (II.57), which will form the basis for developing the finite-difference implementation of the NRBCs in

Chapters IV–VI. We will begin with a simplified prototype implementation of the automated Higdon NRBCs with no advection or forcing terms, and we will build the implementation to include Coriolis, gravity, and non-zero mean flow. We will also develop auxiliary variable forms which eliminate the high-order derivative terms, using both the Givoli-Neta and the Hagstrom-Warburton auxiliary variable NRBC formulations.

C. LINEARIZED EULER EQUATIONS

Having derived the non-linear equations, we now seek to simplify them into a linear form. We assume that each state variable consists of a time-independent mean value and a small perturbation from that mean. Thus,

$$\varphi = \bar{\varphi} + \varphi^*, \tag{II.58}$$

where the overbar denotes the reference value, and the asterisk denotes the $O(\delta)$ perturbation variable. Before we can derive this linearized form, we must first define our reference variables. We will perform the linearization on (II.57).

1. Defining the Reference Variables

The reference values are time-independent by definition, but they may not necessarily be constant in space. It is reasonable to believe that the reference values for the velocity variables u, v, and w will be constant; however, this may not be true for the density ρ and pressure p. In the presence of gravity, a volume of compressible fluid will be compressed by the weight of the fluid above it, increasing the density and pressure. Therefore, it is reasonable to expect that our reference states for density and pressure will vary with z.

Let us consider a constant domain governed by (II.57). With everything at rest, we set all time derivative terms and all velocity terms to zero. This leaves us with

$$\partial_x \bar{p} \;=\; 0$$

15

$$\partial_y \bar{p} = 0 \tag{II.59}$$

$$\partial_z \bar{p} = -g\bar{\rho}$$

This confirms our expectation that our reference values for ρ and p are dependent on z. So for our reference values, we let u_0, v_0, and w_0 define our constant mean velocities; $\bar{\rho}$ denotes our z-dependent density reference state, with ρ_0 the density at $z = 0$; and $\bar{p}$ denotes our z-dependent pressure reference state, with p_0 the pressure at $z = 0$.

2. Linearizing the Equations

Begin with the first equation of (II.57):

$$\partial_t \rho + \partial_x (\rho u) + \partial_y (\rho v) + \partial_z (\rho w) = 0. \tag{II.60}$$

Expand the derivatives via the product rule, and substitute the reference/perturbation variable expansion in (II.58) to get

$$\left. \begin{aligned} \partial_t(\bar{\rho} + \rho^*) + (\bar{\rho} + \rho^*)\,\partial_x(u_0 + u^*) + (u_0 + u^*)\,\partial_x(\bar{\rho} + \rho^*) \\ + (\bar{\rho} + \rho^*)\,\partial_y(v_0 + v^*) + (v_0 + v^*)\,\partial_y(\bar{\rho} + \rho^*) \\ + (\bar{\rho} + \rho^*)\,\partial_z(w_0 + w^*) + (w_0 + w^*)\,\partial_z(\bar{\rho} + \rho^*) \end{aligned} \right\} = 0 \,. \tag{II.61}$$

Recalling which reference variables are independent in space and time, and eliminating all terms of $O(\delta^2)$, we get

$$\partial_t \rho^* + \bar{\rho}\left(\partial_x u^* + \partial_y v^* + \partial_z w^*\right) + u_0 \partial_x \rho^* + v_0 \partial_y \rho^* + w_0 \partial_z \rho^* = -\partial_z \bar{\rho}\left(w_0 + w^*\right). \tag{II.62}$$

We leave the equation in this form, rather than reverting it to the whole state variable. By considering only the perturbation variable, we eliminate the possibility of the reference value overwhelming the perturbation, introducing unnecessary round-off errors into the finite-precision calculations.

When we apply this same process to the velocity and pressure equations of (II.57), using (II.59) to simplify the equation for w, we get

$$\partial_t \vec{\varphi} + A \partial_x \vec{\varphi} + B \partial_y \vec{\varphi} + C \partial_z \vec{\varphi} = D \vec{\varphi} + E, \tag{II.63}$$

where

$$\vec{\varphi} \;=\; \begin{pmatrix} \rho^* & u^* & v^* & w^* & p^* \end{pmatrix}^T$$

$$A \;=\; \begin{pmatrix} u_0 & \bar{\rho} & 0 & 0 & 0 \\ 0 & u_0 & 0 & 0 & \frac{1}{\bar{\rho}} \\ 0 & 0 & u_0 & 0 & 0 \\ 0 & 0 & 0 & u_0 & 0 \\ 0 & \gamma\bar{p} & 0 & 0 & u_0 \end{pmatrix}$$

$$B \;=\; \begin{pmatrix} v_0 & 0 & \bar{\rho} & 0 & 0 \\ 0 & v_0 & 0 & 0 & 0 \\ 0 & 0 & v_0 & 0 & \frac{1}{\bar{\rho}} \\ 0 & 0 & 0 & v_0 & 0 \\ 0 & 0 & \gamma\bar{p} & 0 & v_0 \end{pmatrix}$$

$$C \;=\; \begin{pmatrix} w_0 & 0 & 0 & \bar{\rho} & 0 \\ 0 & w_0 & 0 & 0 & 0 \\ 0 & 0 & w_0 & 0 & 0 \\ 0 & 0 & 0 & w_0 & \frac{1}{\bar{\rho}} \\ 0 & 0 & 0 & \gamma\bar{p} & w_0 \end{pmatrix}$$

$$D \;=\; \begin{pmatrix} 0 & 0 & 0 & -\partial_z\bar{\rho} & 0 \\ 0 & 0 & f & 0 & 0 \\ 0 & -f & 0 & 0 & 0 \\ -g\frac{1}{\bar{\rho}} & 0 & 0 & 0 & 0 \\ 0 & 0 & 0 & g\bar{\rho} & 0 \end{pmatrix}$$

$$E \;=\; \begin{pmatrix} -\partial_z\bar{\rho}w_0 \\ fv_0 \\ -fu_0 \\ 0 \\ g\bar{\rho}w_0 \end{pmatrix} \tag{II.64}$$

17

For the $\frac{1}{\rho}\{\partial_x p,\ \partial_y p,\ \partial_z p\}$ terms in the momentum equations, we use the following linearization:

$$
\begin{aligned}
\frac{\partial_x p}{\rho} &= \frac{\partial_x\,(\bar{p}+p^*)}{\bar{\rho}+\rho^*} \\[2mm]
&= \frac{\partial_x p^*}{\bar{\rho}}\left(\frac{1}{1+\frac{\rho^*}{\bar{\rho}}}\right) \\[2mm]
&\approx \frac{\partial_x p^*}{\bar{\rho}}\left(1-\frac{\rho^*}{\bar{\rho}}+\left(\frac{\rho^*}{\bar{\rho}}\right)^2-\cdots\right) \\[2mm]
&\approx \frac{\partial_x p^*}{\bar{\rho}} \\[2mm]
\frac{\partial_y p}{\rho} &\approx \frac{\partial_y p^*}{\bar{\rho}} \\[2mm]
\frac{\partial_z p}{\rho} &\approx \frac{\partial_z p^*+\partial_z \bar{p}}{\bar{\rho}}\left(1-\frac{\rho^*}{\bar{\rho}}+\left(\frac{\rho^*}{\bar{\rho}}\right)^2-\cdots\right) \\[2mm]
&\approx \frac{\partial_z p^*}{\bar{\rho}}-\frac{g\bar{\rho}}{\bar{\rho}}\left(1-\frac{\rho^*}{\bar{\rho}}\right) \\[2mm]
&\approx \frac{\partial_z p^*}{\bar{\rho}}-g\left(1-\frac{\rho^*}{\bar{\rho}}\right)\ ,
\end{aligned}
$$

where we use (II.59) in the next to last line.

Note that the matrix A is singular if $u_0=0$ or $u_0^2=\gamma\bar{p}/\bar{\rho}$. Similarly, B is singular if $v_0=0$ or $v_0^2=\gamma\bar{p}/\bar{\rho}$, and C is singular if $w_0=0$ or $w_0^2=\gamma\bar{p}/\bar{\rho}$.

So what have we lost by this linearization? The main difference between non-linear flow and linear flow is the non-linear interaction between vortices [69]. For example, Fig. 4 shows a rising thermal bubble using non-linear equations (left) and their linearized form (right). The turbulence is clearly absent in the linearized case. However, wave motion is not noticeably affected. Fig. 5 shows an acoustic wave using the non-linear (left) and linearized equations (right). The differences are negligible. (These figures were generated during some early work, applying a spectral element implementation of the non-linear system (II.55) in the xz plane influenced by gravity, and to the linearized form of the same system.) Since our non-reflecting boundary

conditions are intended for wave propagation, we do not need to keep the non-linear effects of vorticity.
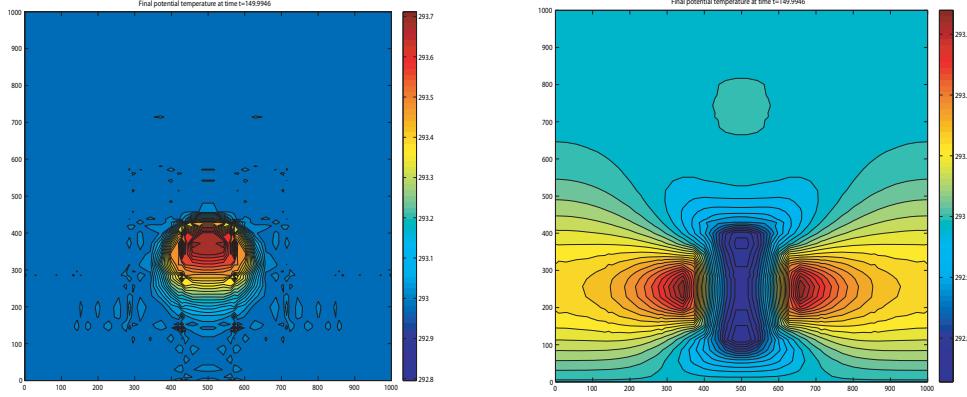
Figure 4. A Rising Thermal Bubble Using Non-linear (left) and Linear (right) Equations
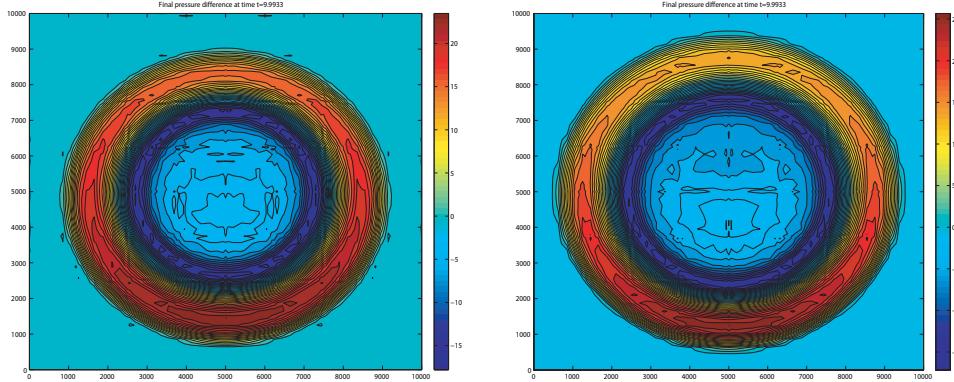
Figure 5. An Acoustic Wave Using Non-linear (left) and Linear (right) Equations

Before we begin developing NRBCs for this equation system, let us spend some time discussing NRBCs in general, with particular emphasis on the scalar-equation implementations of the NRBCs we are here adapting for a linear first-order system. This discussion will be the subject of the next chapter, and then the new NRBC implementations will be developed in Chapters IV–VI.

19

THIS PAGE INTENTIONALLY LEFT BLANK

III.   NON-REFLECTING BOUNDARY CONDITIONS

A.   OVERVIEW AND HISTORY

We wish to solve fluid flow problems in only a portion of a large or infinite domain. By restricting our area of interest, we effectively create a boundary $\mathcal{B}$ where none exists physically, dividing our computational domain Ω from the rest of the domain $\mathcal{D}$. Implicit in our choice of $\mathcal{B}$ is the assumption that everything we wish to model is contained inside Ω; nothing external impinges on our computational domain. The challenge we must overcome, then, is defining $\mathcal{B}$ in such a way that it behaves computationally as if there were no physical boundary. How, then, do we specify what occurs at these boundaries? The usual answer is to claim that waves flow out of the domain at the boundary, but they do not flow into the domain. If defined correctly, this claim will result in waves which propagate out of the computational domain without any reflection, so that the computational boundary is transparent to these outgoing waves, mimicking the real-world behavior where no such physical boundary exists.

In general, there are two ways to simulate an open boundary. One may either surround the domain with an artificial absorbing medium, so that outgoing waves are diffused to zero before they return to the computational domain, or one may use a differential operator to prescribe the wave behavior at the boundary, so that only outgoing waves are permitted.

Research into modeling open boundaries has been active since the late 1960s. Zienkiewicz and Newton [121] first derived the Sommerfeld radiation condition for outgoing wave propagation in 1969. In hindsight, this differential operator is surprisingly obvious and easy to derive. Beginning with the known general solution to the one-dimensional scalar wave equation

$$\partial_{tt} u = c^2 \partial_{xx} u \ , \tag{III.1}$$

we have

$$u(x, t) = F(x - ct) + G(x + ct) \tag{III.2}$$

for some functions F and G [105]. If F denotes the outgoing waves, and G the incoming, then we insist on $G \equiv 0$ on the boundary. Differentiating u with respect to x and t, this gives us

$$\partial_t u = -cF' \quad , \quad \partial_x u = F' . \tag{III.3}$$

From here we easily get the Sommerfeld boundary condition:

$$\partial_t u + c\partial_x u = 0 . \tag{III.4}$$

This boundary condition can be interpreted in two ways. The characteristic-based interpretation uses this condition as prescribing the Riemann invariant of the solution (see Ch. 8 of [24]). The wave-based interpretation describes it as requiring waves on the boundary to satisfy the one-way advection equation. Several early NRBCs were developed in the 1970s using these two interpretations. Wurtele et al. [119] used the characteristic method, while Pearson [93] and Orlanski [92] took the wave-based approach. Engquist and Majda [25, 26] extended the wave-based method, defining a pseudo-differential operator solution to the 2-D wave equation and deriving Padé approximations thereto in a sequence of ever-more-accurate boundary conditions. Smith [101] took a simplistic, albeit computationally intensive, approach: Apply a Dirichlet boundary condition to one solution, apply a Neumann boundary condition to another, and then add the two solutions, cancelling the two reflections and leaving only the non-reflecting solution within the accuracy of the Neumann operator. One of the first absorbing layer methods was also published around this time by Davies [17] for the linearized Euler equations in a nested environment, using a "relaxation" function near the boundary to match the small-scale interior scheme with the large-scale outer model. Later NRBCs built on these methods or developed new approaches.

In the 1980s, several new NRBC techniques appeared. Bayliss and Turkel [9, 10] developed a sequence of increasing-order boundary conditions based on an-

nihilating the first terms of the asymptotic expansion of the scalar wave equation. Miller and Thorpe [87] proposed a modified Orlanski scheme based on alternative time-stepping methods. Ferm and Gustafsson [27] used Fourier transformations to devise a downstream boundary condition for the steady-state linearized Euler equations. Klemp and Durran [79] developed a "sponge layer" to absorb outgoing gravity waves, applied to the linear Boussinesq equations, later applied to the non-linear Euler equations by Giraldo and Restelli [32]. Davies [18] compared various techniques, including "diffusion zones," relaxation functions, and radiation boundary conditions. Raymond and Kuo [95] modified the Sommerfeld condition to consider tangential as well as normal derivatives in multi-dimensional flows. Ting and Miksis [110] proposed using Kirchhoff's formula to determine the boundary values of waves exterior to a scatterer. Trefethen and Halpern [111] analyzed the Engquist-Majda method; considering different approaches to approximating the pseudo-differential operator, they demonstrated its well-posedness and proved Engquist's and Majda's proposition concerning which classes of Padé approximations are well-posed. Higdon [62, 64] developed a sequence of increasing-order boundary conditions based on a product of Sommerfeld conditions at various incidence angles. Keller and Givoli [78] developed the "Dirichlet-to-Neumann" (DtN) mapping, an NRBC method which converts the Dirichlet condition at infinity to a Neumann condition at the computational domain boundary; they then used this DtN mapping in a finite element solution of Laplace's equation on an infinite domain [38]. See also Givoli's 1991 paper [33] reviewing the then-current state of the art.

The 1990s saw an explosion in NRBC development. Kröner [82] adapted the Engquist-Majda scheme to the 2-D linearized Euler equations, using Fourier transformations rather than pseudo-differential operators to define the boundary condition; Giles [30] performed a similar technique, also using Fourier transformations to derive an NRBC for the 2-D linearized Euler equations. G. Kreiss [80] used a simple Dirichlet condition at the downstream end for the pressure term of the linearized

Euler equations, and he showed that the resulting error decreases exponentially upstream of the open boundary. Collino [15] extended the Engquist-Majda scheme to open domains (requiring consideration of corner conditions) and to other wave-like equations. Tam and Webb [106] used the asymptotic expansion to define radiation boundary conditions compatible with their dispersion-relation-preserving finite difference scheme for the linearized Euler equations. Higdon continued his sequence of NRBC papers [65, 66, 67, 68], culminating in a robust NRBC sequence for the dispersive (Klein-Gordon) wave equation. Grote and Keller [47, 48, 49] extended the DtN technique to spherical waves and the Helmholtz equation, in finite difference and finite element methods; Thompson and Huan [109] later modified this formulation to implement a finite element solution of the spherical wave equation. Ren [96] used a 2-D Sommerfeld-like boundary condition,

$$\left(\partial_t + c\left(\alpha_x \partial_x + \alpha_y \partial_y\right)\right)\eta = 0 \tag{III.5}$$
$$\alpha_x^2 + \alpha_y^2 = 1 \ ,$$

to define an open boundary for the 2-D Boussinesq equations. Hagstrom and Hariharan [54] presented an NRBC for the 2-D and 3-D wave equation in polar/spherical coordinates, using auxiliary variables to remove the high-order normal derivative terms; Huan and Thompson [75] later modified this scheme by using a spherical harmonic-based formulation. Safjan [98] also took the auxiliary variable approach, applying them to high-order Padé approximations to the pseudo-differential operator of the scalar wave equation. Jensen [77] compared several techniques, including NRBCs and sponge layers, for modeling open boundaries in a stratified ocean model.

The 1990s also saw the development of the Perfectly Matched Layer (PML), first defined by Bérenger [11] for the 2-D Maxwell equations. This absorbing layer method surrounds the computational domain with a dispersive medium, defined in such a way that incoming waves *at any incidence angle* pass from the interior to the dispersive layer without any (theoretical) reflection. A 2007 paper by Skelton et al. [100] claimed to find over 1,000 references to Bérenger's paper in the literature.

This technique has been applied to the linearized Euler equations by Abarbanel et al. [1], Goodrich and Hagstrom [45], Hu [71, 72, 73], and Nataf [88]; to the linearized shallow-water equations by Navon et al. [89]; to Maxwell's equations using a second-order discretization scheme by Sjögreen and Petersson [99]; to the linearized and non-linear wave equation by Appelö and G. Kreiss [7] (following Appelö et al.'s well-posedness and stability theory in [6]); to elastic waveguides by Skelton et al. [100]; to the time-harmonic wave equation by Bermúdez et al. [12]; and to the non-linear Euler and Navier-Stokes equations by Hu et al. [74].

NRBC development continued in this decade as well, with new techniques and new applications of old techniques. Oliveira [91] combined a Sommerfeld condition with an absorbing layer to develop an NRBC for the transient mild-slope equation:

$$\nabla \left(CC_g \nabla \eta \right) + \left(k^2 CC_g - \omega^2 \right) \eta - \partial_{tt} \eta = 0 \qquad \text{(III.6)}$$

(see Eqn. (9) of [91]). Grote and Keller [50] developed an exact NRBC for the 3-D elastic wave equation with a spherical open boundary, based on annihilating the first terms of the wave's spherical harmonics. Alpert et al. [4, 5] developed two NRBCs for the scalar wave equation, one using Hankel functions and Laplace transforms, and one using Fourier-Laplace transformations. Lie [83] used Fourier-Laplace transformations to derive an NRBC for the shallow-water equations. Colonius and Ran [16] developed an absorbing buffer technique for conservation law-based systems by using Fourier transformations to filter the outgoing flow disturbances. McDonald [85, 86] derived a characteristic-based NRBC for the shallow-water equations and compared the performance of NRBCs and "relaxation zone" boundaries in nested-model environments. Hagstrom and Nordström [56] analyzed the use of extrapolation boundary values in solving the steady-state linearized Euler equations, showing the relationship between the position of the artificial far-field boundary and the error norm of the discrete solution. Blayo and Debreu [13] considered a characteristic variable approach to NRBCs in first-order systems for ocean and atmospheric models. Chang et al. [14] used a Space-Time Conservation Element and Solution Element (CE/SE)

method to solve the 1-D Euler equations, which effectively handled shockwaves inside the domain (although the results were good within the domain, the numerical results published showed poorer performance closer to the boundary). Guddati and Lim [51] used continued fractions (rather than the Engquist-Majda Padé approximations) to approximate the pseudo-differential operator, and they devised a formulation that could be applied to any convex polygon boundary (rather than the usual straight-line boundaries). Zahid and Guddati [120] incorporated PML-like "padding elements" into a continued fraction NRBC for dispersive waves. Atassi and Galán [8] used Fourier-Bessel modes to derive an NRBC for the non-linear Euler equations in an annular duct. Song and Bazyar [102] derived an NRBC for finite element frequency-domain wave analysis based on Padé approximations.

The 2000s also saw a revived interest in the Higdon NRBC sequence. Givoli and Neta created an algorithm to compute high-order finite difference derivatives automatically, removing the algebraic complexity which limited the original Higdon sequence to third-order. This automation, along with an auxiliary variable method which removed the high-order normal derivatives, was applied to the Klein-Gordon equation and the shallow-water equations in a sequence of papers by them and their students and colleagues [39, 40, 41, 42, 43, 90, 113, 114, 115, 116]. Givoli again published a review of current NRBC techniques in [35]. In addition, Hagstrom and Warburton [57] developed a modified form of the Givoli-Neta auxiliary variable NRBC for the scalar wave equation. This new method was expanded and analyzed in [37, 53, 55, 84].

In this dissertation, we use the Givoli-Neta automation to apply the Higdon NRBCs to the linearized Euler equations; we also extend the Givoli-Neta and Hagstrom-Warburton auxiliary variable NRBCs thereto. Some of the results presented in the following chapters have been published or submitted for publication [19, 20, 21, 22]. The remainder of this chapter is devoted to the scalar form of the Higdon, Givoli-Neta, and Hagstrom-Warburton NRBC sequences, laying the ground-

work for their application to the linearized Euler equations.

B. NRBCS FOR SCALAR EQUATIONS
1. Higdon

One of the simplest non-reflecting boundary conditions (NRBCs) is the Sommerfeld radiation condition:

$$(\partial_t + c_0 \partial_x) u = 0, \tag{III.7}$$

where u is the unknown solution to our problem, and c_0 is the wave propagation speed in the positive x direction (for a right-side boundary; on other sides, replace ∂_x with the appropriate normal derivative). In essence, this boundary condition says that the outgoing wave at the boundary satisfies the one-dimensional advection equation with advection speed c_0. This boundary condition is most easily applied to the standard wave equation,

$$\partial_{tt} u = c_0^2 \nabla^2 u \tag{III.8}$$

It can also apply to the linearized shallow water equations (see [41]),

$$\begin{align}
\partial_t u - fv &= -g \partial_x \eta \\
\partial_t v + fu &= -g \partial_y \eta \\
\partial_t \eta + h_0 (\partial_x u + \partial_y v) &= 0
\end{align} \tag{III.9}$$

whose surface height component η can be converted (see [113]) to the dispersive (Klein-Gordon) wave equation,

$$\partial_{tt} \eta = c_0^2 \nabla^2 \eta - f^2 \eta \quad , \quad c_0 = \sqrt{gh_0} \tag{III.10}$$

The difficulty in (III.9) and (III.10) is that there is more than one wave speed. The same problem afflicts the standard wave equation in more than one dimension, as waves travelling in directions other than normal to the boundary have wave speeds whose normal components are not equal to c_0. Higdon proposed [68] defining a boundary condition as a product of J Sommerfeld-like terms:

$$\prod_{j=1}^{J} (\partial_t + c_j \partial_x) u = 0 \tag{III.11}$$

Just as "$xy = 0$" is a consolidation of "$x = 0$ or $y = 0$", this product consolidates, into a single equation, numerous Sommerfeld conditions with different advection speeds. Since the differential operator is linear, it is easy to show that if any one of the individual Sommerfeld conditions is satisfied, then the consolidated Higdon condition is also satisfied.

a.   Reflection Coefficient

Let us analyze the claim that this boundary condition is non-reflecting. Consider a wave-like equation with a solution of the form

$$u(x,t) = e^{i(x - c_x t)} \tag{III.12}$$

This solution defines a wave with speed c_x. Applying the Higdon boundary condition to this equation, we claim that

$$\prod_{j=1}^{J} \left(\partial_t + c_j \partial_x \right) e^{i(x - c_x t)} = 0 \tag{III.13}$$

If c_x does not exactly equal one of the c_j, this statement may not be true. To make it true, we must add a reflected wave, thus:

$$\prod_{j=1}^{J} \left(\partial_t + c_j \partial_x \right) \left(e^{i(x - c_x t)} + R_J e^{i(x + c_x t)} \right) = 0 \tag{III.14}$$

The magnitude of R_J is the *reflection coefficient* associated with the boundary condition. (If (III.13) is true, then $R_J = 0$.) Higdon [68] claims that this reflection coefficient is always less than one, and that it decreases as J increases. We present the proof here in more detail.

Lemma III.1 *The magnitude of the reflection coefficient R_J of the Higdon NRBC defined in (III.11), applied to a wave with speed c_x, is*

$$|R_J| = \prod_{j=1}^{J} \left| \frac{c_x - c_j}{c_x + c_j} \right| \tag{III.15}$$

Proof. We prove by induction. For the $J = 1$ case, we have

$$\left(\partial_t + c_1 \partial_x \right) \left[e^{i(x - c_x t)} + R_1 e^{i(x + c_x t)} \right] = 0 , \tag{III.16}$$

28

and it is easy to show that

$$|R_1| = \left| \frac{c_x - c_1}{c_x + c_1} \right| . \tag{III.17}$$

Having proven there exists a J such that this lemma is true, we consider the $J + 1$ case:

$$\prod_{j=1}^{J+1} (\partial_t + c_j \partial_x) \left(e^{i(x - c_x t)} + R_{J+1} e^{i(x + c_x t)} \right) = 0 \tag{III.18}$$

Since the differential operators are linear, we can write

$$\prod_{j=1}^{J} (\partial_t + c_j \partial_x) \left[(\partial_t + c_{J+1} \partial_x) \left(e^{i(x - c_x t)} + R_{J+1} e^{i(x + c_x t)} \right) \right] = 0 . \tag{III.19}$$

Expanding the derivatives inside the brackets and combining terms, we get

$$\prod_{j=1}^{J} (\partial_t + c_j \partial_x) \left(e^{i(x - c_x t)} + \left(\frac{c_{J+1} + c_x}{c_{J+1} - c_x} \right) R_{J+1} e^{i(x + c_x t)} \right) = 0 . \tag{III.20}$$

Comparing this equation with (III.14), we see that

$$|R_J| = \left| \left(\frac{c_{J+1} + c_x}{c_{J+1} - c_x} \right) R_{J+1} \right| . \tag{III.21}$$

Thus,

$$\begin{aligned}
|R_{J+1}| &= \left| \frac{c_{J+1} - c_x}{c_{J+1} + c_x} \right| |R_J| \\
&= \left| \frac{c_{J+1} - c_x}{c_{J+1} + c_x} \right| \prod_{j=1}^{J} \left| \frac{c_x - c_j}{c_x + c_j} \right| \\
&= \prod_{j=1}^{J+1} \left| \frac{c_x - c_j}{c_x + c_j} \right| \quad \square
\end{aligned} \tag{III.22}$$

Since these c_j and c_x are positive, each term in the product is less than one. Thus, as J increases, the reflection coefficient gets smaller. Of course, well-chosen c_j's will reduce the reflection coefficient more rapidly, but even poor choices (for example, failing to consider possible incidence angles or phase speeds) will still bring improvements. Hence, we can get good absorption either with a high J or with well-chosen c_j's.

b. *A Simplifying Assumption*

The difficulty in using (III.11) comes from the rapidly increasing algebraic complexity for large J. At $J = 2$, we have

$$\left(\frac{\partial^2}{\partial t^2} + c_1\frac{\partial^2}{\partial t \partial x} + c_2\frac{\partial^2}{\partial t \partial x} + c_1 c_2 \frac{\partial^2}{\partial x^2}\right) u = 0 \tag{III.23}$$

At $J = 3$, it becomes

$$\left.\begin{array}{c} \left(\frac{\partial^3}{\partial t^3} + c_1\frac{\partial^3}{\partial t^2 \partial x} + c_2\frac{\partial^3}{\partial t^2 \partial x} + c_3\frac{\partial^3}{\partial t^2 \partial x}\right. \\ \left. +c_1 c_2 \frac{\partial^3}{\partial t \partial x^2} + c_1 c_3 \frac{\partial^3}{\partial t \partial x^2} + c_2 c_3 \frac{\partial^3}{\partial t \partial x^2} + c_1 c_2 c_3 \frac{\partial^3}{\partial x^3}\right) u \end{array}\right\} = 0 \;, \tag{III.24}$$

and so forth. The Givoli-Neta algorithm automates the finite difference computation of these high-order derivatives, but at a cost of $O(3^J)$ operations per time step. However, if we simply make all c_j equal to a single wave speed c, then (III.11) can be written as

$$\left(\partial_t + c\partial_x\right)^J u = 0 \tag{III.25}$$

(see [90]), or, expanding the polynomial,

$$\left(\sum_{j=0}^{J} \frac{J!}{j!(J-j)!} c^j \frac{\partial^J}{\partial t^{(J-j)} \partial x^j}\right) u = 0 \tag{III.26}$$

We will show in the next section that this simplification, when applied to a finite difference formulation, requires only $O(J^2)$ operations per time step.

c. *Discretization of Higdon NRBCs*

For our finite difference implementation of the NRBCs, we use first-order differences for each derivative, with the difference pointing into the domain and backward in time. Higdon [68] demonstrated that this discretization scheme is stable when used in conjunction with the Klein-Gordon equation. For an open boundary on a rectangular domain, we have

$$\text{Top:} \quad \left(\frac{I - S_t^-}{\delta t} + c_0 \left(\frac{I - S_y^-}{\delta y}\right)\right)^J \sigma_{i,N}^n \;\; = \;\; 0$$

$$\text{Left:} \quad \left(\frac{I - S_t^-}{\delta t} - c_0 \left(\frac{S_x^+ - I}{\delta x}\right)\right)^J \sigma_{W,j}^n \;\; = \;\; 0$$

$$\text{Right:} \quad \left(\frac{I - S_t^-}{\delta t} + c_0 \left(\frac{I - S_x^-}{\delta x}\right)\right)^J \sigma_{E,j}^n \quad = \quad 0 \qquad \text{(III.27)}$$

$$\text{Bottom:} \quad \left(\frac{I - S_t^-}{\delta t} - c_0 \left(\frac{S_y^+ - I}{\delta y}\right)\right)^J \sigma_{i,S}^n \quad = \quad 0,$$

where I denotes the identity operator; S^- and S^+ backward and forward shifts in the subscript variable, e.g.,

$$S_x^+ \sigma_{i,j}^n = \sigma_{i+1,j}^n \quad , \quad S_t^- \sigma_{i,j}^n = \sigma_{i,j}^{n-1};$$

δt our grid spacing in time; δx and δy our grid spacing in x and y, respectively; $\sigma_{i,j}^n$ the value of a generic state variable σ at grid point (i, j) at time step n; and subscripts N, W, E, S denoting the north, west, east, or south boundaries, respectively. If we multiply each term by δt, clearing it out of the denominator, and then group terms by shift operator, we get

$$\text{Top:} \quad \left(a_y I + b S_t^- + c_y S_y^-\right)^J \sigma_{i,N}^n \quad = \quad 0$$

$$\text{Left:} \quad \left(a_x I + b S_t^- + c_x S_x^+\right)^J \sigma_{W,j}^n \quad = \quad 0$$

$$\text{Right:} \quad \left(a_x I + b S_t^- + c_x S_x^-\right)^J \sigma_{E,j}^n \quad = \quad 0 \qquad \text{(III.28)}$$

$$\text{Bottom:} \quad \left(a_y I + b S_t^- + c_y S_y^+\right)^J \sigma_{i,S}^n \quad = \quad 0,$$

where

$$a_x \quad = \quad 1 - c_x$$

$$a_y \quad = \quad 1 - c_y$$

$$b \quad = \quad -1$$

$$c_x \quad = \quad -c_0 \frac{\delta t}{\delta x}$$

$$c_y \quad = \quad -c_0 \frac{\delta t}{\delta y}$$

Expanding these operators as polynomials, we have

$$\text{Top:} \quad \left(\sum_{\beta=0}^{J} \sum_{\gamma=0}^{J-\beta} \frac{J!}{\alpha! \beta! \gamma!} a_y^\alpha b^\beta c_y^\gamma S_t^{-\beta} S_y^{-\gamma}\right) \sigma_{i,N}^n \quad = \quad 0$$

$$\text{Left: } \left(\sum_{\beta=0}^{J} \sum_{\gamma=0}^{J-\beta} \frac{J!}{\alpha!\beta!\gamma!} a_x^{\alpha} b^{\beta} c_x^{\gamma} S_t^{-\beta} S_x^{+\gamma} \right) \sigma_{W,j}^n = 0$$

$$\text{Right: } \left(\sum_{\beta=0}^{J} \sum_{\gamma=0}^{J-\beta} \frac{J!}{\alpha!\beta!\gamma!} a_x^{\alpha} b^{\beta} c_x^{\gamma} S_t^{-\beta} S_x^{-\gamma} \right) \sigma_{E,j}^n = 0 \qquad \text{(III.29)}$$

$$\text{Bottom: } \left(\sum_{\beta=0}^{J} \sum_{\gamma=0}^{J-\beta} \frac{J!}{\alpha!\beta!\gamma!} a_y^{\alpha} b^{\beta} c_y^{\gamma} S_t^{-\beta} S_y^{+\gamma} \right) \sigma_{i,S}^n = 0$$

where $\alpha = J - \beta - \gamma$.

Note. From this point forward in the dissertation, we will only show the NRBC formula for one side rather than all four. On the other three sides, the appropriate changes should be made for the correct normal derivative.

2.   Givoli-Neta

The greatest problem afflicting these high-order NRBCs is the presence of high-order spatial and temporal derivatives. With the spatial derivatives, the NRBC algorithm must look deep into the domain, and an incoming wave can begin to affect the boundary long before it actually reaches the boundary. High temporal derivatives require a long "history" of past values, increasing memory requirements. In both cases, and with the high-order mixed derivatives, increasing the number of terms in the NRBC calculation increases the danger of round-off errors corrupting the solution and destabilizing the system.

In addition, the NRBC order is inherently limited by the size of the domain. This is true in a finite difference setting, but it is even more restrictive in dealing with finite elements. In a finite element scheme, the spatial derivatives generally limit the NRBC order to that of the element polynomials, unless one is willing to use derivative approximations which are not local to a single element.

The way out of this dilemma is to introduce *auxiliary variables* [34] which require only low-order derivative calculations. In this section and the one following, we consider two methods for implementing these auxiliary variable techniques.

The Givoli-Neta NRBC was first proposed in [39, 42, 43] for the Klein-Gordon

equation in finite difference and finite element schemes. (In this dissertation, the term "Givoli-Neta NRBC" refers to the auxiliary variable implementation, not their automated high-order Higdon NRBC.) This NRBC follows directly from the Higdon NRBC. Where the Higdon NRBC uses one high-order equation on the boundary, the Givoli-Neta NRBC of order J uses a system of J low-order equations, defined thus:

$$\varphi_{j+1} = \left(\partial_x + \frac{1}{c_{j+1}}\partial_t\right)\varphi_j \tag{III.30}$$
$$\varphi_0 \equiv u$$
$$\varphi_J \equiv 0 .$$

Direct substitution shows that (III.30) is equivalent to (III.11). The above definition applies to an NRBC on the right side of the domain; on other sides, replace ∂_x with the appropriate normal derivative.

To illustrate the utility of this formulation, let us apply the NRBC to the Klein-Gordon equation (III.10). As this work has already been done by Givoli and Neta [39, 42, 43], we will not repeat the derivations here.

It is easy to show that the auxiliary variables also satisfy the Klein-Gordon equation, that is,

$$\partial_{tt}\varphi_j = c_0^2\nabla^2\varphi_j - f^2\varphi_j , \tag{III.31}$$

for all $j \in 1 \ldots J-1$. Armed with that fact, we can then combine (III.30) and (III.10) to remove the normal derivative terms from our NRBC. When we do so, our resulting NRBC is

$$\left(\frac{1}{c_0^2} - \frac{1}{c_j^2}\right)\partial_{tt}\varphi_{j-1} + \left(\frac{1}{c_j} + \frac{1}{c_{j+1}}\right)\partial_t\varphi_j - \varphi_{j+1} = \partial_{yy}\varphi_{j-1} - \frac{f^2}{c_0^2}\varphi_{j-1} . \tag{III.32}$$

This equation gives us a tri-diagonal system of equations to solve for our auxiliary variables. With an efficient matrix solver, the effort required is $O(J)$, rather than the $O(J^2)$ required for the original formulation, and it is $O(J)$ even without setting the c_j values to c_0. Furthermore, since the auxiliary variables are defined solely using temporal and tangential derivatives, we can restrict them to the boundary,

reducing the amount of memory needed to store their values. Finally, since the NRBC uses no derivatives beyond second order, they can be easily applied to a finite element system to any order. There are three downsides, however. NRBCs on two adjacent sides require consideration of corner compatibility conditions (due to the presence of tangential derivatives), their numeric stability is less robust over long time-integrations [37], and the conversion to remove the normal derivatives introduces an additional source of discretization error which produces an "error floor" that cannot be overcome by simply increasing J [36].

3.   Hagstrom-Warburton

The Hagstrom-Warburton NRBCs were first presented in [57] for the scalar wave equation, with subsequent extensions and analysis in [37, 53, 55]. This NRBC scheme also uses a system of low-order auxiliary variable equations instead of a single high-order boundary equation. The Hagstrom-Warburton NRBC of order J is given by

$$
\begin{aligned}
\partial_t \varphi_1 &= a_0 \partial_t u + c_0 \partial_x u \\
a_j \partial_t \varphi_{j+1} - c_0 \partial_x \varphi_{j+1} &= a_j \partial_t \varphi_j + c_0 \partial_x \varphi_j \\
\varphi_{J+1} &\equiv 0 \,,
\end{aligned}
\tag{III.33}
$$

where the parameters $a_j \in (0, 1]$ are chosen by the user. Hagstrom and Warburton show that this definition, applied to a plane wave traveling at speed c_0 and incidence angle θ, results in a reflection coefficient of

$$
R = -\frac{a_0 - \cos\theta}{a_0 + \cos\theta} \prod_{j=1}^{J} \left(\frac{a_j - \cos\theta}{a_j + \cos\theta} \right)^2 \,,
\tag{III.34}
$$

which, like the Higdon scheme's reflection coefficient, is a product of J terms, each of which is less than unity. Hence, as J increases, the reflection coefficient decreases. However, with the squaring of each term in the product, the reflection coefficient for the Hagstrom-Warburton scheme decreases significantly more rapidly than the Higdon reflection coefficient.

No physical interpretation of the NRBC formulation is given. One way to interpret (III.33b) is that the outgoing characteristic of φ_j is matched by the incoming characteristic of φ_{j+1}. However, that does not explain the form of (III.33a). It could be that the authors wanted an NRBC scheme with a quadratically-decaying reflection coefficient, and they reverse-engineered this NRBC formulation to get one that works.

As with the Givoli-Neta NRBCs, the auxiliary variables presented here also satisfy the Klein-Gordon equation (III.31) for all $j \in 1 \ldots J$. We can use that fact to remove the normal derivative term from (III.33b), replacing that equation with

$$
\left.
\begin{array}{c}
a_j \left(a_{j-1}^2 - 1\right) \partial_{tt}\varphi_{j-1} + a_{j-1}\left(a_j^2 - 1\right) \partial_{tt}\varphi_{j+1} \\
- \left(a_{j-1} + a_j\right)\left(a_{j-1}a_j + 1\right) \partial_{tt}\varphi_j
\end{array}
\right\}
=
\left\{
\begin{array}{l}
a_j \left(f^2\varphi_{j-1} - c_0^2\partial_{yy}\varphi_{j-1}\right) \\
+ \left(a_{j-1} + a_j\right)\left(f^2\varphi_j - c_0^2\partial_{yy}\varphi_j\right) \\
+ a_{j-1}\left(f^2\varphi_{j+1} - c_0^2\partial_{yy}\varphi_{j+1}\right)
\end{array}
\right. .
$$
(III.35)

(again, see [55] for details). Once again, we have a system of auxiliary variables defined solely on the boundary, and a boundary condition consisting entirely of low-order derivatives. As with the Givoli-Neta system, this system also requires $O(J)$ operations to solve.

C. NRBCS FOR FIRST-ORDER SYSTEMS

In general, the three NRBC techniques discussed in the previous section have only been implemented for scalar wave-like equations, not for first-order systems. The exception is the Hagstrom-Warburton NRBC, where one section of [57] briefly discusses the characteristic-based implementation for a symmetric first-order system of the form

$$
\partial_t\vec{\varphi} + A\partial_x\vec{\varphi} + B\partial_y\vec{\varphi} = 0 .
$$
(III.36)

However, that discussion does not consider corner conditions or the presence of un-differentiated terms on the right-hand side. In Chapter VI we develop these NRBCs in more depth.

While the Higdon and Givoli-Neta NRBC methods have been developed for the shallow-water equations (e.g., [113]), those implementations involve converting the system to a scalar Klein-Gordon equation for the surface height state variable; hence, they are not truly implemented for the first-order system. In the next two chapters, we will develop these NRBC methods for a true first-order system. While the Higdon implementation is specific to the linearized Euler equations, the Givoli-Neta implementation (not including gravitational effects (Sec. V.C)) can be extended easily to any first-order system.

IV.   HIGDON NRBCS FOR THE LINEARIZED EULER EQUATIONS

A.   OVERVIEW

This chapter develops the finite difference implementation of the high-order NRBCs for the linearized Euler equations in two dimensions. We begin with the simplest possible equation set, with no advection or forcing terms. After demonstrating the validity of this prototypical implementation in Section B, we proceed to incorporate the effects of Coriolis (Sec. C), gravity (Sec. D), and advection (Sec. E).

B.   AN INITIAL PROTOTYPE

We begin with the simplest possible implementation of the linearized 2-D Euler equations: zero advection, no Coriolis or gravitational forces.

$$
\begin{aligned}
\partial_t \rho + \rho_0 \left(\partial_x u + \partial_y v \right) &= 0 \\
\partial_t u + \frac{1}{\rho_0} \partial_x p &= 0 \\
\partial_t v + \frac{1}{\rho_0} \partial_y p &= 0 \\
\partial_t p + \gamma p_0 \left(\partial_x u + \partial_y v \right) &= 0
\end{aligned}
\tag{IV.1}
$$

The variables here are the perturbation variables from the linearization in Sec. II.C.2; we remove the asterisks here and in all subsequent equations for textual clarity. In addition, we use ρ_0 and p_0 instead of $\bar{\rho}$ and $\bar{p}$ because we have no z-dependency in these equations. This set is mostly useless for real-world modeling, especially considering the fact that ρ has no impact on any of the other state variables. However, it will serve as an initial prototype for developing this implementation (see also [19]).

1.   Equivalence of (IV.1) and the Scalar Wave Equation—Continuous Case

In [68], Higdon proved that the J-order NRBC is compatible and stable when applied to the dispersive wave equation (and thus the standard wave equation by

setting $f = 0$), based on stability criteria developed by H.-O. Kreiss [81] (with a geometric characteristic-based interpretation provided by Higdon [63]). Therefore, if we can convert these simplified Euler equations to the standard wave equation, we will know that they too will be stable with this NRBC formulation.

Differentiate (IV.1b,c,d) with respect to x, y, and t, respectively, and get (ignoring the equation for ρ)

$$
\begin{aligned}
\partial_{xt} u &= -\frac{1}{\rho_0} \partial_{xx} p \\
\partial_{yt} v &= -\frac{1}{\rho_0} \partial_{yy} p \\
\partial_{tt} p &= -\gamma p_0 \left(\partial_{xt} u + \partial_{yt} v \right)
\end{aligned}
\tag{IV.2}
$$

Substituting the first and second of these new equations into the third gives

$$
\partial_{tt} p = \frac{\gamma p_0}{\rho_0} \left(\partial_{xx} p + \partial_{yy} p \right),
\tag{IV.3}
$$

which is the standard wave equation for p, with the wave speed given by

$$
c_0 = \sqrt{\frac{\gamma p_0}{\rho_0}},
\tag{IV.4}
$$

reflecting the value given in the literature [24, 76, 107, 108]. Therefore, this system of equations, combined with the Higdon-like NRBCs, will be stable. It may seem a bit shaky to make this claim, since we have only proven that the system can be converted to the wave equation for p, not for the other variables. Might they still be unstable in u and v? The answer is no. Since p depends on u and v, if they are unstable, then they will destabilize p. Since p is stable, it follows that u and v must also be stable. (The stability of ρ is somewhat irrelevant, as it has no impact on the other state variables.)

In Sec. VI.1, we will show that all four state variables satisfy the scalar wave equation, and we will derive its exact form. For now, it is sufficient to note that we can convert this equation set to the scalar wave equation in p.

2. Equivalence of (IV.1) and the Scalar Wave Equation— Discrete Case

Using stability criteria developed by Gustafsson et.al. [52], Higdon showed [68] that the discretization scheme in Sec. III.B.1.c is compatible with the standard second-order discretization scheme for the standard wave equation (solving for $u_{i,j}^{n+1}$):

$$\frac{u_{i,j}^{n+1} - 2u_{i,j}^n + u_{i,j}^{n-1}}{(\delta t)^2} = c_0^2 \left(\frac{u_{i+1,j}^n - 2u_{i,j}^n + u_{i-1,j}^n}{(\delta x)^2} + \frac{u_{i,j+1}^n - 2u_{i,j}^n + u_{i,j-1}^n}{(\delta y)^2} \right) \quad (\text{IV.5})$$

However, this scheme is for solving a single second-order PDE, not a system of first-order PDEs, as we have. Even though we have shown that this system is equivalent, in one of the state variables, to the standard wave equation, creating a discretization scheme which is also consistent and stable is a matter of some delicacy.

Givoli and Neta described a similar difficulty they encountered in developing a stable discretization scheme for the shallow water equations [39]. After numerous failed efforts, whose results were unstable for any $J \geq 2$, they defined a scheme which was equivalent to the dispersive wave equation discretization scheme proved stable by Higdon in [68]. We use a similar approach here. Let Δ_t denote a second-order centered difference in time, with similar notation for difference approximations in x and y; thus,

$$\begin{aligned}
\Delta_a &= \frac{S_a^+ - S_a^-}{2\delta a} \\
a &\in \{x, y, t\},
\end{aligned} \quad (\text{IV.6})$$

where δa is the step size in a. Use the following discretization for (IV.1):

$$\begin{aligned}
\Delta_t \rho &= -\rho_0 \left(\Delta_x u + \Delta_y v \right) \\
\Delta_t u &= \frac{\Delta_x p}{\rho_0} \\
\Delta_t v &= \frac{\Delta_y p}{\rho_0} \\
\Delta_t p &= -\gamma p_0 \left(\Delta_x u + \Delta_y v \right) \quad (\text{IV.7})
\end{aligned}$$

As with converting (IV.1) to (III.8), apply Δ_x to (IV.7b), Δ_y to (IV.7c), Δ_t to (IV.7d), and then make the appropriate substitution. This gives us

$$\Delta_t \Delta_t p = \frac{\gamma p_0}{\rho_0} \left(\Delta_x \Delta_x p + \Delta_y \Delta_y p \right) . \tag{IV.8}$$

If we expand these differences, we get

$$\frac{p_{i,j}^{n+2} - 2p_{i,j}^{n} + p_{i,j}^{n-2}}{(2\delta t)^2} = \frac{\gamma p_0}{\rho_0} \left(\frac{p_{i+2,j}^{n} - 2p_{i,j}^{n} + p_{i-2,j}^{n}}{(2\delta x)^2} + \frac{p_{i,j+2}^{n} - 2p_{i,j}^{n} + p_{i,j-2}^{n}}{(2\delta y)^2} \right) , \tag{IV.9}$$

which is the scalar wave equation *on a double-sized grid*. Hence, to make our discretization scheme fully compatible, we use the following discretization for the NRBC on each side of the domain:

$$\left(\frac{I - S_t^{-2}}{2\delta t} + c_0 \frac{I - S_x^{-2}}{2\delta x} \right)^J \sigma_{i,j}^{n} = 0 \tag{IV.10}$$

where σ denotes any one of our state variables ρ, u, v, p.

A reviewer for [21] noted that this NRBC cannot resolve the shortest wavelengths resolvable by the interior scheme. Subsequent experiments showed no new instabilities generated by these short wavelengths.

In [19], the authors showed that a certain choice of one-sided differencing can also yield a compatible scheme, one which is compatible with the scalar wave equation on the same size grid. However, subsequent experimentation revealed deeper flaws in that approach. First, it could not be extended to match the Klein-Gordon equation when Coriolis forces are included. Second, its semi-implicit nature became fully implicit under advection. (An attempt to avoid an implicit scheme, based on a quadrant-based interior discretization method, proved to be unstable under advection.) The scheme devised here avoids these flaws, as subsequent sections will show.

3.   Numerical Example—Semi-Infinite Channel

Consider a simple numerical example. Define a square domain 10 km on each side, with walls on three sides and open on the top (see Fig. 6). We truncate the

domain Ω with an artificial north boundary Γ and impose the non-reflecting boundary condition on the state variables. We define the hard wall as

$$
\begin{aligned}
\partial_{\vec{n}} \rho &= 0 \\
\vec{u} \cdot \vec{n} &= 0 \\
\partial_{\vec{n}} p &= 0
\end{aligned}
\tag{IV.11}
$$

The open boundary is defined by a Higdon-type NRBC of order J. Using a sea-level
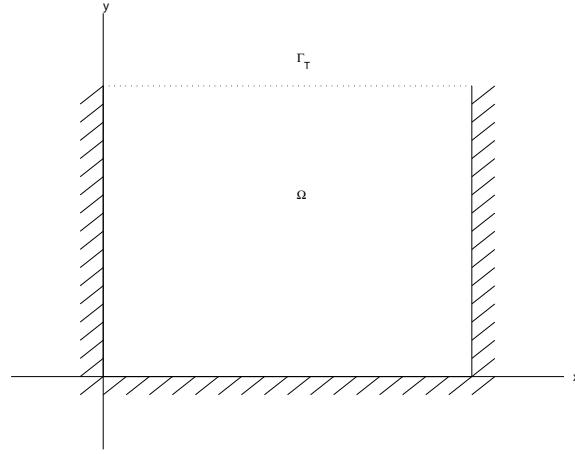
Figure 6. A semi-infinite channel domain Ω truncated by an artifical boundary Γ_T [After [40], Fig. 1b, p. 259]

atmospheric density $\rho_0 = 1.2 \frac{\text{kg}}{\text{m}^3}$ and pressure $p_0 = 1.01 \times 10^5 \frac{\text{N}}{\text{m}^2}$ [58], our initial condition is a pressure bubble in the center of the domain:

$$
p_{x,z}^0 = \begin{cases} p_0 \left(1 + \frac{\cos\left(\frac{\pi}{2}\frac{d}{r}\right)}{100}\right) &: \quad d \leq r \\ \\ p_0 &: \quad \text{otherwise} \end{cases}
$$

$$
\tag{IV.12}
$$

$$
\rho_{x,z}^0 = \begin{cases} \rho_0 \left(\frac{p_{x,y}^0}{\bar{p}_z}\right)^{\frac{c_v}{c_p}} &: \quad d \leq r \\ \\ \rho_0 &: \quad \text{otherwise,} \end{cases}
$$

41

where

$$c_v = 717.5 \ \frac{\text{J}}{\text{kg} \cdot \text{K}}$$

$$c_p = 1004.67 \ \frac{\text{J}}{\text{kg} \cdot \text{K}}$$

$$d = \sqrt{(x - x_c)^2 + (y - y_c)^2} \ \text{m}$$

$$r = 1 \ \text{km} ,$$

and (x_c, y_c) denotes the center of the domain. The initial perturbation of ρ is defined to maintain a constant potential temperature in the pressure perturbation bubble [24]. We divide the domain into a 100×100 grid and run the simulation up to $t = 24$ s, which is sufficient time for the wave trough to reach the corners. We also run a reference solution on a 10×20 km domain consisting of 100×200 grid points; this reference solution has hard walls on all four sides, and the simulation duration is short enough that reflections from the top boundary will not re-enter the original domain. By using a computed reference solution rather than an analytic solution, we can attribute all differences to the NRBC error rather than the discretization scheme's truncation error. Our time step is chosen as 90% of the CFL limit [64],

$$\left(c_0 \frac{\delta t}{\delta x} \right)^2 + \left(c_0 \frac{\delta t}{\delta y} \right)^2 \leq 1 , \tag{IV.13}$$

where c_0 is the wave speed $\sqrt{\gamma p_0 / \rho_0}$. (We have observed experimentally [21] that setting δt to the maximum allowed by the CFL limit results in reduced effectiveness for the higher J NRBCs.) We use this same c_0 for the NRBC wave speed. Define the error norm, for each state variable φ, to be

$$E_\varphi = \frac{\sqrt{\sum_{i=1}^{N_x} \sum_{j=1}^{N_y} \left(\varphi_J(i,j) - \varphi_0(i,j) \right)^2}}{\sqrt{\sum_{i=1}^{N_x} \sum_{j=1}^{N_y} \varphi_0(i,j)^2}} , \tag{IV.14}$$

where φ_J is the state variable computed using the order J NRBC; φ_0 is the reference solution state variable; N_x and N_y are the number of points in the x and y directions, respectively; and we normalize the error norm by the norm of the reference state

variable (so that all four state variables' error norms are approximately the same order of magnitude). Using the perturbation variables defined in (IV.1), the interior discretization scheme (IV.7), and the Higdon NRBC discretization (IV.10a), we run the simulation using different values of J for the NRBC order. Figs. 7–10 show the perturbation variables ρ, u, v, and p, respectively, for the $J = 10$ case. Fig. 11 contrasts the computed solutions and error deltas for v between the $J = 1$ and $J = 10$ cases. Table I shows the error norms for each state variable for $J \in 1 \ldots 10$.
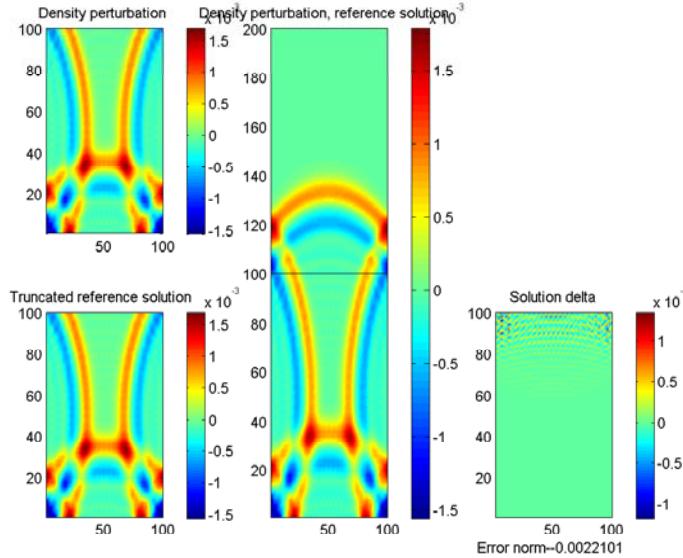
Figure 7. Plot of ρ in basic system (IV.1) with $J = 10$ in a semi-infinite channel. (TL) Computed solution. (Center) Reference solution; the area corresponding to the computed solution is contained below the horizontal line. (BL) Reference solution truncated to computed solution domain. (BR) Delta between reference solution and computed solution, with error norm computed by (IV.14).
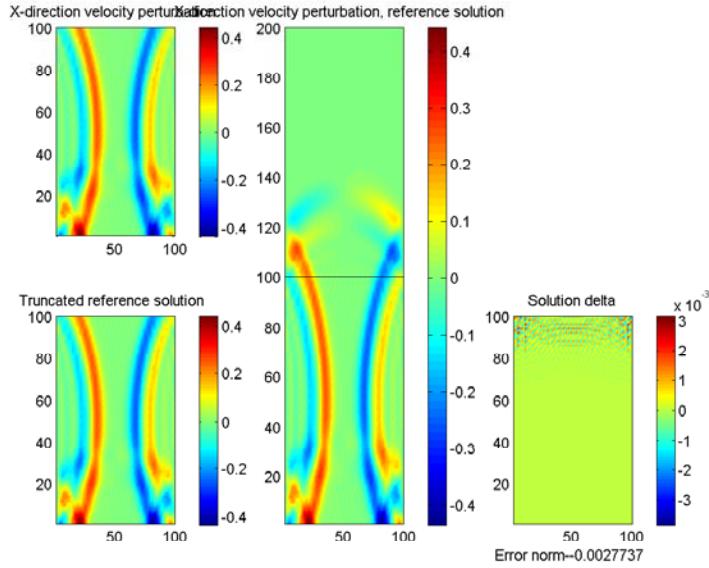
Figure 8. Plot of u in basic system (IV.1) with $J = 10$ in a semi-infinite channel. (TL) Computed solution. (Center) Reference solution; the area corresponding to the computed solution is contained below the horizontal line. (BL) Reference solution truncated to computed solution domain. (BR) Delta between reference solution and computed solution, with error norm computed by (IV.14).

J	E_ρ	E_u	E_v	E_p
1	0.12361	0.077449	0.1674	0.12361
2	0.039728	0.020397	0.047278	0.039727
3	0.026079	0.010879	0.022051	0.026078
4	0.022763	0.0077222	0.014192	0.022763
5	0.021505	0.0060029	0.010178	0.021505
6	0.020889	0.0049066	0.0078822	0.020889
7	0.020551	0.0041032	0.0063328	0.020551
8	0.020362	0.0035019	0.0052668	0.020361
9	0.020249	0.0030695	0.0044665	0.020249
10	0.020176	0.0027737	0.0038836	0.020176

Table I. Error norms for basic system (IV.1) with $J \in 1 \ldots 10$ in a semi-infinite channel
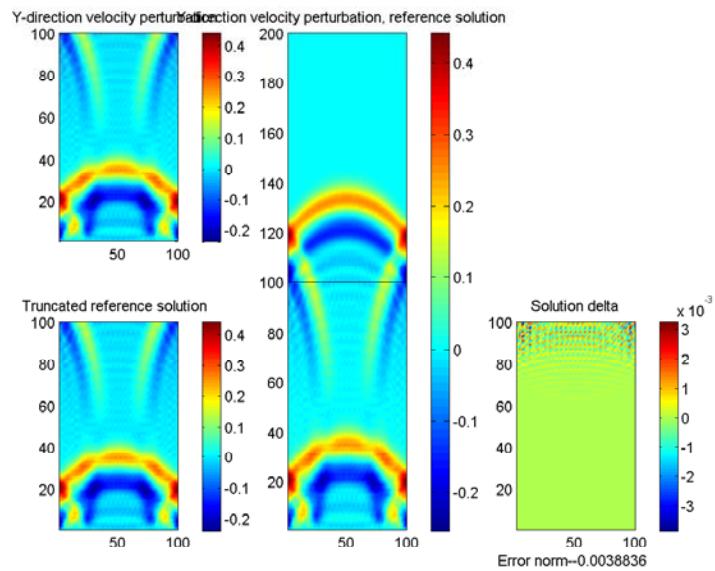
Figure 9. Plot of v in basic system (IV.1) with $J = 10$ in a semi-infinite channel. (TL) Computed solution. (Center) Reference solution; the area corresponding to the computed solution is contained below the horizontal line. (BL) Reference solution truncated to computed solution domain. (BR) Delta between reference solution and computed solution, with error norm computed by (IV.14).
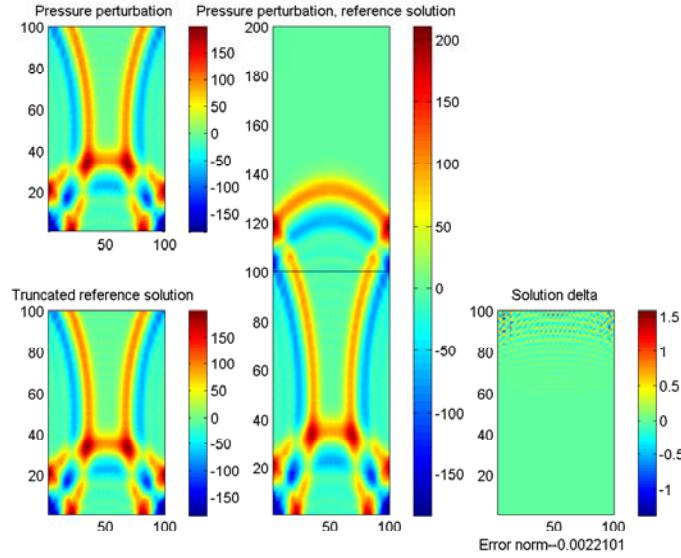
Figure 10. Plot of p in basic system (IV.1) with $J = 10$ in a semi-infinite channel. (TL) Computed solution. (Center) Reference solution; the area corresponding to the computed solution is contained below the horizontal line. (BL) Reference solution truncated to computed solution domain. (BR) Delta between reference solution and computed solution, with error norm computed by (IV.14).
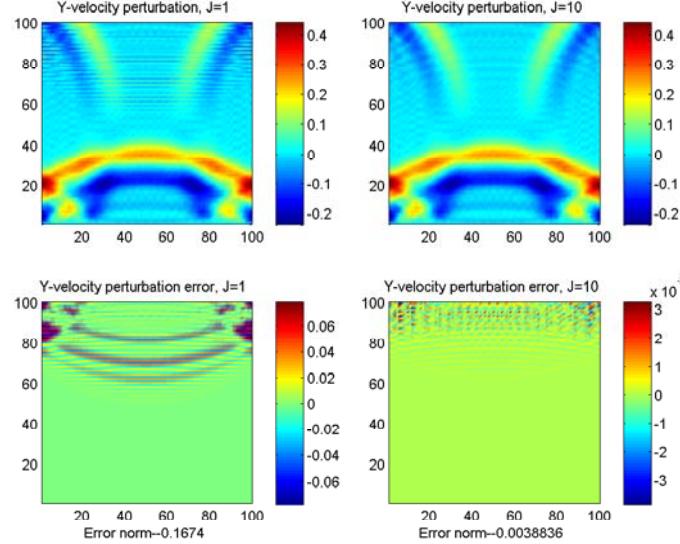
Figure 11. Comparison of v in basic system (IV.1) computed with $J = 1$ and $J = 10$ in a semi-infinite channel, with error norms computed by (IV.14). (TL) Computed solution for $J = 1$. (TR) Computed solution for $J = 10$. (BL) Delta between reference solution and $J = 1$ computed solution. (BR) Delta between reference solution and $J = 10$ computed solution.

46

4. Numerical Example—Open Domain

We now perform the same simulation in an open domain (see Fig. 12), using NRBCs on all four sides for the state variables. Before proceeding, we note that we
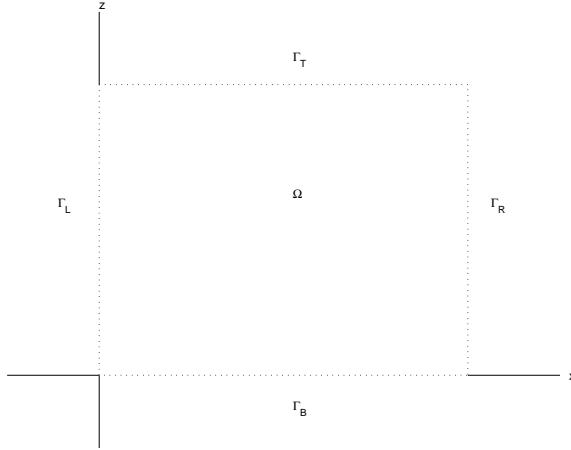
Figure 12. An open domain Ω truncated by artificial boundaries Γ_L, Γ_T, Γ_R and Γ_B [After [19], Fig. 1, p. 1]

now have points which are on the corners of two open boundaries, and we pause to address this potential complication. Looking at (IV.10), we see that for each point on an open boundary, that point only depends on itself at previous times and on the adjacent interior points. The boundary points are independent of each other. Furthermore, due to the discretization (IV.7) of the interior scheme, there are no interior points which depend on the corner points. Fig. 13 illustrates this dependency for the top-right corner of an open domain. Notice that no other point depends on the corner. Hence, our boundary condition at the corner is, by and large, irrelevant. For our implementation here, we decree that the corners are considered part of the top/bottom boundaries. Our reference solution is a 30×30 km domain with 300×300 grid points, situated so that the center of the reference domain corresponds to the computational domain. When we run this simulation, we get results such as those in Figs. 14, 15, and Table II. (From here on, we will only plot the results for one state

47
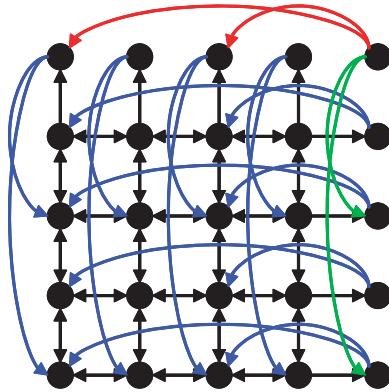
Figure 13. Interior and boundary discretization dependencies for points near the top-right corner of an open domain. The black arrows show the interior dependecies based on the discretization scheme (IV.7). Blue arrows show the dependencies of the boundary points except for the corner. Green arrows show the dependency if the corner is considered part of the top; red arrows show the dependency if the corner is considered part of the right.

variable, rather than all four.) Not surprisingly, given the symmetry of the domain and the discretization scheme, the errors for u and v are the same.

J	E_ρ	E_u	E_v	E_p
1	1.5544	2.0918	2.0918	1.5558
2	0.4589	0.61777	0.61777	0.45933
3	0.22861	0.30055	0.30055	0.22882
4	0.15198	0.19766	0.19766	0.15212
5	0.11326	0.14588	0.14588	0.11336
6	0.089796	0.11564	0.11564	0.08988
7	0.074067	0.095798	0.095798	0.074136
8	0.06246	0.082285	0.082285	0.062519
9	0.053427	0.071617	0.071617	0.053476
10	0.046644	0.062478	0.062476	0.046687

Table II. Error norms for basic system (IV.1) with $J \in 1 \ldots 10$ in an open domain
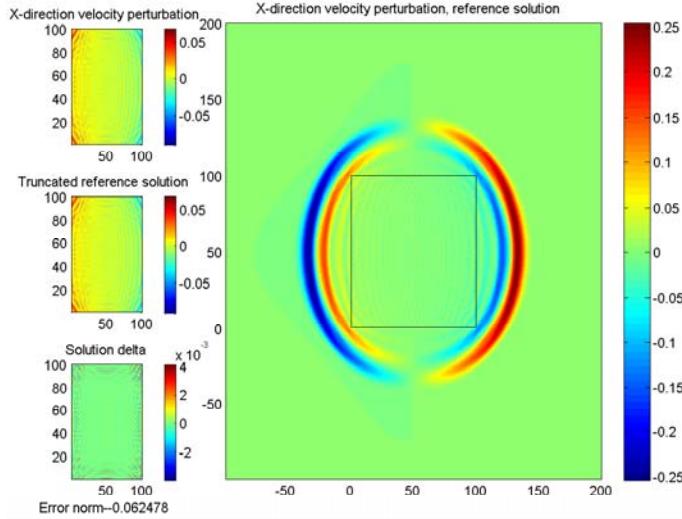
Figure 14. Plot of u in basic system (IV.1) with $J = 10$ in an open domain. (TL) Computed solution. (Right) Reference solution; the area corresponding to the computed solution is contained within the center box. (CL) Reference solution truncated to computed solution domain. (BL) Delta between reference solution and computed solution, with error norm computed by (IV.14).
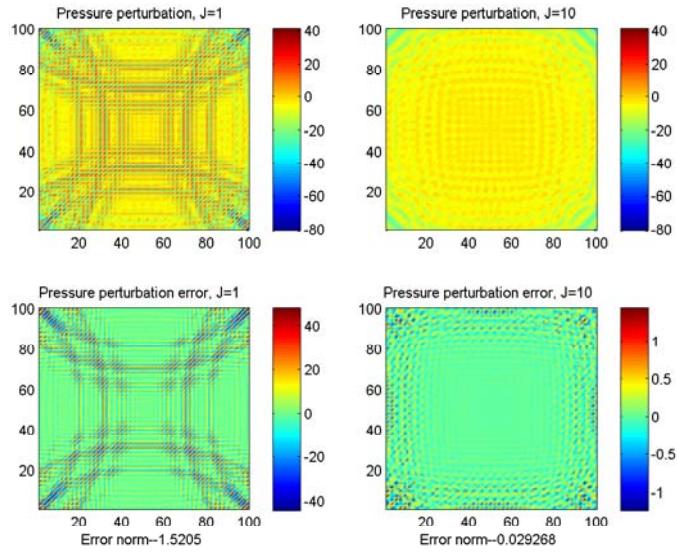
Figure 15. Comparison of p in basic system (IV.1) computed with $J = 1$ and $J = 10$ in an open domain, with error norms computed by (IV.14). (TL) Computed solution for $J = 1$. (TR) Computed solution for $J = 10$. (BL) Delta between reference solution and $J = 1$ computed solution. (BR) Delta between reference solution and $J = 10$ computed solution.

49

C. CORIOLIS FORCES IN THE XY PLANE

Let us now add Coriolis forces to our equation set [21]. Leaving the advection terms zero, our equation set is

$$
\begin{aligned}
\partial_t \rho + \rho_0 \left(\partial_x u + \partial_y v \right) &= 0 \\
\partial_t u + \frac{1}{\rho_0} \partial_x p &= fv \\
\partial_t v + \frac{1}{\rho_0} \partial_y p &= -fu \\
\partial_t p + \gamma p_0 \left(\partial_x u + \partial_y v \right) &= 0
\end{aligned}
\tag{IV.15}
$$

This set is somewhat more useful for atmospheric modeling, although we still have ρ decoupled from the rest of the system. As with the preceding section, we now wish to show that (IV.15) is equivalent to the Klein-Gordon equation $\partial_{tt} p = c_0^2 \nabla^2 p - f^2 p$, which, as noted previously, Higdon proved is stable with this NRBC formulation [68].

1. Equivalence of (IV.15) and the Klein-Gordon Equation— Continuous Case

This conversion begins the same as in the previous section. Differentiate (IV.15d) with respect to t

$$
\partial_{tt} p + \gamma p_0 (\partial_{xt} u + \partial_{yt} v) = 0
\tag{IV.16}
$$

Now differentiate (IV.15b) with respect to x and (IV.15c) with respect to y and add

$$
\partial_{xt} u + \partial_{yt} v + \frac{1}{\rho_0} \left(\partial_{xx} p + \partial_{yy} p \right) = f \left(\partial_x v - \partial_y u \right)
\tag{IV.17}
$$

Now substitute (IV.17) into (IV.16)

$$
\partial_{tt} p - \frac{\gamma p_0}{\rho_0} \nabla^2 p + f \gamma p_0 \left(\partial_x v - \partial_y u \right) = 0 \ .
\tag{IV.18}
$$

Differentiate (IV.15b) with respect to y and (IV.15c) with respect to x and subtract

$$
\partial_{yt} u - \partial_{xt} v + \frac{1}{\rho_0} \left(\underbrace{\partial_{yx} p - \partial_{xy} p}_{=0} \right) = f \left(\partial_y v + \partial_x u \right) \ .
\tag{IV.19}
$$

Combine terms to get

$$f \left(\partial_x u + \partial_y v \right) = -\partial_t \left(\partial_x v - \partial_y u \right) . \tag{IV.20}$$

Combine (IV.15d) and (IV.20) to get

$$f \partial_t p = \gamma p_0 \partial_t \left(\partial_x v - \partial_y u \right) . \tag{IV.21}$$

Integrate (IV.21) with respect to time to get

$$f \left(p - p_0 \right) = \gamma p_0 \left(\partial_x v - \partial_y u \right) . \tag{IV.22}$$

Finally, substitute (IV.22) into (IV.18)

$$\partial_{tt} p - \frac{\gamma p_0}{\rho_0} \nabla^2 p + f^2 (p - p_0) = 0 , \tag{IV.23}$$

which gives us the Klein-Gordon equation for the pressure perturbation $p - p_0$, again with wave speed $\sqrt{\gamma p_0 / \rho_0}$. As an aside, we notice that (IV.20) involves the time derivative of the curl of $\vec{u}$ on the right-hand side. Thus, if $f = 0$, then $\nabla \times \vec{u}$ is constant.

2.   Equivalence of (IV.15) and the Klein-Gordon Equation— Discrete Case

We would like to find a discretization scheme which is equivalent to the discrete Klein-Gordon equation

$$\frac{u_{i,j}^{n+1} - 2u_{i,j}^n + u_{i,j}^{n-1}}{\delta t^2} = c_0^2 \left(\frac{u_{i+1,j}^n - 2u_{i,j}^n + u_{i-1,j}^n}{\delta_x^2} + \frac{u_{i,j+1}^n - 2u_{i,j}^n + u_{i,j-1}^n}{\delta_y^2} \right) - f^2 u_{i,j}^n \tag{IV.24}$$

Given the similarity to the discrete scalar wave equation, we begin by using the discretization scheme in Sec. B.2, adding the Coriolis terms to the right-hand side to get

$$
\begin{aligned}
\Delta_t \rho &= -\rho_0 \left(\Delta_x u + \Delta_y v \right) \\
\Delta_t u &= -\frac{\Delta_x p}{\rho_0} + fv \\
\Delta_t v &= -\frac{\Delta_y p}{\rho_0} - fu \\
\Delta_t p &= -\gamma p_0 \left(\Delta_x u + \Delta_y v \right)
\end{aligned}
\tag{IV.25}
$$

Apply Δ_x to (IV.25b), Δ_y to (IV.25c), Δ_t to (IV.25d), and then make the appropriate substitution. This gives us

$$\Delta_t\Delta_t p = \frac{\gamma p_0}{\rho_0}\left(\Delta_x\Delta_x p + \Delta_y\Delta_y p\right) - f\gamma p_0\left(\Delta_x v - \Delta_y u\right), \qquad\text{(IV.26)}$$

Next, apply Δ_y to (IV.25b) and Δ_x to (IV.25c), then subtract and combine terms to get

$$\Delta_t\left(\Delta_y u - \Delta_x v\right) = f\left(\Delta_x u + \Delta_y v\right) \qquad\text{(IV.27)}$$

We substitute (IV.25d) into (IV.27) to get

$$\Delta_t\left(\Delta_y u - \Delta_x v\right) = -\frac{f}{\gamma p_0}\Delta_t p \qquad\text{(IV.28)}$$

If we apply Δ_t to (IV.26) and incorporate (IV.28) into it, we get

$$\Delta_t\left[\Delta_t\Delta_t p - \frac{\gamma p_0}{\rho_0}\left(\Delta_x\Delta_x p + \Delta_y\Delta_y p\right) + f^2 p\right] = 0 \qquad\text{(IV.29)}$$

Thus, the quantity inside the brackets is constant in time. Since we are assuming a closed system with no source functions (other than the Coriolis force itself), then this quantity must initially be zero and will thus always be zero. Expanding the differencing terms gives us

$$\frac{p_{i,j}^{n+2} - 2p_{i,j}^n + p_{i,j}^{n-2}}{(2\delta t)^2} = \frac{\gamma p_0}{\rho_0}\left(\frac{p_{i+2,j}^n - 2p_{i,j}^n + p_{i-2,j}^n}{(2\delta x)^2} + \frac{p_{i,j+2}^n - 2p_{i,j}^n + p_{i,j-2}^n}{(2\delta y)^2}\right) - f^2 p_{i,j}^n$$
$$\text{(IV.30)}$$

As with equating the initial basic case to the scalar wave equation, we now have a system which is compatible with the Klein-Gordon equation on a double-size grid. So again, our NRBC will be given by (IV.10).

3.   Numerical Examples

For this example, we use the same domain and initial conditions as with the basic system in Sec. B. Our Coriolis force f is based on an angular momemtum $\Omega = 7.292116 \times 10^{-5}$ s^{-1} [112] at a latitude ϕ of $30°$ N, thus,

$$f = 2\Omega\sin\phi = 7.292116 \times 10^{-5}\text{ s}^{-1}$$

J	E_ρ	E_u	E_v	E_p
1	0.12361	0.077448	0.1674	0.12361
2	0.039728	0.020397	0.047278	0.039727
3	0.026079	0.010879	0.022051	0.026078
4	0.022763	0.0077222	0.014192	0.022763
5	0.021505	0.0060029	0.010178	0.021505
6	0.020889	0.0049066	0.0078821	0.020889
7	0.020551	0.0041032	0.0063328	0.020551
8	0.020362	0.0035019	0.0052668	0.020361
9	0.020249	0.0030695	0.0044665	0.020249
10	0.020176	0.0027737	0.0038836	0.020176

Table III. Error norms for Coriolis-influenced system (IV.15) with $J \in 1 \ldots 10$ in a semi-infinite channel

When we apply this force to our domains, we get results which are virtually indistinguishable from those in the preceding section. This is not too surprising, since the Coriolis force is so small that its effects are unnoticeable over such short timeframes [28]. Tables III and IV show the error norms for all four state variables for $J \in 1 \ldots 10$ in the channel and open domain, respectively. Suppose, just for curiosity's sake, we make the Earth rotate much more rapidly and increase f by a factor of a thousand,

J	E_ρ	E_u	E_v	E_p
1	1.5544	2.0917	2.0917	1.5558
2	0.4589	0.61777	0.61777	0.45933
3	0.22861	0.30055	0.30054	0.22882
4	0.15198	0.19766	0.19766	0.15212
5	0.11326	0.14588	0.14588	0.11336
6	0.089797	0.11564	0.11564	0.08988
7	0.074067	0.095798	0.095797	0.074136
8	0.062461	0.082285	0.082284	0.062519
9	0.053427	0.071617	0.071617	0.053476
10	0.046645	0.062478	0.062476	0.046689

Table IV. Error norms for Coriolis-influenced system (IV.15) with $J \in 1 \ldots 10$ in an open domain

J	E_ρ	E_u	E_v	E_p
1	1.4093	0.70281	0.70253	1.4033
2	0.4086	0.20314	0.20309	0.40687
3	0.20321	0.098226	0.098178	0.20235
4	0.13492	0.064387	0.064365	0.13435
5	0.10056	0.047464	0.047443	0.10013
6	0.079742	0.037609	0.037594	0.079405
7	0.065817	0.031154	0.031144	0.065539
8	0.055543	0.026777	0.026767	0.055308
9	0.047521	0.023331	0.023321	0.04732
10	0.041445	0.020369	0.020361	0.04127

Table V. Error norms with $J \in 1 \ldots 10$ in an open domain under artifically-large Coriolis (IV.15)

to $f = 0.07292116$ s^{-1}, just to make its effects noticeable. If we do that, we get the error norms given in Table V for the open domain. A comparison of the results for small and large J is exemplified in Figs. 16 and 17. If we look at the u and v plots side-by-side (Fig. 18), we can discern the clockwise rotation generated by the Coriolis force.
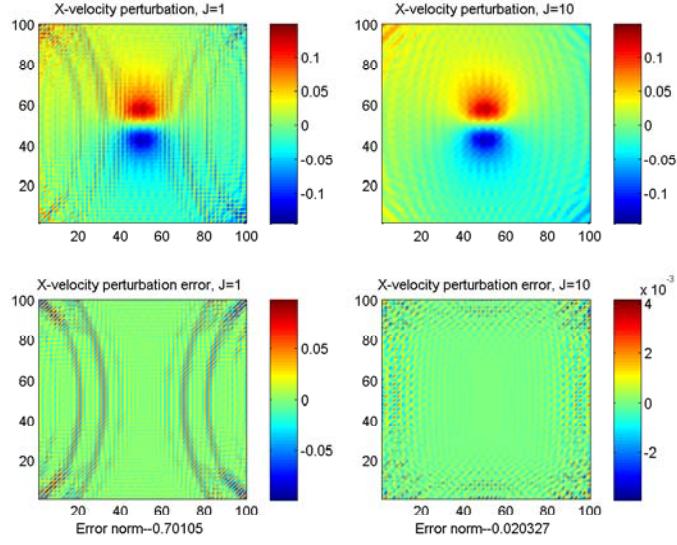
Figure 16. Comparison of u in Coriolis-influenced system (IV.15), using artificially-large Coriolis, computed with $J = 1$ and $J = 10$ in an open domain, with error norms computed by (IV.14). (TL) Computed solution for $J = 1$. (TR) Computed solution for $J = 10$. (BL) Delta between reference solution and $J = 1$ computed solution. (BR) Delta between reference solution and $J = 10$ computed solution.
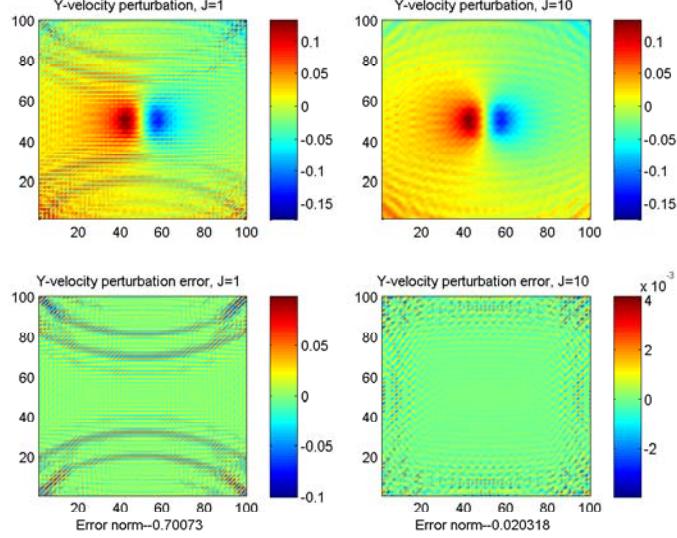
Figure 17. Comparison of v in Coriolis-influenced system (IV.15), using artificially-large Coriolis, computed with $J = 1$ and $J = 10$ in an open domain, with error norms computed by (IV.14). (TL) Computed solution for $J = 1$. (TR) Computed solution for $J = 10$. (BL) Delta between reference solution and $J = 1$ computed solution. (BR) Delta between reference solution and $J = 10$ computed solution.
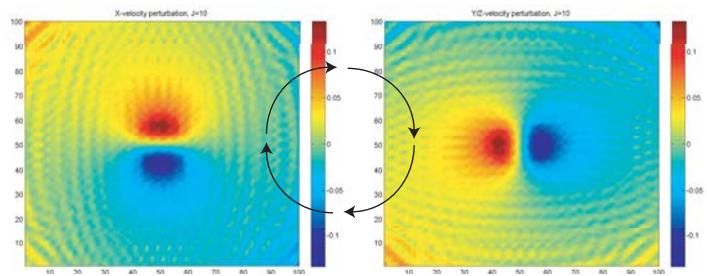
Figure 18. Side-by-side plot of u and v, illustrating the rotation generated by the Coriolis acceleration. The superimposed clockwise arrows highlight the combined result of the u and v values.

D. GRAVITATIONAL FORCES IN THE XZ PLANE

Now we shift from the xy plane to the xz plane and consider what happens when we add the effects of gravity to our system. Still keeping the advection terms equal to zero, we now have the equation set

$$
\begin{aligned}
\partial_t \rho + \bar{\rho}\left(\partial_x u + \partial_z w\right) &= -\bar{\rho}' w \\
\partial_t u + \frac{1}{\rho}\partial_x p &= 0 \\
\partial_t w + \frac{1}{\rho}\partial_z p &= -\frac{g}{\rho}\rho \\
\partial_t p + \gamma \bar{p}\left(\partial_x u + \partial_z w\right) &= g\bar{\rho}w
\end{aligned}
\tag{IV.31}
$$

where we now must use $\bar{\rho}$ and $\bar{p}$ for our z-dependent reference states. We use $\bar{\rho}'$ to denote the derivative of $\bar{\rho}$, which depends only on z. Note that ρ finally makes an impact on the other state variables.

1. Defining the Reference State for Density and Pressure

Eq. (II.59) sets a compatibility condition between our reference states for density and pressure. This restriction is a fairly loose one, however, requiring us to look to other sources for possible functions which satisfy this condition. Since these equations are derived from the ideal gas law, we look to the literature for atmospheric models on which we can base these initial conditions.

Although several atmospheric models exist [24, 112], for ease of differentiation we will use an exponentially-decaying model

$$
\bar{p} = p_0 e^{-\alpha z} \;,
\tag{IV.32}
$$

where α is a scaling height needed to match the surface $(z = 0)$ pressure and density values. Applying (II.59) to this model, we get

$$
\bar{\rho} = \frac{p_0 \alpha}{g}e^{-\alpha z} \;.
\tag{IV.33}
$$

2. Deriving a Wave-Like Equation from (IV.31)

As with the basic system and the system subject to Coriolis forces, we now attempt to convert the gravity-affected system to a wave-like equation. First, we differentiate (IV.31d) with respect to time to get

$$\partial_{tt}p = g\bar{\rho}\partial_t w - \gamma\bar{p}\left(\partial_{xt}u + \partial_{zt}w\right) \tag{IV.34}$$

Differentiating (IV.31b) with respect to x and (IV.31c) with respect to z (remembering that $\bar{\rho}$ depends on z) gives us

$$\partial_{xt}u = -\frac{1}{\bar{\rho}}\partial_{xx}p \tag{IV.35}$$

$$\partial_{zt}w = -g\left(\frac{\bar{\rho}\partial_z\rho - \bar{\rho}'\rho}{\bar{\rho}^2}\right) - \frac{\bar{\rho}\partial_{zz}p - \bar{\rho}'\partial_z p}{\bar{\rho}^2} \tag{IV.36}$$

Substituting these results into (IV.34) gives us

$$\begin{aligned}
\partial_{tt}p &= g\bar{\rho}\partial_t w + \frac{\gamma\bar{p}}{\bar{\rho}}\left(\partial_{xx}p + g\partial_z\rho - \frac{g\bar{\rho}'}{\bar{\rho}}\rho + \partial_{zz}p - \frac{\bar{\rho}'}{\bar{\rho}}\partial_z p\right) \\
&= \frac{\gamma\bar{p}}{\bar{\rho}}\nabla^2 p + g\bar{\rho}\partial_t w + \frac{\gamma\bar{p}}{\bar{\rho}}\left(g\partial_z\rho - \frac{g\bar{\rho}'}{\bar{\rho}}\rho - \frac{\bar{\rho}'}{\bar{\rho}}\partial_z p\right)
\end{aligned} \tag{IV.37}$$

Using (IV.31c) to remove the $\bar{\rho}\partial_t w$ term from (IV.37) gives us

$$\begin{aligned}
\partial_{tt}p &= \frac{\gamma\bar{p}}{\bar{\rho}}\nabla^2 p - g^2\rho - g\partial_z p + \frac{\gamma\bar{p}}{\bar{\rho}}\left(g\partial_z\rho - \frac{g\bar{\rho}'}{\bar{\rho}}\rho - \frac{\bar{\rho}'}{\bar{\rho}}\partial_z p\right) \\
&= \frac{\gamma\bar{p}}{\bar{\rho}}\nabla^2 p - g\left(g + \frac{\gamma\bar{p}\bar{\rho}'}{\bar{\rho}^2}\right)\rho + g\frac{\gamma\bar{p}}{\bar{\rho}}\partial_z\rho - \left(g + \frac{\gamma\bar{p}\bar{\rho}'}{\bar{\rho}^2}\right)\partial_z p
\end{aligned} \tag{IV.38}$$

If we solve (IV.31a) and (IV.31d) for $\partial_x u + \partial_z w$, we get

$$\frac{g\bar{\rho}w - \partial_t p}{\gamma\bar{p}} = \frac{-\bar{\rho}'w - \partial_t\rho}{\bar{\rho}} \ , \tag{IV.39}$$

which we can solve for w and differentiate with respect to time to get

$$\partial_t w = \frac{\bar{\rho}\partial_{tt}p - \gamma\bar{p}\partial_{tt}\rho}{g\bar{\rho}^2 + \gamma\bar{p}\bar{\rho}'} \ , \ g \neq 0 \tag{IV.40}$$

Equating this with $\partial_t w$ in (IV.31c) and solving for ρ gives

$$\rho = \frac{\bar{\rho}}{g}\left(\frac{\bar{\rho}\partial_{tt}p - \gamma\bar{p}\partial_{tt}\rho}{g\bar{\rho}^2 + \gamma\bar{p}\bar{\rho}'} - \frac{1}{\bar{\rho}}\partial_z p\right) \tag{IV.41}$$

Substituting this result into (IV.38) gives us

$$
\begin{aligned}
\partial_{tt}p &= \begin{cases} \frac{\gamma\bar{p}}{\bar{\rho}}\nabla^2 p - \bar{\rho}\left(g + \frac{\gamma\bar{p}\bar{\rho}'}{\bar{\rho}^2}\right)\left(\frac{\bar{\rho}\partial_{tt}p - \gamma\bar{p}\partial_{tt}\rho}{g\bar{\rho}^2 + \gamma\bar{p}\bar{\rho}'} - \frac{1}{\bar{\rho}}\partial_z p\right) \\ +g\frac{\gamma\bar{p}}{\bar{\rho}}\partial_z\rho - \left(g + \frac{\gamma\bar{p}\bar{\rho}'}{\bar{\rho}^2}\right)\partial_z p \end{cases} \\
&= \frac{\gamma\bar{p}}{\bar{\rho}}\nabla^2 p - \frac{g\gamma\bar{p}\bar{\rho}\partial_{tt}\rho - g\bar{\rho}^2\partial_{tt}p}{g\bar{\rho}^2 + \gamma\bar{p}\bar{\rho}'} - \frac{\gamma\bar{p}\bar{\rho}'}{\bar{\rho}}\frac{\gamma\bar{p}\partial_{tt}\rho - \bar{\rho}\partial_{tt}p}{\gamma\bar{\rho}^2 + \gamma\bar{p}\bar{\rho}'} + g\frac{\gamma\bar{p}}{\bar{\rho}}\partial_z\rho \quad\text{(IV.42)}
\end{aligned}
$$

after combining and cancelling terms. Now let us use an exponential atmospheric model. Combining (IV.32) and (II.59) gives us

$$
\bar{\rho} = \frac{\bar{p}\alpha}{g}
$$

$$
\bar{\rho}' = -\frac{\bar{p}\alpha^2}{g}
$$

Substituting these values into (IV.42) gives us

$$
\begin{aligned}
\partial_{tt}p &= \frac{\gamma\bar{p}}{\bar{\rho}}\nabla^2 p - \frac{g\gamma\frac{\alpha}{g}\partial_{tt}\rho - g\frac{\alpha^2}{g^2}\partial_{tt}p}{g\frac{\alpha^2}{g^2} - \gamma\frac{\alpha^2}{g}} + \frac{\gamma\frac{\alpha^2}{g}}{\frac{\alpha}{g}}\left(\frac{\gamma\partial_{tt}\rho - \frac{\alpha}{g}\partial_{tt}p}{g\frac{\alpha^2}{g^2} - \gamma\frac{\alpha^2}{g}}\right) + g\frac{\gamma\bar{p}}{\bar{\rho}}\partial_z\rho \\
&= \frac{\gamma\bar{p}}{\bar{\rho}}\nabla^2 p - \gamma\frac{g}{\alpha}\partial_{tt}\rho + \partial_{tt}p + g\frac{\gamma\bar{p}}{\bar{\rho}}\partial_z\rho \quad\text{(IV.43)}
\end{aligned}
$$

Noting that $\bar{p}/\bar{\rho} = g/\alpha$, this simplifies to

$$
\partial_{tt}\rho = \nabla^2 p + g\partial_z\rho \quad\text{(IV.44)}
$$

We almost have a wave-like equation. The only thing missing is having the time derivative and the Laplace operator in the same variable. Look again at (IV.41). If we solve it for $\partial_{tt}\rho$ and use (IV.32) to cancel and combine terms, we have

$$
\partial_{tt}\rho = \frac{\bar{\rho}}{\gamma\bar{p}}\partial_{tt}p + \frac{\alpha(1-\gamma)}{\gamma}\left(g\rho + \partial_z p\right) \quad\text{(IV.45)}
$$

Substituting this result into (IV.44) gives us

$$
\partial_{tt}p = \frac{\gamma\bar{p}}{\bar{\rho}}\left(\nabla^2 p + g\partial_z\rho\right) + g\left(1-\gamma\right)\bar{\rho}\partial_t w \ , \quad\text{(IV.46)}
$$

where we use (IV.31c) to make the substitution

$$
\bar{\rho}\partial_t w = -g\rho - \partial_z p \ ,
$$

and we keep the usual $\frac{\gamma \bar{p}}{\bar{\rho}}$ as the wave speed term rather than simplify it. If we try to remove the ρ and w terms, we go around in circles, never quite replacing them all in terms of p. Hence, this is the closest we can come to deriving a wave-like equation that is equivalent to (IV.31). Our wave equation for p is altered by the vertical derivative of ρ and the time derivative of w.

Note, however, that if we set $\gamma = 1$, differentiate (IV.46) with respect to time, and make the appropriate substitutions, we can get

$$\partial_t \left(\partial_{tt} p - \frac{g}{\alpha} \nabla^2 p \right) - g \partial_{zt} p = 0 \; , \tag{IV.47}$$

which more nearly resembles a wave equation, only for the time derivative of the pressure, rather than for the pressure itself. However, due to the definitions of the atmospheric constants, $\gamma = 1$ means $R = 0$, which causes problems with the ideal gas law $p = \rho R T$ on which we base our model. Hence, this contrivance is purely academic.

3.   Numerical Examples

For our first example, we consider an open boundary on the sides of the domain, so that the normal derivative is perpendicular to the force of gravity (see Fig. 19). We discretize (IV.31) according to the same second-order centered-difference scheme in Sec. B, which gives us

$$
\begin{aligned}
\Delta_t \rho &= -\bar{\rho}\left(\Delta_x u + \Delta_z w\right) - \bar{\rho}' w \\
\Delta_t u &= -\frac{\Delta_x p}{\bar{\rho}} \\
\Delta_t w &= -\frac{\Delta_z p}{\bar{\rho}} - \frac{g}{\bar{\rho}} \rho \\
\Delta_t p &= -\gamma \bar{p}\left(\Delta_x u + \Delta_z w\right) + g \bar{\rho} w
\end{aligned}
\tag{IV.48}
$$

where we use z, w, $\bar{\rho}$, and $\bar{p}$ instead of y, v, ρ_0, and p_0, respectively, to emphasize that our concern is now with a vertical, rather than horizontal, plane. As before, we use the same domain size and initial conditions. However, we now have hard walls on the top and bottom and NRBCs on the left and right, and the reference solution
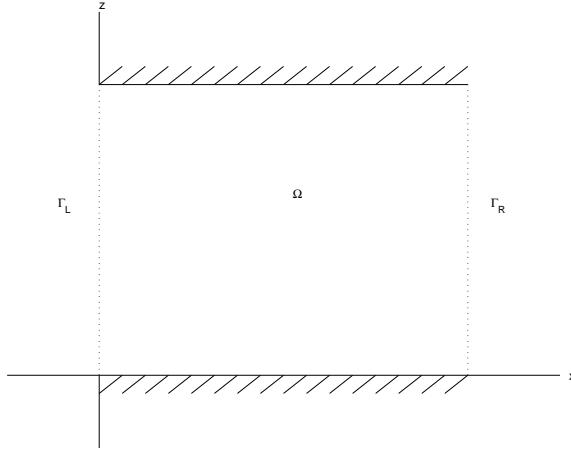
Figure 19. An infinite channel domain Ω truncated by artifical boundaries Γ_L and Γ_R [After [22], Fig. 1, p. 2]

is a 30×10 km channel, with the domain of interest in the center. The error norms are given in Table VI, with a comparison of pressure plots given by Fig. 20.

Having successfully implemented gravity perpendicular to the open boundaries' normal vector, we now implement it parallel to the open boundary's normal vector. Using again the same initial conditions, our domain is now a "bucket," i.e., a semi-infinite channel with the open boundary on top (Fig. 6). Table VII shows the

J	E_ρ	E_u	E_v	E_p
1	0.23241	0.52603	0.12775	0.23171
2	0.065394	0.14839	0.033298	0.065251
3	0.03214	0.069192	0.017724	0.032071
4	0.021193	0.04438	0.012525	0.021144
5	0.015814	0.031941	0.0096649	0.015776
6	0.012458	0.024676	0.007901	0.012429
7	0.010184	0.019914	0.0066308	0.01016
8	0.0086452	0.016684	0.0056677	0.0086248
9	0.0076161	0.01435	0.0049472	0.0075982
10	0.0068845	0.012637	0.0044394	0.0068682

Table VI. Error norms with $J \in 1 \ldots 10$ in a horizontal channel with gravitational forces (IV.31)
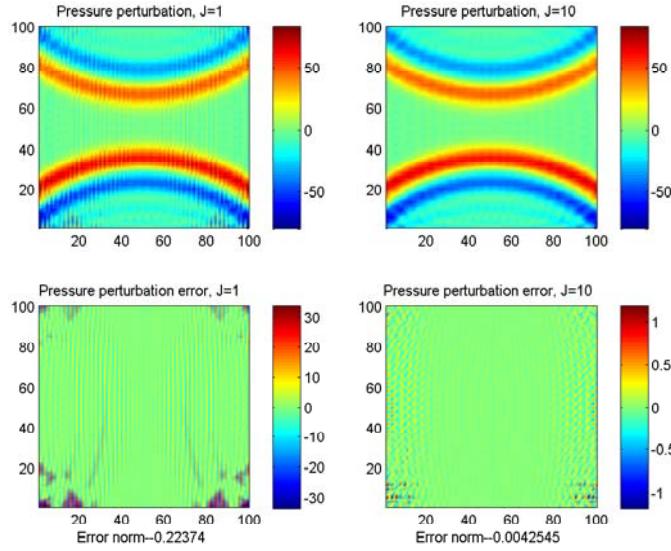
Figure 20. Comparison of p in gravity-influenced system (IV.31) computed with $J = 1$ and $J = 10$ in an infinite horizontal channel, with error norms computed by (IV.14). (TL) Computed solution for $J = 1$. (TR) Computed solution for $J = 10$. (BL) Delta between reference solution and $J = 1$ computed solution. (BR) Delta between reference solution and $J = 10$ computed solution.

error norms, and Fig. 21 compares the z-velocity perturbations for $J = 1$ and $J = 10$.

Next we combine these results into a domain open on three sides, with a hard wall on the bottom (see Fig. 22). Table VIII shows the error norms, and Fig. 23 compares the x-velocity perturbations for $J = 1$ and $J = 10$.

J	E_ρ	E_u	E_v	E_p
1	0.097404	0.10278	0.22495	0.096936
2	0.034899	0.027336	0.063934	0.034738
3	0.026286	0.014095	0.030089	0.026195
4	0.024522	0.0098734	0.019451	0.024443
5	0.023927	0.00764	0.013899	0.023852
6	0.023651	0.0062309	0.010768	0.023578
7	0.023506	0.0052081	0.0086306	0.023433
8	0.023425	0.0044326	0.0071758	0.023353
9	0.023378	0.0038462	0.0060809	0.023307
10	0.023348	0.00339	0.0052913	0.023276

Table VII. Error norms with $J \in 1 \ldots 10$ in a vertical bucket with gravitational forces (IV.31)

J	E_ρ	E_u	E_v	E_p
1	0.31226	0.85386	0.30744	0.30865
2	0.088812	0.24972	0.089607	0.087862
3	0.043421	0.11951	0.04392	0.042972
4	0.028607	0.077987	0.029393	0.028308
5	0.021264	0.057307	0.021724	0.021042
6	0.016764	0.04499	0.017264	0.016589
7	0.01378	0.036859	0.014216	0.013637
8	0.011743	0.031518	0.012194	0.01162
9	0.010292	0.027596	0.010665	0.010185
10	0.0091922	0.024287	0.0094066	0.0090963

Table VIII. Error norms with $J \in 1 \ldots 10$ in an open-air domain with gravitational forces (IV.31)
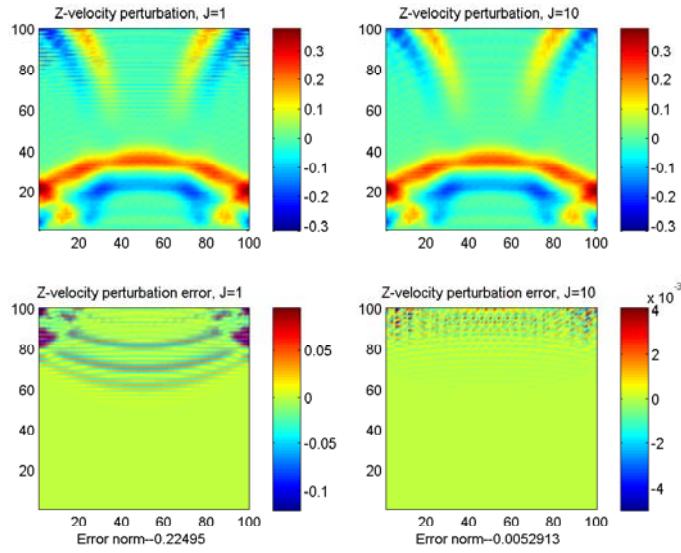
Figure 21. Comparison of w in gravity-influenced system (IV.31) computed with $J = 1$ and $J = 10$ in a semi-infinite vertical channel, with error norms computed by (IV.14). (TL) Computed solution for $J = 1$. (TR) Computed solution for $J = 10$. (BL) Delta between reference solution and $J = 1$ computed solution. (BR) Delta between reference solution and $J = 10$ computed solution.
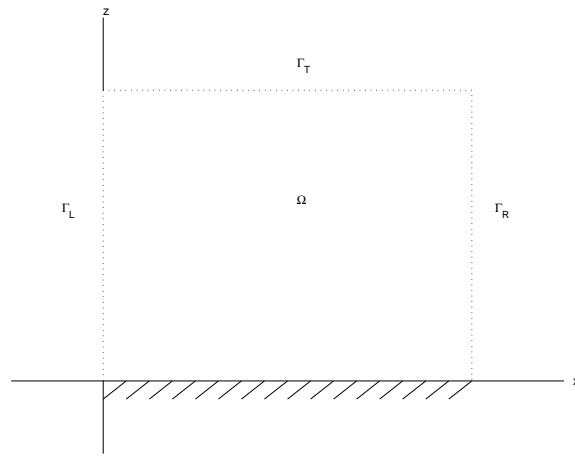
Figure 22. A half-plane domain Ω truncated by artificial boundaries Γ_L, Γ_T and Γ_R [After [20], Fig. 1, p. 3]
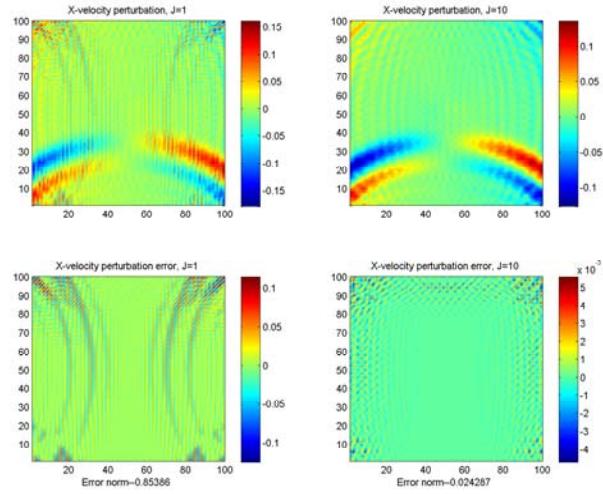
Figure 23. Comparison of u in gravity-influenced system (IV.31) computed with $J = 1$ and $J = 10$ in an open-air domain, with error norms computed by (IV.14). (TL) Computed solution for $J = 1$. (TR) Computed solution for $J = 10$. (BL) Delta between reference solution and $J = 1$ computed solution. (BR) Delta between reference solution and $J = 10$ computed solution.

E.   ADVECTION

Now we consider the case of non-zero mean flow. Beginning with the simple case, we have

$$
\begin{aligned}
\partial_t \rho + u_0 \partial_x \rho + v_0 \partial_y \rho + \rho_0 \left(\partial_x u + \partial_y v \right) &= 0 \\
\partial_t u + u_0 \partial_x u + v_0 \partial_y u + \frac{1}{\rho_0} \partial_x p &= 0 \\
\partial_t v + u_0 \partial_x v + v_0 \partial_y v + \frac{1}{\rho_0} \partial_y p &= 0 \\
\partial_t p + u_0 \partial_x p + v_0 \partial_y p + \gamma p_0 \left(\partial_x u + \partial_y v \right) &= 0
\end{aligned}
\tag{IV.49}
$$

Define a Lagrangian derivative

$$
\frac{D}{Dt} = \partial_t + u_0 \partial_x + v_0 \partial_y
\tag{IV.50}
$$

If we use this definition in (IV.49), we get

$$
\begin{aligned}
\frac{D\rho}{Dt} + \rho_0 \left(\partial_x u + \partial_y v \right) &= 0 \\
\frac{Du}{Dt} + \frac{1}{\rho_0} \partial_x p &= 0 \\
\frac{Dv}{Dt} + \frac{1}{\rho_0} \partial_y p &= 0 \\
\frac{Dp}{Dt} + \gamma p_0 \left(\partial_x u + \partial_y v \right) &= 0 \ ,
\end{aligned}
\tag{IV.51}
$$

and we can easily show that this formulation is equivalent to a Lagrangian scalar wave equation

$$
\frac{D^2 p}{Dt^2} = \frac{\gamma p_0}{\rho_0} \nabla^2 p
\tag{IV.52}
$$

If we incorporate Coriolis forces, then our equation set is

$$
\begin{aligned}
\frac{D\rho}{Dt} + \rho_0 \left(\partial_x u + \partial_y v \right) &= 0 \\
\frac{Du}{Dt} + \frac{1}{\rho_0} \partial_x p &= f \left(v + v_0 \right) \\
\frac{Dv}{Dt} + \frac{1}{\rho_0} \partial_y p &= -f \left(u + u_0 \right) \\
\frac{Dp}{Dt} + \gamma p_0 \left(\partial_x u + \partial_y v \right) &= 0
\end{aligned}
\tag{IV.53}
$$

Using our now-familiar conversion technique, we have

$$\frac{D^2 p}{Dt^2} = \frac{\gamma p_0}{\rho_0} \nabla^2 p - \gamma p_0 f \left(\partial_x v - \partial_y u \right) \qquad \text{(IV.54)}$$

Now (IV.49) and (IV.53) both imply $\frac{Dp}{Dt} = \frac{\gamma p_0}{\rho_0} \frac{D\rho}{Dt}$, so if we apply $\frac{D}{Dt}$ to (IV.54), we get

$$\frac{D}{Dt} \left(\frac{D^2 p}{Dt^2} - \frac{\gamma p_0}{\rho_0} \nabla^2 p + \gamma p_0 f \left(\partial_x v - \partial_y u \right) \right) = 0 \qquad \text{(IV.55)}$$

Using the same approach we used to convert the no-mean-flow form to the Klein-Gordon equation, we apply ∂_y to (IV.53b), ∂_x to (IV.53c), and subtract to get

$$\frac{D}{Dt} \left(\partial_x v - \partial_y u \right) = -f \left(\partial_x u + \partial_y v \right) \qquad \text{(IV.56)}$$

Substituting this result into (IV.55) removes the vorticity term and gives us

$$\frac{D}{Dt} \left(\frac{D^2 p}{Dt^2} p - \frac{\gamma p_0}{\rho_0} \nabla^2 p \right) - \gamma p_0 f^2 \left(\partial_x u + \partial_y v \right) = 0$$

$$\frac{D}{Dt} \left(\frac{D^2 p}{Dt^2} p - \frac{\gamma p_0}{\rho_0} \nabla^2 p \right) + f^2 \frac{Dp}{Dt} = 0 \qquad \text{(IV.57)}$$

Integrate along characteristics, assuming an initial value of zero, to get

$$\frac{D^2 p}{Dt^2} p = \frac{\gamma p_0}{\rho_0} \nabla^2 p - f^2 p \ . \qquad \text{(IV.58)}$$

So our system is still equivalent to the Klein-Gordon equation, using Lagrangian derivatives rather than time derivative. However, we will show in Sec. 3 that such a system is inherently unstable under long-time integration.

1. Interior Discretization Scheme

Similar to (IV.50), if we define the Lagrangian difference

$$\vec{\Delta} = \Delta_t + u_0 \Delta_x + v_0 \Delta_y \ , \qquad \text{(IV.59)}$$

then the discrete basic system is given by

$$\begin{aligned} \vec{\Delta}\rho + \rho_0 \left(\Delta_x u + \Delta_y v \right) &= 0 \\ \vec{\Delta}u + \frac{1}{\rho_0} \Delta_x p &= 0 \\ \vec{\Delta}v + \frac{1}{\rho_0} \Delta_y p &= 0 \\ \vec{\Delta}p + \gamma p_0 \left(\Delta_x u + \Delta_y v \right) &= 0 \ , \end{aligned} \qquad \text{(IV.60)}$$

67

which is easily shown to be equivalent to

$$\vec{\Delta}\vec{\Delta}p = \frac{\gamma p_0}{\rho_0}\left(\Delta_x\Delta_x p + \Delta_y\Delta_y p\right) \tag{IV.61}$$

Hence, the basic system under advection should be stable when implemented in conjunction with the Higdon NRBC defined for a double-sized grid. Likewise, if we include Coriolis, we have the discrete system

$$
\begin{aligned}
\vec{\Delta}\rho + \rho_0\left(\Delta_x u + \Delta_y v\right) &= 0 \\
\vec{\Delta}u + \frac{1}{\rho_0}\Delta_x p &= f\left(\frac{v_0}{\rho_0}\rho + v + v_0\right) \\
\vec{\Delta}v + \frac{1}{\rho_0}\Delta_y p &= -f\left(\frac{u_0}{\rho_0}\rho + u + u_0\right) \\
\vec{\Delta}p + \gamma p_0\left(\Delta_x u + \Delta_y v\right) &= 0 \;,
\end{aligned}
\tag{IV.62}
$$

and if we use the discrete analog to the continuous case derivation in the preceding section, we can easily show that this system is equivalent to

$$\vec{\Delta}\left[\vec{\Delta}\vec{\Delta}p = \frac{\gamma p_0}{\rho_0}\left(\Delta_x\Delta_x p + \Delta_y + \Delta_y p\right) - f^2 p\right] \;, \tag{IV.63}$$

which again should be stable when the Higdon scheme is used on a double-sized grid. Since the inclusion of gravity creates a system which is not compatible in the continuous case with a wave-like equation, its discrete formulation will also not be equivalent to a discrete wave-like equation. The discretization scheme in the xz plane under the influence of gravity is given by

$$
\begin{aligned}
\vec{\Delta}\rho + \bar{\rho}\left(\Delta_x u + \Delta_z w\right) &= -\bar{\rho}'\left(w + w_0\right) \\
\vec{\Delta}u + \frac{1}{\bar{\rho}}\Delta_x p &= 0 \\
\vec{\Delta}w + \frac{1}{\bar{\rho}}\Delta_z p &= -\frac{g}{\bar{\rho}}\rho \\
\vec{\Delta}p + \gamma\bar{p}\left(\Delta_x u + \Delta_z w\right) &= g\bar{\rho}\left(w + w_0\right) \;,
\end{aligned}
\tag{IV.64}
$$

where we replace the constants ρ_0 and p_0 with the z-dependent values $\bar{\rho}$ and $\bar{p}$. Note that w_0 appears on the right-hand side of the equations for ρ and p because of the linearization process in Sec. II.C.2. In practice, however, the presence of the ground will require $w_0 = 0$.

68

2. NRBC Formulation

The addition of advection changes our wave speed with respect to the boundary. To determine the new "correct" wave speed estimate, replace the time derivative in the Higdon NRBC definition (III.11) with the Lagrangian derivative (expressed for a right-side boundary):

$$\prod_{j=1}^{J}\left(\frac{D}{Dt}+c_{j}\partial_{x}\right)u=0 \tag{IV.65}$$

For waves striking the boundary, we are only concerned with the velocity normal to the boundary. Thus, we remove the tangential component of the Lagrangian derivative, expand and combine terms, and use our simplification $c_j = c_0$, giving

$$\left(\partial_{t}+\left(c_{0}+u_{0}\right)\partial_{x}\right)^{J}u=0 \tag{IV.66}$$

Since our interior discretization scheme is equivalent (or approximately so) to a wave equation on a double-sized grid, our NRBC discretization for these equations is given by

$$\left(\frac{I-S_{t}^{-2}}{2\delta t}+\left(c_{0}+u_{0}\right)\frac{I-S_{x}^{-2}}{2\delta x}\right)^{J}\sigma=0 \tag{IV.67}$$

3. Long-Term Instability of Advection with Coriolis

Let us briefly consider the discrete form of (II.63) in the xy plane with Coriolis forces. Using our usual second-order centered-difference scheme, we have

$$
\begin{aligned}
\Delta_{t}\rho+u_{0}\Delta_{x}\rho+v_{0}\Delta_{y}\rho+\rho_{0}\Delta_{x}u+\rho_{0}\Delta_{y}v &= 0\\
\Delta_{t}u+u_{0}\Delta_{x}u+v_{0}\Delta_{y}u+\frac{1}{\rho_{0}}\Delta_{x}p &= f\left(v+v_{0}\right)\\
\Delta_{t}v+u_{0}\Delta_{x}v+v_{0}\Delta_{y}v+\frac{1}{\rho_{0}}\Delta_{y}p &= -f\left(u+u_{0}\right)\\
\Delta_{t}p+u_{0}\Delta_{x}p+v_{0}\Delta_{y}p+\gamma p_{0}\Delta_{x}u+\gamma p_{0}\Delta_{y}v &= 0
\end{aligned} \tag{IV.68}
$$

Assume everything is initially at rest (no perturbations), and $u_0 v_0 \neq 0$. With every perturbation variable equal to zero at times $n \leq 0$, our values at time $n = 1$ become

$$\frac{\rho_{i,j}^{1}}{2\delta t} = 0$$

$$\frac{u_{i,j}^1}{2\delta t} = fv_0$$

$$\frac{v_{i,j}^1}{2\delta t} = -fu_0$$

$$\frac{p_{i,j}^1}{2\delta t} = 0 \tag{IV.69}$$

So, having started from a zero-perturbation domain, the combination of advection and Coriolis creates non-zero perturbations in u and v. In fact, u and v are still constant in the domain, but now the constant is non-zero. We note that ρ and p are still uniformly zero throughout the domains, and it is easy to show that they will always be zero. However, if we look at u and v at the next time step, noting that all spatial differences are zero, we get

$$\frac{u_{i,j}^2}{2\delta t} = f\left(v_{i,j}^1 + v_0\right)$$

$$\frac{v_{i,j}^2}{2\delta t} = -f\left(u_{i,j}^1 + u_0\right) \tag{IV.70}$$

Substituting the previously determined values for $u_{i,j}^1$ and $v_{i,j}^1$, we get

$$u_{i,j}^2 = 2\delta t f v_0 - (2\delta t f)^2 u_0$$

$$v_{i,j}^2 = -2\delta t f u_0 - (2\delta t f)^2 v_0 \tag{IV.71}$$

Proceeding to time step $n = 3$, we have

$$u_{i,j}^3 \approx 2\left(2\delta t f v_0\right) + O\left((2\delta t f)^2\right)$$

$$v_{i,j}^3 \approx -2\left(2\delta t f u_0\right) + O\left((2\delta t f)^2\right) \tag{IV.72}$$

where we are only concerned with the terms which are linear in $2\delta t f$. It can be shown that

$$u_{i,j}^n \approx \lfloor \frac{n}{2} \rfloor (2\delta t f) v_0 + O\left((2\delta t f)^2\right)$$

$$v_{i,j}^n \approx -\lfloor \frac{n}{2} \rfloor (2\delta t f) u_0 + O\left((2\delta t f)^2\right) , \tag{IV.73}$$

where $\lfloor \cdot \rfloor$ denotes the floor function.

Remark 1: If $f \neq 0$ and either $u_0 \neq 0$ or $v_0 \neq 0$, then our zero-perturbation domain grows linearly, without bound, in u and/or v. While the growth will be slow due to the magnitude of f, it will still be present. Hence, the combination of Coriolis forces and non-zero advection is inherently unstable in the linearized Euler equations. We can only use this equation set for short-time integrations, not for longer durations.

Remark 2: If we perform a similar analysis in the case of gravity and non-zero advection, we see that that system is inherently unstable if $w_0 \neq 0$. Horizontal advection does not cause any problems. Any physical problem which considers gravity and vertical advection is unsuited to this equation set. Meteorological problems, however, will generally include the ground and thus not have any constant vertical advection.

4.   Numerical Examples
a.   *Basic System, Infinite Channel*

For the examples in this section, we use the same domain and initial conditions as before. Our first example is a basic system in an infinite channel with a constant lateral advection of $u_0 = 100\frac{m}{s}$. Again running the simulation up until $t = 24$, we get the error norms listed in Table IX. Fig. 24 shows the density preturbation ρ for the $J = 10$ case. Note the faint wave propagating in the opposite direction; this false wave is a consequence of using centered-differences for our spatial discretization [24]. Fig. 25 compares the pressure perturbation p for low- and high-order NRBCs.

J	E_ρ	E_u	E_v	E_p
1	0.22447	0.30496	0.18074	0.22447
2	0.06216	0.09791	0.059247	0.062159
3	0.026666	0.041939	0.021853	0.026666
4	0.017115	0.025099	0.012509	0.017115
5	0.01258	0.019265	0.0097557	0.01258
6	0.010007	0.014986	0.0074502	0.010007
7	0.0082563	0.012216	0.0059657	0.0082562
8	0.0070098	0.010347	0.0051175	0.0070098
9	0.0060805	0.0090438	0.0044283	0.0060805
10	0.0053682	0.0079242	0.003876	0.0053683

Table IX. Error norms with $J \in 1 \ldots 10$ in an infinite channel with horizontal advection
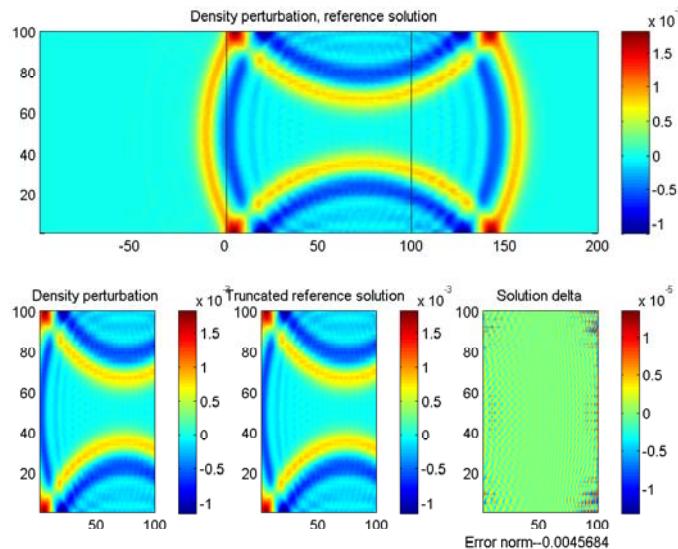
Figure 24. Plot of ρ in basic system (IV.49) with left-to-right advection with $J = 10$ in an infinite channel. (BL) Computed solution. (Top) Reference solution; the area corresponding to the computed solution is contained between the vertical lines. (BC) Reference solution truncated to computed solution domain. (BR) Delta between reference solution and computed solution, with error norm computed by (IV.14).

72
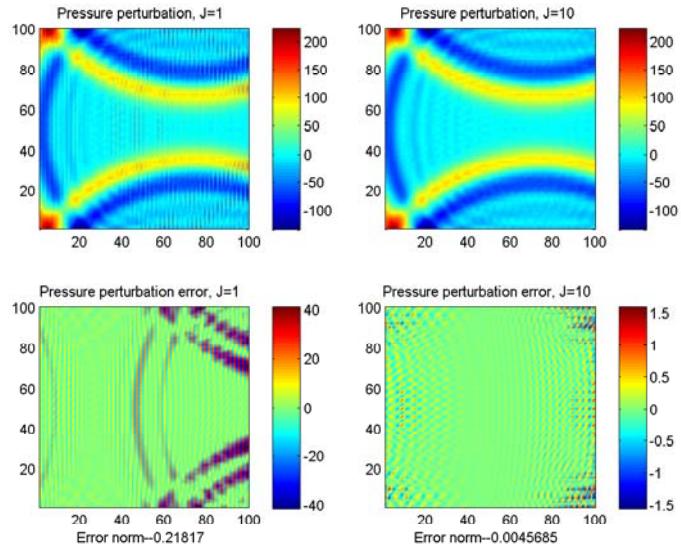
Figure 25. Comparison of p in basic system (IV.49) with left-to-right advection computed with $J = 1$ and $J = 10$ in an infinite channel, with error norms computed by (IV.14). (TL) Computed solution for $J = 1$. (TR) Computed solution for $J = 10$. (BL) Delta between reference solution and $J = 1$ computed solution. (BR) Delta between reference solution and $J = 10$ computed solution.

J	E_ρ	E_u	E_v	E_p
1	0.33816	0.36566	0.36566	0.33819
2	0.091059	0.10563	0.10563	0.091066
3	0.043514	0.050827	0.050827	0.043517
4	0.028633	0.032601	0.032601	0.028635
5	0.021446	0.023794	0.023794	0.021447
6	0.0172	0.018581	0.018581	0.017201
7	0.014495	0.015508	0.015508	0.014496
8	0.012603	0.013347	0.013347	0.012604
9	0.011967	0.013011	0.012734	0.011969
10	0.078775	0.10216	0.082933	0.078757

Table X. Error norms with $J \in 1 \ldots 10$ in an open domain with diagonal advection

b.   *Basic System, Open Domain*

Now consider the basic system in an open domain with a constant diagonal advection of $u_0 = 90$ m/s, $v_0 = 90$ m/s. This time, we get the error norms listed in Table X. Not surprisingly, the error norms for u and v are identical up to $J = 8$ (with v slightly better than u in the $J = 9$ case). In this example, we see that the $J = 10$ error norms are larger than those for $J = 9$. Fig. 26 shows the x-velocity preturbation u for the $J = 8$ case; Figs. 27 and 28 shows the same variable for the $J = 9$ and $J = 10$ cases, respectively. We see from the latter two that the system begins to destabilize at the top-right corner. The reason for this destabilization is still under investigation. Fig. 29 compares the y-velocity perturbation v for low- and high-order NRBCs.
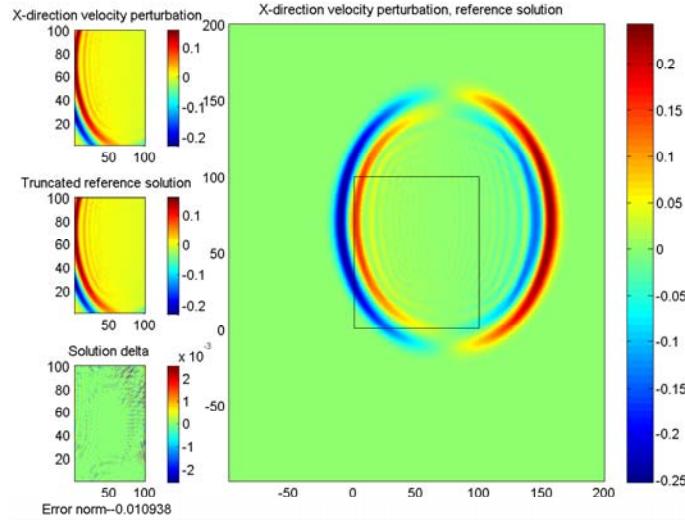
Figure 26. Plot of u in basic system (IV.49) with bottom-left-to-top-right advection with $J = 8$ in an open domain. (TL) Computed solution. (Right) Reference solution; the area corresponding to the computed solution is contained in the center box. (CL) Reference solution truncated to computed solution domain. (BL) Delta between reference solution and computed solution, with error norm computed by (IV.14).
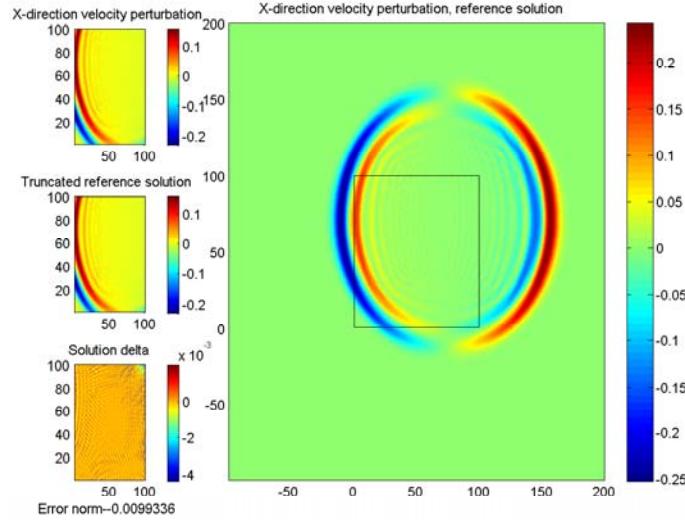
Figure 27. Plot of u in basic system (IV.49) with bottom-left-to-top-right advection with $J = 9$ in an open domain. (TL) Computed solution. (Right) Reference solution; the area corresponding to the computed solution is contained in the center box. (CL) Reference solution truncated to computed solution domain. (BL) Delta between reference solution and computed solution, with error norm computed by (IV.14).
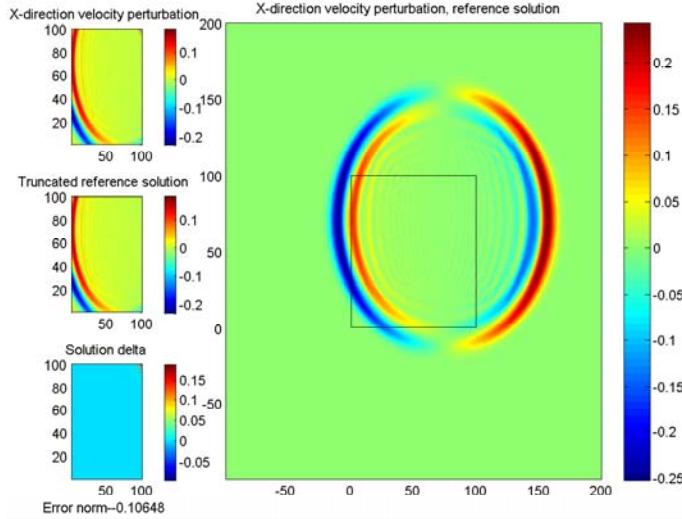
Figure 28. Plot of u in basic system (IV.49) with bottom-left-to-top-right advection with $J = 10$ in an open domain. (TL) Computed solution. (Right) Reference solution; the area corresponding to the computed solution is contained in the center box. (CL) Reference solution truncated to computed solution domain. (BL) Delta between reference solution and computed solution, with error norm computed by (IV.14).
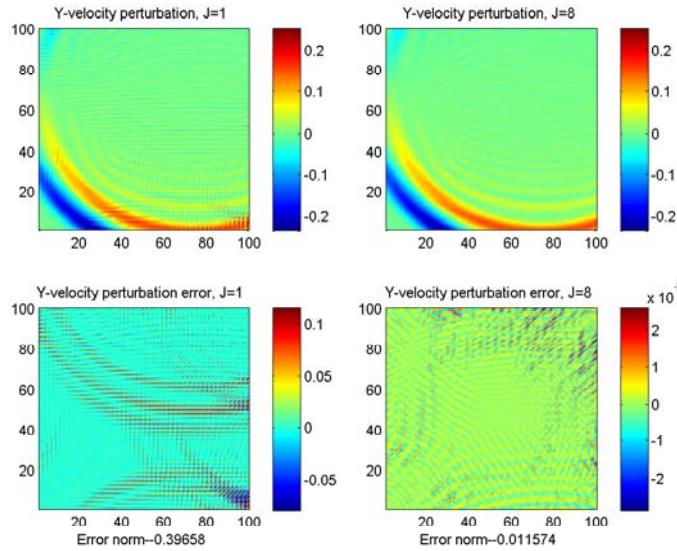
Figure 29. Comparison of v in basic system (IV.49) with bottom-left-to-top-right advection computed with $J = 1$ and $J = 8$ in an open domain, with error norms computed by (IV.14). (TL) Computed solution for $J = 1$. (TR) Computed solution for $J = 8$. (BL) Delta between reference solution and $J = 1$ computed solution. (BR) Delta between reference solution and $J = 8$ computed solution.

J	E_ρ	E_u	E_v	E_p
1	0.22154	0.59249	0.25232	0.22154
2	0.10104	0.3566	0.15752	0.10104
3	0.34963	1.3304	0.39134	0.34963
4	1.4844	5.1058	1.391	1.4844
5	2.3286	7.4879	3.3526	2.3286
6	34.219	98.952	36.169	34.219
7	71.57	277.37	83.65	71.57
8	4971.8	14265	4154	4971.8

Table XI. Error Norms with $J \in 1 \ldots 8$ in an Infinite Channel with Horizontal Advection and Coriolis

c.   *Coriolis Forces, Infinite Channel*

Having shown already that the system is inherently unstable for long-time integrations involving both advection and Coriolis, let us look briefly at the effectiveness of the Higdon NRBCs for a short-duration simulation. We first consider an infinite channel with left-to-right advection, $u_0 = 100\frac{\text{m}}{\text{s}}$. Incorporating Coriolis forces, we use the discretization scheme (IV.62) for the interior. Table XI shows the error norms for $J \in 1 \ldots 8$. We see some improvement between $J = 1$ and $J = 2$, but the system fails for higher J. We will not show any plots of these results.

J	E_ρ	E_u	E_v	E_p
1	0.86499	0.31392	0.33843	0.86506
2	0.58828	0.26882	0.2833	0.58833
3	6.288	2.5314	2.67	6.2885
4	327.16	134.55	141.92	327.18
5	14895	4854.5	5120.1	14896
6	278880	87044	91822	278900

Table XII. Error Norms with $J \in 1 \ldots 6$ in an Open Domain with Diagonal Advection and Coriolis

d. Coriolis Forces, Open Domain

Likewise, when we consider the system in an open domain, with the NRBC on all four sides, using a diagonal advection, $u_0 = v_0 = 100\frac{\text{m}}{\text{s}}$, we get the results shown in Table XII. A slight improvement from $J = 1$ to $J = 2$ is followed by massive instability for higher J. Again, we will omit any plots of these results.

J	E_ρ	E_u	E_v	E_p
1	0.2251	0.29999	0.18206	0.22442
2	0.062733	0.096051	0.059583	0.062517
3	0.027088	0.041293	0.022049	0.027048
4	0.017524	0.024613	0.012558	0.017488
5	0.012913	0.018886	0.0098005	0.012887
6	0.010289	0.014672	0.0074523	0.01027
7	0.0085063	0.011944	0.0059542	0.0084902
8	0.007226	0.010119	0.005107	0.0072123
9	0.0062668	0.0088368	0.0044166	0.0062548
10	0.0055272	0.0077406	0.0038622	0.0055167

Table XIII. Error norms with $J \in 1 \ldots 10$ in an infinite channel with horizontal advection and gravity

e.   *Gravity, Infinite Channel*

Turning our attention now to the inclusion of gravity, we again consider an infinite channel with horizontal advection, $u_0 = 100\frac{\mathrm{m}}{\mathrm{s}}$. Using the discretization scheme (IV.64), we get the error norms shown in Table XIII. Unlike the Coriolis case, this time we get good results all the way up to $J = 10$. Fig. 30 illustrates the difference in pressure perturbation results for small and large J.
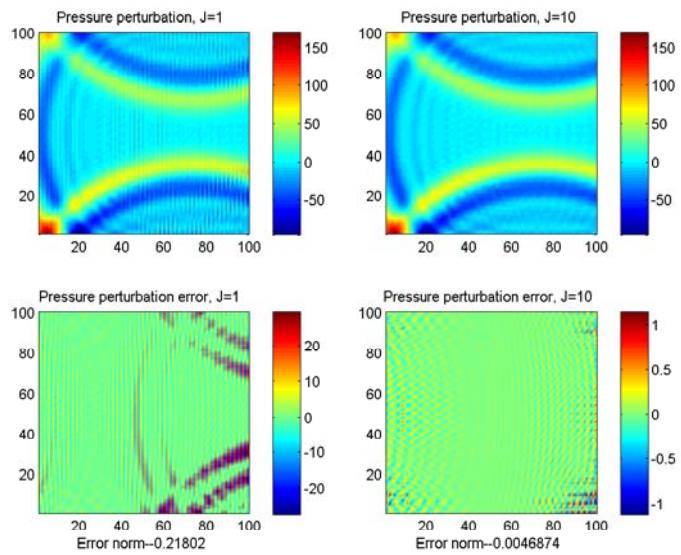
Figure 30. Comparison of p in gravity-influenced system (IV.64) with left-to-right advection computed with $J = 1$ and $J = 10$ in an infinite channel, with error norms computed by (IV.14). (TL) Computed solution for $J = 1$. (TR) Computed solution for $J = 10$. (BL) Delta between reference solution and $J = 1$ computed solution. (BR) Delta between reference solution and $J = 10$ computed solution.

J	E_ρ	E_u	E_v	E_p
1	0.25917	0.35427	0.28085	0.25639
2	0.072395	0.11036	0.084279	0.071655
3	0.032031	0.050496	0.036455	0.03179
4	0.020847	0.03178	0.022262	0.020674
5	0.015383	0.023689	0.016319	0.015259
6	0.012198	0.018435	0.012387	0.012104
7	0.010073	0.01515	0.0099833	0.0099939
8	0.0085547	0.012836	0.0084265	0.0084879
9	0.0074187	0.011229	0.007244	0.0073608
10	0.0066163	0.010216	0.0066934	0.0065656

Table XIV. Error norms with $J \in 1\ldots 10$ in a half-plane with horizontal advection and gravity

f.   Gravity, Ground and Open Air

Looking now at an "open" domain in the presence of gravity, we consider the open-air domain of Fig. 22. This domain matches the physical idea of modeling an open atmosphere bounded by the ground. While the presence of the ground prevents us from considering vertical or diagonal advection, it still presents us with a domain containing two adjacent open boundaries. We keep $u_0 = 100\frac{\mathrm{m}}{\mathrm{s}}$ for our advection speed and run our standard simulation. The error norms for different values of J are given in Table XIV. Fig. 31 illustrates the differences between low and high J.

F.   SUMMARY

This high-order NRBC implementation provides high accuracy with little computational overhead. However, it has three significant limitations:

1. The formulation requires one-sided high-order spatial and temporal derivatives.

2. These one-sided derivatives limit the NRBC order to the size of the domain.

3. Coriolis and advection cannot be used together stably.
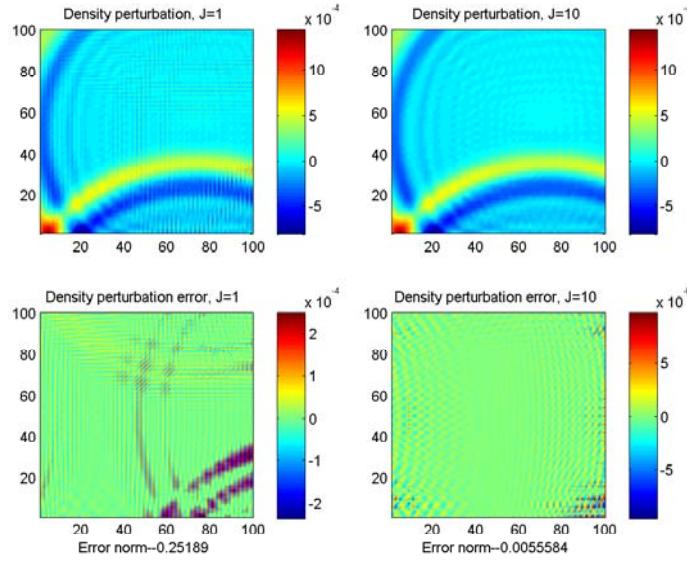
Figure 31. Comparison of ρ in gravity-influenced system (IV.64) with left-to-right advection computed with $J = 1$ and $J = 10$ in an open-air domain, with error norms computed by (IV.14). (TL) Computed solution for $J = 1$. (TR) Computed solution for $J = 10$. (BL) Delta between reference solution and $J = 1$ computed solution. (BR) Delta between reference solution and $J = 10$ computed solution.

In the next chapter, we will look at another NRBC implementation, one which does not suffer from these limitations.

V. GIVOLI-NETA NRBCS FOR THE LINEARIZED EULER EQUATIONS

A. INITIAL IMPLEMENTATION FOR FIRST-ORDER SYSTEMS

1. Derivation

Let us now consider the Givoli-Neta auxiliary variable NRBC described in Sec. III.B.2. That section described this NRBC formulation for a scalar wave-like equation. In this chapter we apply it to the linearized Euler system. We first define the auxiliary variables in vector form:

$$\left(\partial_{\vec{n}} + \frac{1}{c_j}\partial_t\right)\vec{\varphi}_j = \vec{\varphi}_{j+1} \tag{V.1}$$

$$\vec{\varphi}_0 \equiv \vec{\varphi}$$

Note that we have left off the truncation condition $\vec{\varphi}_J \equiv 0$ from our formulation. As we derive the implementation below, we shall see that we need to modify the truncation condition slightly; the modified truncation condition will be given as part of the characteristic-based derivation (V.10).

Givoli and Neta [39, 40] show how to manipulate the Klein-Gordon equation to remove the normal derivatives. We will show briefly how to do so with the linearized Euler equations. For definiteness, we proceed for the right-side boundary; thus, $\vec{n} = x$.

Begin with the equation system in vector form:

$$\partial_t\vec{\varphi} + A\partial_x\vec{\varphi} + B\partial_y\vec{\varphi} = C\vec{\varphi} + \vec{D} , \tag{V.2}$$

where

$$\vec{\varphi} = \begin{pmatrix} \rho & u & v & p \end{pmatrix}^T$$

$$A = \begin{pmatrix} u_0 & \rho_0 & 0 & 0 \\ 0 & u_0 & 0 & \frac{1}{\rho_0} \\ 0 & 0 & u_0 & 0 \\ 0 & \gamma p_0 & 0 & u_0 \end{pmatrix}$$

$$B = \begin{pmatrix} v_0 & 0 & \rho_0 & 0 \\ 0 & v_0 & 0 & 0 \\ 0 & 0 & v_0 & \frac{1}{\rho_0} \\ 0 & 0 & \gamma p_0 & v_0 \end{pmatrix}$$

In the basic system, C and $\vec{D}$ are both zero. With Coriolis, we have

$$C = \begin{pmatrix} 0 & 0 & 0 & 0 \\ 0 & 0 & f & 0 \\ 0 & -f & 0 & 0 \\ 0 & 0 & 0 & 0 \end{pmatrix}$$

$$\vec{D} = \begin{pmatrix} 0 & fv_0 & -fu_0 & 0 \end{pmatrix}^T$$

With gravity, replace v, v_0, ρ_0, and p_0 in A and B with w, w_0, $\bar{\rho}$, and $\bar{p}$, respectively, and use

$$C = \begin{pmatrix} 0 & 0 & -\bar{\rho}' & 0 \\ 0 & 0 & 0 & 0 \\ -g\frac{1}{\bar{\rho}} & 0 & 0 & 0 \\ 0 & 0 & g\bar{\rho} & 0 \end{pmatrix}$$

$$\vec{D} = \begin{pmatrix} -\bar{\rho}'w_0 & 0 & 0 & g\bar{\rho}w_0 \end{pmatrix}^T$$

Define the linear differential operator $L(\vec{\varphi})$ to be

$$L(\vec{\varphi}) \equiv \partial_t \vec{\varphi} + A\partial_x \vec{\varphi} + B\partial_y \vec{\varphi} - C\vec{\varphi} \tag{V.3}$$

By definition, $L(\vec{\varphi}) = \vec{D}$. A more useful result is the following lemma:

Lemma V.1 *The auxiliary variables $\vec{\varphi}_j$ satisfy*

$$L(\vec{\varphi}_j) = 0 \tag{V.4}$$

for all $j \in 1 \ldots J$. The only exception to this lemma is when both of the following conditions are met:

- $\vec{n} = \pm\hat{k}$

- $g \neq 0$

Proof. Apply the operator L to (V.1) to get

$$
\begin{aligned}
L(\vec{\varphi}_1) &= L\left(\left(\partial_{\vec{n}} + \frac{1}{c_j}\partial_t\right)\varphi\right) \\
&= \partial_{\vec{n}}\left(L(\vec{\varphi})\right) + \frac{1}{c_j}\partial_t\left(L(\vec{\varphi})\right) \\
&= \partial_{\vec{n}}\vec{D} + \frac{1}{c_j}\partial_t\vec{D} \\
&= 0
\end{aligned}
\tag{V.5}
$$

Then proceed by induction to prove the lemma for all j $\square$.

(Note that if both conditions in Lemma V.1's exception are met, then $L\left(\partial_z\vec{\varphi}\right) \neq \partial_z\left(L\left(\vec{\varphi}\right)\right)$, and we cannot proceed with this proof or the overall derivation. The NRBC which handles these conditions will be given in Sec. C.)

Solve (V.1) for $\partial_x\vec{\varphi}_j$ and, using Lemma V.1, substitute the result into (V.2):

$$
A\vec{\varphi}_{j+1} = \left(\frac{1}{c_j}A - I\right)\partial_t\vec{\varphi}_j - B\partial_t\vec{\varphi}_j + C\vec{\varphi}_j \ , \ \ \forall j \in 1\dots J
\tag{V.6}
$$

We now have an auxiliary variable equation which need be defined only on the boundary. However, as it is defined solely on the boundary, and given that everything on the boundary is initially zero, we have an equation system which will always be identically zero. We will take a characteristic-based approach similar to that presented in Sec. 6 of [57].

Let Λ be the diagonal matrix of the eigenvalues of A in decreasing order, with R the corresponding right eigenvectors. With two degrees of freedom for the eigenvectors associated with $\lambda = u_0$, we choose eigenvectors which do not map one characteristic variable to one state variable, which we would get if we chose $\begin{pmatrix} 1 & 0 & 0 & 0 \end{pmatrix}^T$ and $\begin{pmatrix} 0 & 0 & 1 & 0 \end{pmatrix}^T$ for our u_0 eigenvectors. Instead, we use the following:

$$
\Lambda = \text{diag}\begin{pmatrix} u_0 + c_0 & u_0 & u_0 & u_0 - c_0 \end{pmatrix}
$$

$$R = \begin{pmatrix} \frac{\rho_0}{c_0} & 1 & 1 & -\frac{\rho_0}{c_0} \\ 1 & 0 & 0 & 1 \\ 0 & -1 & 1 & 0 \\ \rho_0 c_0 & 0 & 0 & -\rho_0 c_0 \end{pmatrix}$$

$$R^{-1} = \begin{pmatrix} 0 & \frac{1}{2} & 0 & \frac{1}{2\rho_0 c_0} \\ \frac{1}{2} & 0 & -\frac{1}{2} & -\frac{1}{2c_0^2} \\ \frac{1}{2} & 0 & \frac{1}{2} & -\frac{1}{2c_0^2} \\ 0 & \frac{1}{2} & 0 & -\frac{1}{2\rho_0 c_0} \end{pmatrix} \tag{V.7}$$

$$A = R\Lambda R^{-1}$$

With this definition, left-multiply (V.6) by R^{-1} and insert RR^{-1} as needed to get

$$\Lambda \vec{\xi}_1 = \left(\frac{1}{c_j}\Lambda - I\right)\partial_t \vec{\xi}_0 - \tilde{B}\partial_t \vec{\xi}_0 + \tilde{C}\vec{\xi}_0 + \tilde{D}$$

$$\Lambda \vec{\xi}_{j+1} = \left(\frac{1}{c_j}\Lambda - I\right)\partial_t \vec{\xi}_j - \tilde{B}\partial_t \vec{\xi}_j + \tilde{C}\vec{\xi}_j \ , \ j \in 1\ldots J \ , \tag{V.8}$$

where

$$\vec{\xi}_j = R^{-1}\vec{\varphi}_j$$

$$\tilde{B} = R^{-1}BR$$

$$\tilde{C} = R^{-1}CR \tag{V.9}$$

$$\tilde{D} = R^{-1}\vec{D}$$

However, we still have a system which is defined exclusively on the boundary. To overcome this problem, use (V.6) in characteristic form as a natural boundary condition for the outgoing characteristics. To close the system, use a Dirichlet condition for the highest-order auxiliary variables corresponding to the incoming characteristics. The final system then is

$$\left[\partial_t \vec{\xi}_0 = -\Lambda \partial_x \vec{\xi}_0 - \tilde{B}\partial_y \vec{\xi}_0 + \tilde{C}\vec{\xi}_0 + \tilde{D}\right]_+$$

$$\left(I - \frac{1}{c_j}\Lambda\right)\partial_t \vec{\xi}_0 + \Lambda \vec{\xi}_1 = -\tilde{B}\partial_y \vec{\xi}_0 + \tilde{C}\vec{\xi}_0 + \tilde{D}$$

$$\left(I - \frac{1}{c_j}\Lambda\right)\partial_t\vec{\xi}_j + \Lambda\vec{\xi}_{j+1} = -\tilde{B}\partial_y\vec{\xi}_j + \tilde{C}\vec{\xi}_j \, , \, j \in 1\ldots J$$

$$\left[\vec{\varphi}_J = 0\right]_- \, , \tag{V.10}$$

where the subscripts $+$ and $-$ mean we apply these equations only to the outgoing and incoming characteristics, respectively; that is, the first equation only applies to the outgoing characteristic variables, the second and third equations apply to all four characteristic auxiliary variables (for each j), and the final equation only applies to the incoming characteristic auxiliary variables. For example, if we have $J = 1$, $u_0 > 0$, $C = 0$, $\vec{D} = 0$, and we use standard first-order forward-differences in time, first-order backward-differences in x, and second-order centered-differences in y, then (V.10) defines the matrix system

$$
\begin{pmatrix}
1 & 0 & 0 & 0 & 0 & 0 & 0 & 0 \\
0 & 1 & 0 & 0 & 0 & 0 & 0 & 0 \\
0 & 0 & 1 & 0 & 0 & 0 & 0 & 0 \\
1-\lambda_a & 0 & 0 & 0 & \delta t\lambda_a & 0 & 0 & 0 \\
0 & 1-\lambda_b & 0 & 0 & 0 & \delta t\lambda_b & 0 & 0 \\
0 & 0 & 1-\lambda_c & 0 & 0 & 0 & \delta t\lambda_c & 0 \\
0 & 0 & 0 & 1-\lambda_d & 0 & 0 & 0 & \delta t\lambda_d \\
0 & 0 & 0 & 0 & 0 & 0 & 0 & 1
\end{pmatrix}
\begin{pmatrix}
\xi^n_{a,E,i} \\
\xi^n_{b,E,i} \\
\xi^n_{c,E,i} \\
\xi^n_{d,E,i} \\
\xi^n_{1,a,E,i} \\
\xi^n_{1,b,E,i} \\
\xi^n_{1,c,E,i} \\
\xi^n_{1,d,E,i}
\end{pmatrix}
$$

$$
=
\begin{pmatrix}
\xi^{n-1}_{a,E,i} + \delta t\left(-\left[\Lambda\left(\frac{\vec{\xi}^{n-1}_{E,i}-\vec{\xi}^{n-1}_{E-1,i}}{\delta x}\right)\right]_a - \left[\tilde{B}\left(\frac{\vec{\xi}^{n-1}_{E,i+1}-\vec{\xi}^{n-1}_{E,i-1}}{2\delta y}\right)\right]_a\right) \\
\xi^{n-1}_{b,E,i} + \delta t\left(-\left[\Lambda\left(\frac{\vec{\xi}^{n-1}_{E,i}-\vec{\xi}^{n-1}_{E-1,i}}{\delta x}\right)\right]_b - \left[\tilde{B}\left(\frac{\vec{\xi}^{n-1}_{E,i+1}-\vec{\xi}^{n-1}_{E,i-1}}{2\delta y}\right)\right]_b\right) \\
\xi^{n-1}_{c,E,i} + \delta t\left(-\left[\Lambda\left(\frac{\vec{\xi}^{n-1}_{E,i}-\vec{\xi}^{n-1}_{E-1,i}}{\delta x}\right)\right]_c - \left[\tilde{B}\left(\frac{\vec{\xi}^{n-1}_{E,i+1}-\vec{\xi}^{n-1}_{E,i-1}}{2\delta y}\right)\right]_c\right) \\
(1-\lambda_a)\xi^{n-1}_{a,E,i} + \delta t\left(-\left[\tilde{B}\left(\frac{\vec{\xi}^{n-1}_{E,i+1}-\vec{\xi}^{n-1}_{E,i-1}}{2\delta y}\right)\right]_a\right) \\
(1-\lambda_b)\xi^{n-1}_{b,E,i} + \delta t\left(-\left[\tilde{B}\left(\frac{\vec{\xi}^{n-1}_{E,i+1}-\vec{\xi}^{n-1}_{E,i-1}}{2\delta y}\right)\right]_b\right) \\
(1-\lambda_c)\xi^{n-1}_{c,E,i} + \delta t\left(-\left[\tilde{B}\left(\frac{\vec{\xi}^{n-1}_{E,i+1}-\vec{\xi}^{n-1}_{E,i-1}}{2\delta y}\right)\right]_c\right) \\
(1-\lambda_d)\xi^{n-1}_{d,E,i} + \delta t\left(-\left[\tilde{B}\left(\frac{\vec{\xi}^{n-1}_{E,i+1}-\vec{\xi}^{n-1}_{E,i-1}}{2\delta y}\right)\right]_d\right) \\
0
\end{pmatrix}
, \tag{V.11}
$$

87

where λ denotes the individual eigenvalues of the diagonal matrix Λ; the subscript 1 denotes the first (and only) auxiliary variable; the subscripts a, b, c, d denote the individual components of the characteristic/state/auxiliary variable vectors; the subscripts E and $E-1$ denote the eastern boundary and the point adjacent to it, respectively; the subscripts i, $i+1$, and $i-1$ denote the grid point in the y direction; and the superscripts n and $n-1$ denote the current and previous time steps, respectively.

Note that if we are applying this NRBC in the presence of gravity, *even in a horizontal channel*, we must take care to consider the z-derivative of the eigenvector matrix R when we convert from state variables to characteristics. In such a case, (V.10) becomes

$$
\begin{aligned}
\left[\partial_t \vec{\xi}_0 \right. &= \left. -\Lambda \partial_x \vec{\xi}_0 - \tilde{B}\partial_z\vec{\xi}_0 + \left(\tilde{B}\left(\partial_z R^{-1}\right) R + \tilde{C}\right)\vec{\xi}_0 + \tilde{D}\right]_+ \\
\left(I - \frac{1}{c_j}\Lambda\right)\partial_t\vec{\xi}_0 + \Lambda\vec{\xi}_1 &= -\tilde{B}\partial_z\vec{\xi}_0 + \left(\tilde{B}\left(\partial_z R^{-1}\right) R + \tilde{C}\right)\vec{\xi}_0 + \tilde{D} \\
\left(I - \frac{1}{c_j}\Lambda\right)\partial_t\vec{\xi}_j + \Lambda\vec{\xi}_{j+1} &= -\tilde{B}\partial_z\vec{\xi}_j + \left(\tilde{B}\left(\partial_z R^{-1}\right) R + \tilde{C}\right)\vec{\xi}_j \ , \ j \in 1 \ldots J \\
\left[\vec{\varphi}_J\right. &= \left. 0\right]_- \ .
\end{aligned}
\tag{V.12}
$$

2.   Incompatibility with Zero Advection

Note that, because of the Λ on the left-hand side of (V.10b,c), all of the eigenvalues must be non-zero. Requiring the advection be subsonic is trivial; it can be a constraint of the model. But the case of zero advection is trickier. The answer is to define a "false" non-zero advection, small enough that there will be no drift from one point to an adjacent point over the duration of the simulation:

$$
\|u_0\| < \frac{\min(\delta x)}{2t_{max}} \ ,
\tag{V.13}
$$

where $\min(\delta x)$ is the smallest grid spacing in the x direction, and t_{max} is the duration of the simulation. If the false u_0 is too small, however, there is a risk that the resulting matrix could be numerically singular. Realistically, this concern is unfounded; we have seen experimentally (using Matlab) that the matrix A is not ill-conditioned so long as $\|u_0\| > 10^{-10}\frac{m}{s}$ (approximately an eighth of an inch per year).

J	E_ρ	E_u	E_v	E_p
1	0.15985	0.32103	0.13114	0.15985
2	0.1581	0.32249	0.12376	0.1581
3	0.15697	0.32307	0.12029	0.15697
4	0.15617	0.32308	0.11844	0.15617
5	0.15557	0.32274	0.11729	0.15557
6	0.15506	0.32218	0.11646	0.15506
7	0.15462	0.32151	0.11579	0.15462
8	0.15422	0.32077	0.1152	0.15422
9	0.15384	0.32	0.11465	0.15384
10	0.15347	0.3192	0.11413	0.15347

Table XV. Error norms for Givoli-Neta NRBCs in basic system (IV.1) with $J \in 1 \ldots 10$ in an infinite channel with no advection

3. Numerical Examples

Let us consider some numerical examples. In each example, we use our standard domain and initial condition in an infinite channel (Fig. 19). We first consider the basic case with no advection. Since we have to define a false advection on the boundary, we set

$$u_0 = \frac{\delta x}{3 t_{max}} \tag{V.14}$$

For this domain and simulation duration, that equates to $u_0 = 1.3889 \frac{\text{m}}{\text{s}}$. Furthermore, we set $c_j = 1$ for all j [23, 55], a simplification we will use for all subsequent derivations for these NRBCs. Table XV shows the state variable error norms for $J \in 1 \ldots 10$, Fig. 32 shows the state variable ρ for the $J = 10$ case, and Fig. 33 compares the state variable u for the $J = 1$ and $J = 10$ cases. We note that there is very little difference between the low-order and high-order results. This is a consequence of the characteristic-based approach [72] as well as a consequence of converting the normal derivative to tangential [36]. If we instead use a horizontal advection $u_0 = 100 \frac{\text{m}}{\text{s}}$, we get the results shown in Table XVI and Figs. 34 and 35.

If we incorporate Coriolis forces in this domain, we see that the Givoli-Neta NRBCs still produce valid results. Tables XVII and XVIII show the error norms for
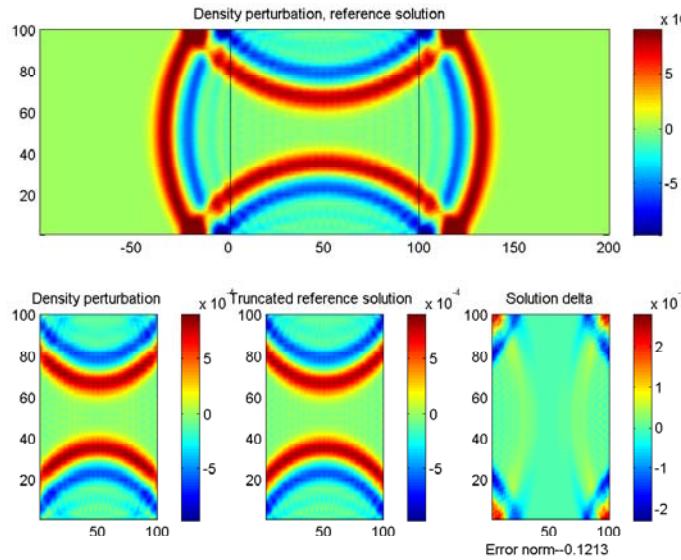
Figure 32. Plot of ρ for Givoli-Neta NRBCs in basic system (IV.1) with $J = 10$ in an infinite channel with no advection. (BL) Computed solution. (Top) Reference solution; the area corresponding to the computed solution is contained between the vertical lines. (BC) Reference solution truncated to computed solution domain. (BR) Delta between reference solution and computed solution, with error norm computed by (IV.14).

the state variables for the $u_0 = 0$ and $u_0 = 100$ cases, respectively. In the interest of brevity, we will omit any figures from these examples.

Similarly, incorporating gravity in the xz plane poses no additional difficulties *in this horizontal channel*, as shown in Tables XIX and XX. We will see in Sec. C how to deal with the effects of gravity on a vertical open boundary.

Interestingly, even though these error norms appear to decrease only slightly as J increases, we can see from a logarithmic plot that they do, in fact, decay exponentially. See Fig. 36 for a graphical representation of the values in Table XX.

J	E_ρ	E_u	E_v	E_p
1	0.1556	0.23218	0.15239	0.1556
2	0.15506	0.23139	0.15096	0.15506
3	0.15452	0.2306	0.14954	0.15452
4	0.15399	0.22982	0.14815	0.15399
5	0.15346	0.22904	0.14679	0.15346
6	0.15293	0.22827	0.14545	0.15293
7	0.1524	0.22751	0.14413	0.1524
8	0.15188	0.22674	0.14283	0.15188
9	0.15136	0.22599	0.14156	0.15136
10	0.15085	0.22523	0.1403	0.15085

Table XVI. Error norms for Givoli-Neta NRBCs in basic system (IV.1) with $J \in 1 \ldots 10$ in an infinite channel with left-to-right advection

J	E_ρ	E_u	E_v	E_p
1	0.12541	0.25444	0.1244	0.12541
2	0.12484	0.25298	0.11594	0.12484
3	0.12438	0.25176	0.11182	0.12438
4	0.12394	0.25063	0.10959	0.12394
5	0.12351	0.24953	0.10822	0.12351
6	0.12307	0.24843	0.10724	0.12307
7	0.12263	0.24734	0.10647	0.12263
8	0.12218	0.24626	0.10581	0.12218
9	0.12174	0.24518	0.10521	0.12174
10	0.1213	0.24411	0.10465	0.1213

Table XVII. Error norms for Givoli-Neta NRBCs in Coriolis-influenced system (IV.15) with $J \in 1 \ldots 10$ in an infinite channel with no advection

J	E_ρ	E_u	E_v	E_p
1	0.24986	0.6637	0.26511	0.24986
2	0.24943	0.66284	0.26447	0.24943
3	0.24901	0.662	0.26385	0.24901
4	0.2486	0.66119	0.26325	0.2486
5	0.24819	0.66039	0.26268	0.24819
6	0.24779	0.65961	0.26213	0.24779
7	0.2474	0.65886	0.2616	0.2474
8	0.24702	0.65812	0.26109	0.24702
9	0.24664	0.6574	0.2606	0.24664
10	0.24626	0.65669	0.26013	0.24627

Table XVIII. Error norms for Givoli-Neta NRBCs in Coriolis-influenced system (IV.15) with $J \in 1 \dots 10$ in an infinite channel with left-to-right advection

J	E_ρ	E_u	E_v	E_p
1	0.12998	0.25364	0.1265	0.1294
2	0.1294	0.25218	0.11796	0.12881
3	0.12893	0.25098	0.11379	0.12833
4	0.12849	0.24986	0.11152	0.12788
5	0.12804	0.24877	0.11012	0.12742
6	0.12758	0.24769	0.10913	0.12697
7	0.12713	0.24662	0.10835	0.12651
8	0.12667	0.24555	0.10768	0.12605
9	0.12621	0.24449	0.10707	0.1256
10	0.12575	0.24343	0.1065	0.12514

Table XIX. Error norms for Givoli-Neta NRBCs in gravity-influenced system (IV.31) with $J \in 1 \dots 10$ in an infinite channel with no advection
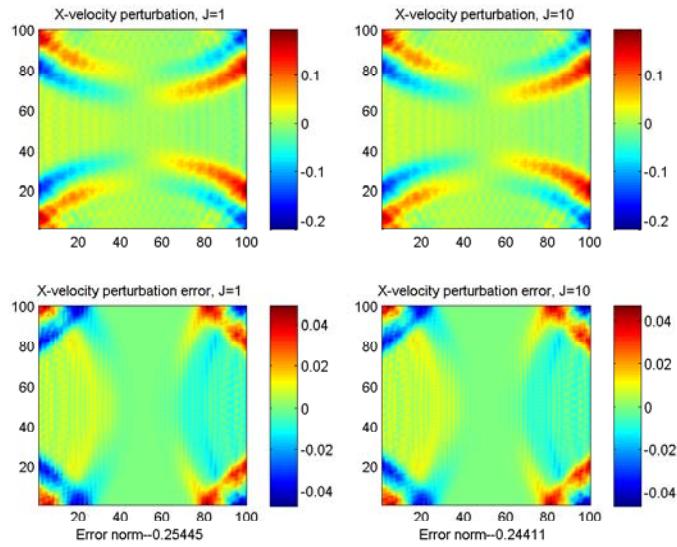
Figure 33. Comparison of u for Givoli-Neta NRBCs in basic system (IV.1) computed with $J = 1$ and $J = 10$ in an infinite channel with no advection, with error norms computed by (IV.14). (TL) Computed solution for $J = 1$. (TR) Computed solution for $J = 10$. (BL) Delta between reference solution and $J = 1$ computed solution. (BR) Delta between reference solution and $J = 10$ computed solution.

J	E_ρ	E_u	E_v	E_p
1	0.1402	0.20569	0.14568	0.13973
2	0.13959	0.20481	0.14417	0.13912
3	0.13899	0.20395	0.14269	0.13852
4	0.13839	0.20309	0.14123	0.13793
5	0.13779	0.20223	0.13979	0.13733
6	0.1372	0.20138	0.13837	0.13674
7	0.1366	0.20053	0.13698	0.13615
8	0.13601	0.19969	0.13561	0.13556
9	0.13543	0.19885	0.13426	0.13498
10	0.13484	0.19802	0.13293	0.1344

Table XX. Error norms for Givoli-Neta NRBCs in gravity-influenced system (IV.31) with $J \in 1 \ldots 10$ in an infinite channel with left-to-right advection
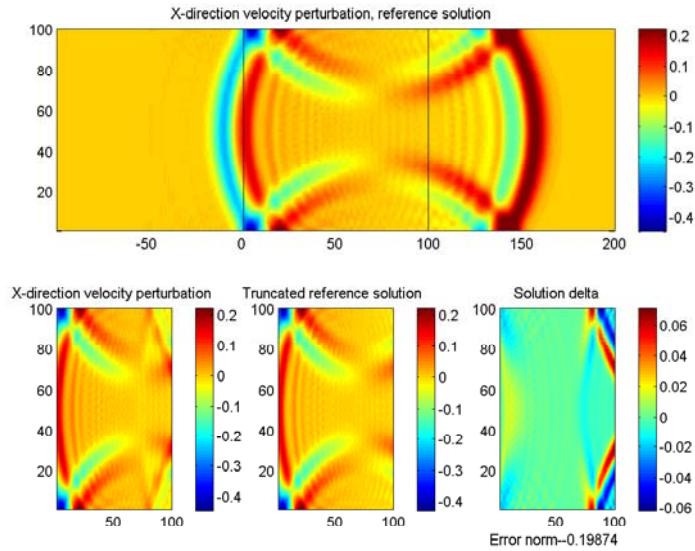
Figure 34. Plot of u for Givoli-Neta NRBCs in basic system (IV.1) with $J = 10$ in an infinite channel with left-to-right advection. (BL) Computed solution. (Top) Reference solution; the area corresponding to the computed solution is contained between the vertical lines. (BC) Reference solution truncated to computed solution domain. (BR) Delta between reference solution and computed solution, with error norm computed by (IV.14).
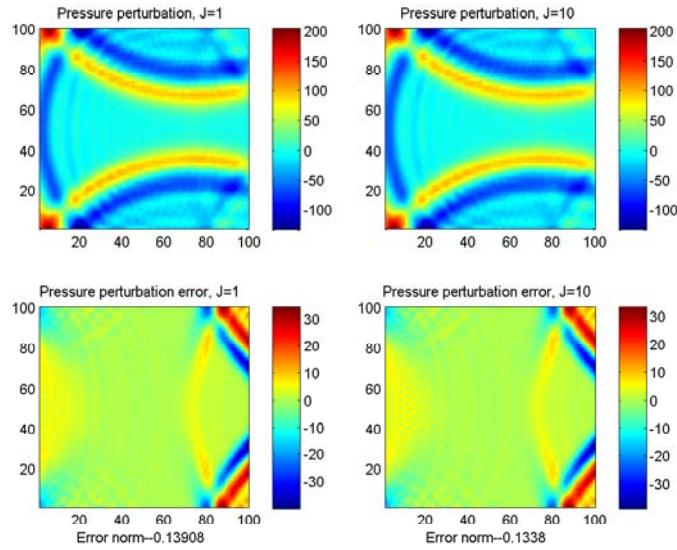
Figure 35. Comparison of p for Givoli-Neta NRBCs in basic system (IV.1) computed with $J = 1$ and $J = 10$ in an infinite channel with left-to-right advection, with error norms computed by (IV.14). (TL) Computed solution for $J = 1$. (TR) Computed solution for $J = 10$. (BL) Delta between reference solution and $J = 1$ computed solution. (BR) Delta between reference solution and $J = 10$ computed solution.
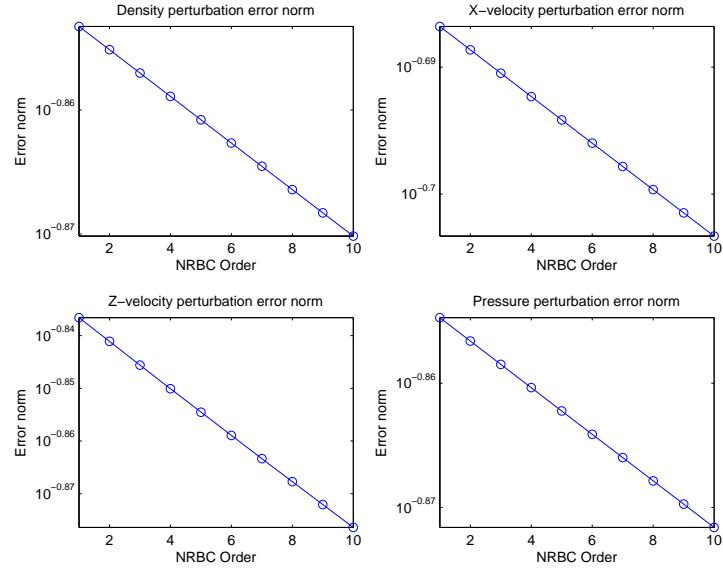
Figure 36. Logarithmic plot of state variable error norms (IV.14) for Givoli-Neta NRBCs applied to gravity-influenced system (IV.31) with $J \in 1 \ldots 10$ in an infinite channel with left-to-right advection. (TL) Error norms for ρ. (TR) Error norms for u. (BL) Error norms for w. (BR) Error norms for p.

95

B. CORNER CONDITIONS IN AN OPEN DOMAIN
1. Derivation

In an auxiliary variable NRBC scheme, the corner where two open boundaries intersect is a source of concern. Assuming the tangential derivatives are approximated with a centered-difference formula, points adjacent to the corner depend on the value at the corner. (This is not the case in a standard high-order NRBC such as the Higdon sequence, where there are no tangential derivatives and thus no dependence on the corner values, as we noted in Sec. IV.B.4.) So how should we treat this corner? Is it to be considered part of one boundary but not the other? Even so, we still have to use a different discretization scheme than that used elsewhere on the boundary. We propose here to treat the corner as if it were part of a curved boundary; define the normal derivative as the $45°$ vector bisecting the normal vector of the two adjacent sides (see Fig. 37). With this definition, we have for the top-left and top-right corners
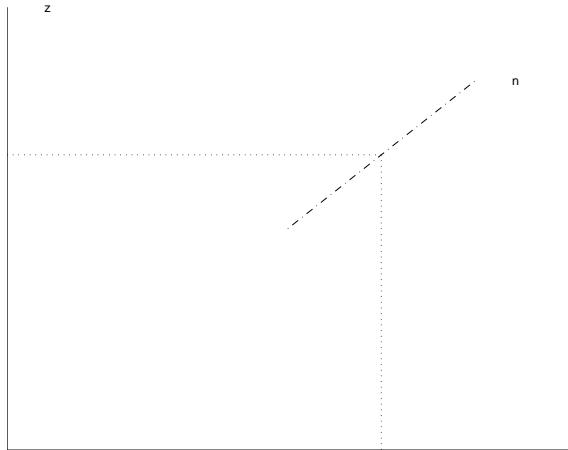
Figure 37. The "normal" derivative for the top-right corner of an open domain

of Fig. 22,

$$\text{Top-left: } \partial_n = \frac{-\partial_x + \partial_z}{\sqrt{2}}$$

$$\text{Top-right: } \partial_n = \frac{\partial_x + \partial_z}{\sqrt{2}}, \tag{V.15}$$

and the associated tangential derivatives are given by

$$\text{Top-left: } \partial_\tau = \frac{\partial_x + \partial_z}{\sqrt{2}}$$

$$\text{Top-right: } \partial_\tau = \frac{\partial_x - \partial_z}{\sqrt{2}} \ . \tag{V.16}$$

In order to derive our characteristic system for the auxiliary variables, we must rewrite (V.2) in terms of normal and tangential derivatives. It is straightforward to show that

$$\partial_t \vec{\varphi} + N \partial_n \vec{\varphi} + T \partial_\tau \vec{\varphi} = C \vec{\varphi} + \vec{D} \ , \tag{V.17}$$

where

$$\text{Top-left: } N = \frac{1}{\sqrt{2}}(-A + B)$$

$$T = \frac{1}{\sqrt{2}}(A + B)$$

$$\text{Top-right: } N = \frac{1}{\sqrt{2}}(A + B)$$

$$T = \frac{1}{\sqrt{2}}(A - B) \ . \tag{V.18}$$

With these definitions, it is easy to show that the characteristic NRBC system for each corner is given by

$$\begin{aligned}
\left[\partial_t \vec{\xi}_0 \right. &= \left. -\Lambda \partial_z \vec{\xi}_0 - \tilde{T} \partial_\tau \vec{\xi}_0 + \tilde{C} \vec{\xi}_0 + \tilde{D} \right]_+ \\
(I - \Lambda) \partial_t \vec{\xi}_j + \Lambda \vec{\xi}_{j+1} &= -\tilde{T} \partial_\tau \vec{\xi}_j + \tilde{C} \vec{\xi}_j \\
\left[\vec{\xi}_J \right. &= \left. 0 \right]_- ,
\end{aligned} \tag{V.19}$$

where

$$\begin{aligned}
\Lambda &= \operatorname{diag} \left(\begin{array}{cccc} n_0 + c_0 & n_0 & n_0 & n_0 - c_0 \end{array} \right)^T \\
\Lambda &= RNR^{-1} \\
\tilde{T} &= R^{-1}TR \ ,
\end{aligned} \tag{V.20}$$

and $\tilde{C}$ and $\tilde{D}$ defined as in (V.9). On the top-left corner, we have

$$n_0 = \frac{-u_0 + w_0}{\sqrt{2}}$$

$$\tau_0 = \frac{u_0 + w_0}{\sqrt{2}}$$

$$R = \begin{pmatrix} 1 & 1 & -1 & 1 \\ -\frac{c_0}{\sqrt{2}\rho_0} & 1 & 1 & \frac{c_0}{\sqrt{2}\rho_0} \\ \frac{c_0}{\sqrt{2}\rho_0} & 1 & 1 & -\frac{c_0}{\sqrt{2}\rho_0} \\ c_0^2 & 0 & 0 & c_0^2 \end{pmatrix}$$

$$R^{-1} = \begin{pmatrix} 0 & -\frac{\sqrt{2}\rho_0}{4c_0} & \frac{\sqrt{2}\rho_0}{4c_0} & \frac{1}{2c_0^2} \\ \frac{1}{2} & \frac{1}{4} & \frac{1}{4} & -\frac{1}{2c_0^2} \\ -\frac{1}{2} & \frac{1}{4} & \frac{1}{4} & \frac{1}{2c_0^2} \\ 0 & \frac{\sqrt{2}\rho_0}{4c_0} & -\frac{\sqrt{2}\rho_0}{4c_0} & -\frac{1}{2c_0^2} \end{pmatrix},$$

and on the top-right corner, we use

$$n_0 = \frac{u_0 + w_0}{\sqrt{2}}$$

$$\tau_0 = \frac{u_0 - w_0}{\sqrt{2}}$$

$$R = \begin{pmatrix} 1 & 1 & 1 & 1 \\ \frac{c_0}{\sqrt{2}\rho_0} & 1 & -1 & -\frac{c_0}{\sqrt{2}\rho_0} \\ \frac{c_0}{\sqrt{2}\rho_0} & -1 & 1 & -\frac{c_0}{\sqrt{2}\rho_0} \\ c_0^2 & 0 & 0 & c_0^2 \end{pmatrix}$$

$$R^{-1} = \begin{pmatrix} 0 & \frac{\sqrt{2}\rho_0}{4c_0} & \frac{\sqrt{2}\rho_0}{4c_0} & \frac{1}{2c_0^2} \\ \frac{1}{2} & \frac{1}{4} & -\frac{1}{4} & -\frac{1}{2c_0^2} \\ \frac{1}{2} & -\frac{1}{4} & \frac{1}{4} & -\frac{1}{2c_0^2} \\ 0 & -\frac{\sqrt{2}\rho_0}{4c_0} & -\frac{\sqrt{2}\rho_0}{4c_0} & -\frac{1}{2c_0^2} \end{pmatrix}.$$

In implementing the finite-difference approximations of ∂_τ, decompose it into its constituent ∂_x and ∂_z components. Use the Γ_T auxiliary variable for ∂_x, and use the Γ_L or Γ_R auxiliary variable for ∂_z, using one-sided differences. Note also that the eigenvalues of N must be non-zero. We can again use a "false" advection to get around this difficulty, if needed.

J	E_ρ	E_u	E_v	E_p
1	0.16986	0.20783	0.19382	0.16986
2	0.16904	0.20686	0.19168	0.16905
3	0.16823	0.20591	0.18957	0.16823
4	0.16742	0.20496	0.18749	0.16742
5	0.16661	0.20401	0.18545	0.16661
6	0.16581	0.20307	0.18344	0.16581
7	0.16501	0.20214	0.18146	0.16502
8	0.16422	0.20121	0.17951	0.16422
9	0.16343	0.20029	0.1776	0.16343
10	0.16265	0.19938	0.17571	0.16265

Table XXI. Error norms for Givoli-Neta NRBCs in basic system (IV.1) with $J \in 1 \ldots 10$ in an open half-plane with left-to-right advection

2. Numerical Examples

For simplicity, let us consider just one example of this open-air domain. We use our standard example with left-to-right advection with no inhomogeneous forces. We require a "false" vertical advection on the top boundary and at the corners; we use $w_0 = \frac{\delta z}{4 t_{max}} = 1.0417 \frac{m}{s}$. Table XXI and Fig. 38 show the error norms for the state variables for $J \in 1 \ldots 10$. Again, although the differences are small, they are nonetheless exponential.

C. GRAVITATIONAL EFFECTS
1. Derivation

Our claim that $L(\vec{\varphi}_j) = 0$ in the preceding section hinges on the fact that the coefficient matrices are constant in the direction of the normal derivative. However, this is not the case when we consider an NRBC on Γ_T in the presence of gravity. In that case, the coefficient terms A, B, C, and $\vec{D}$ all depend on z. Recall the differential operator $L(\vec{\varphi})$ defined in (V.3). We still have $L(\vec{\varphi}) = \vec{D}$ by definition, but what of the auxiliary variables? Since $L(\partial_z \vec{\varphi}) \neq \partial_z (L(\vec{\varphi}))$, we come up against the exception to Lemma V.1. A new derivation is needed. Apply the operator L to both sides of
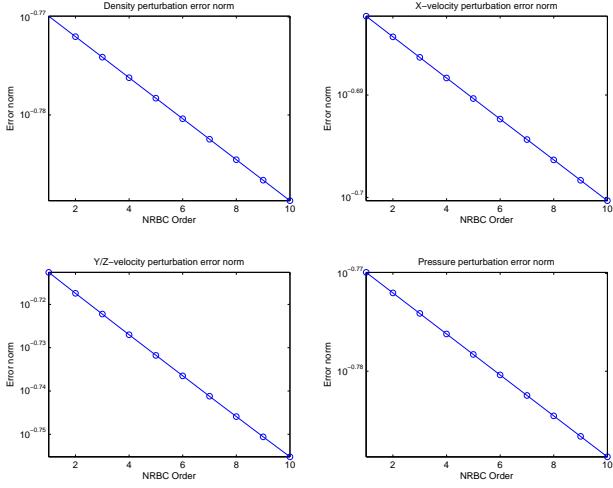
Figure 38. Logarithmic plot of state variable error norms (IV.14) for Givoli-Neta NRBCs applied to basic system (IV.1) with $J \in 1 \ldots 10$ in an open half-plane with left-to-right advection. (TL) Error norms for ρ. (TR) Error norms for u. (BL) Error norms for v. (BR) Error norms for p.

(V.1a, $j = 0$), and simplify

$$
\begin{aligned}
L(\vec{\varphi}_1) &= L(\partial_t \vec{\varphi}) + L(\partial_z \vec{\varphi}) \\
&= \begin{cases} [\partial_{tt}\vec{\varphi} + A\partial_{xt}\vec{\varphi} + B\partial_{zt}\vec{\varphi} - C\partial_t\vec{\varphi}] \\ + [\partial_{zt}\vec{\varphi} + A\partial_{xz}\vec{\varphi} + B\partial_{zz}\vec{\varphi} - C\partial_z\vec{\varphi}] \end{cases} \\
&= \begin{cases} \partial_t \left(\partial_t\vec{\varphi} + A\partial_x\vec{\varphi} + B\partial_z\vec{\varphi} - C\vec{\varphi} \right) \\ + \partial_z \left(\partial_t\vec{\varphi} + A\partial_x\vec{\varphi} + B\partial_z\vec{\varphi} - C\vec{\varphi} \right) \\ - (\partial_z A)\partial_x\vec{\varphi} - (\partial_z B)\partial_z\vec{\varphi} + (\partial_z C)\vec{\varphi} \end{cases} \\
&= \partial_t(L(\vec{\varphi})) + \partial_z(L(\vec{\varphi})) - (\partial_z A)\partial_x\vec{\varphi} - (\partial_z B)\partial_z\vec{\varphi} + (\partial_z C)\vec{\varphi} \\
&= \partial_t\vec{D} + \partial_z\vec{D} - (\partial_z A)\partial_x\vec{\varphi} - (\partial_z B)\partial_z\vec{\varphi} + (\partial_z C)\vec{\varphi} \\
L(\vec{\varphi}_1) &= -(\partial_z A)\partial_x\vec{\varphi} - (\partial_z B)\partial_z\vec{\varphi} + (\partial_z C)\vec{\varphi} + \partial_z\vec{D} \qquad\qquad \text{(V.21)}
\end{aligned}
$$

As we continue applying the operator L to successive $\vec{\varphi}_j$'s, this expression will result in ever-higher z-derivative terms, exactly the case we are trying to avoid. We need to define our reference states in such a way as to remove this difficulty. The most

effective approach is to use the exponentially-decaying atmospheric model (IV.32), given in Sec. IV.D.1.

We can rewrite the matrices A and B as the sum of a constant matrix and a z-dependent one:

$$
\begin{aligned}
A &= u_0 I + A_z \\
B &= w_0 I + B_z \ ,
\end{aligned}
\tag{V.22}
$$

where A_z and B_z are the z-dependent cells of A and B, respectively. Given these z-dependencies, and the definitions for $\bar{\rho}$ and $\bar{p}$, we have

$$
\begin{aligned}
\partial_z A &= -\alpha A_z \\
\partial_z B &= -\alpha B_z \\
\partial_z C &= -\alpha C \\
\partial_z \vec{D} &= -\alpha \vec{D} \ .
\end{aligned}
\tag{V.23}
$$

Continuing our derivation of $L(\vec{\varphi}_1)$ using these definitions, we have

$$
\begin{aligned}
L(\vec{\varphi}_1) &= \alpha A_z \partial_x \vec{\varphi} + \alpha B_z \partial_z \vec{\varphi} - \alpha C \vec{\varphi} - \alpha \vec{D} \\
&= \alpha \left(L(\vec{\varphi}) - \vec{D} - \partial_t \vec{\varphi} - u_0 \partial_x \vec{\varphi} - w_0 \partial_z \vec{\varphi} \right) \\
&= \alpha \left(\vec{D} - \vec{D} - \partial_t \vec{\varphi} - u_0 \partial_x \vec{\varphi} - w_0 \partial_z \vec{\varphi} \right) \\
&= -\alpha \left(\partial_t \vec{\varphi} + u_0 \partial_x \vec{\varphi} + w_0 \partial_z \vec{\varphi} \right) \\
L(\vec{\varphi}_1) &= -\alpha \partial_F \vec{\varphi} \ ,
\end{aligned}
\tag{V.24}
$$

where ∂_F denotes the Lagrangian derivative along the flow. If we continue this derivation for successive $\vec{\varphi}_j$ terms, we get

$$
\begin{aligned}
L(\vec{\varphi}_2) &= -2\alpha \partial_F \vec{\varphi}_1 - \alpha^2 \partial_F \vec{\varphi} \\
L(\vec{\varphi}_3) &= -3\alpha \partial_F \vec{\varphi}_2 - 3\alpha^2 \partial_F \vec{\varphi}_1 - \alpha^3 \partial_F \vec{\varphi}
\end{aligned}
\tag{V.25}
$$

etc.

This leads us to the following lemma:

101

Lemma V.2

$$L(\vec{\varphi}_j) = -\sum_{k=1}^{j} \binom{j}{k} \alpha^k \partial_F \vec{\varphi}_{j-k} \tag{V.26}$$

Proof. Having demonstrated it for the $j=1$ case, we now proceed by induction:

$$
\begin{aligned}
L(\vec{\varphi}_{j+1}) &= L(\partial_t \vec{\varphi}_j) + L(\partial_z \vec{\varphi}_j) && \text{(V.27a)} \\[4pt]
&= \partial_t(L(\vec{\varphi}_j)) + \partial_{zt}\vec{\varphi}_j + A\partial_{xz}\vec{\varphi}_j + B\partial_{zz}\vec{\varphi}_j - C\partial_z\vec{\varphi}_j && \text{(V.27b)} \\[4pt]
&= \begin{cases} \partial_t(L(\vec{\varphi}_j)) + \partial_z\left(\partial_t\vec{\varphi}_j + A\partial_x\vec{\varphi}_j + B\partial_z\vec{\varphi}_j - C\vec{\varphi}_j\right) \\ -(\partial_z A)\partial_x\vec{\varphi}_j - (\partial_z B)\partial_z\vec{\varphi}_j + (\partial_z C)\vec{\varphi}_j \end{cases} && \text{(V.27c)} \\[4pt]
&= \partial_t(L(\vec{\varphi}_j)) + \partial_z(L(\vec{\varphi}_j)) + \alpha A_z \partial_x\vec{\varphi}_j + \alpha B_z \partial_z\vec{\varphi}_j - \alpha C\vec{\varphi}_j && \text{(V.27d)} \\[4pt]
&= \begin{cases} \partial_t(L(\vec{\varphi}_j)) + \partial_z(L(\vec{\varphi}_j)) \\ +\alpha\left(L(\vec{\varphi}_j) - \partial_t\vec{\varphi}_j - u_0\partial_x\vec{\varphi}_j - w_0\partial_z\vec{\varphi}_j\right) \end{cases} && \text{(V.27e)} \\[4pt]
&= \partial_t(L(\vec{\varphi}_j)) + \partial_z(L(\vec{\varphi}_j)) + \alpha L(\vec{\varphi}_j) - \alpha\partial_F\vec{\varphi}_j && \text{(V.27f)} \\[4pt]
&= \begin{cases} \partial_t\left(-\sum_{k=1}^{j}\binom{j}{k}\alpha^k\partial_F\vec{\varphi}_{j-k}\right) + \partial_z\left(-\sum_{k=1}^{j}\binom{j}{k}\alpha^k\partial_F\vec{\varphi}_{j-k}\right) \\ +\alpha\left(-\sum_{k=1}^{j}\binom{j}{k}\alpha^k\partial_F\vec{\varphi}_{j-k}\right) - \alpha\partial_F\vec{\varphi}_j \end{cases} && \text{(V.27g)} \\[4pt]
&= -\sum_{k=1}^{j}\binom{j}{k}\alpha^k\partial_F\left(\partial_t\vec{\varphi}_{j-k} + \partial_z\vec{\varphi}_{j-k}\right) - \sum_{k=0}^{j}\binom{j}{k}\alpha^{k+1}\partial_F\vec{\varphi}_{j-k} && \text{(V.27h)} \\[4pt]
&= -\sum_{k=1}^{j}\binom{j}{k}\alpha^k\partial_F\vec{\varphi}_{j+1-k} - \sum_{k=1}^{j+1}\binom{j}{k-1}\alpha^k\partial_F\vec{\varphi}_{j+1-k} && \text{(V.27i)} \\[4pt]
&= -\sum_{k=1}^{j}\left(\binom{j}{k} + \binom{j}{k-1}\right)\alpha^k\partial_F\vec{\varphi}_{j+1-k} - \alpha^{j+1}\partial_F\vec{\varphi} && \text{(V.27j)} \\[4pt]
&= -\sum_{k=1}^{j}\binom{j+1}{k}\alpha^k\partial_F\vec{\varphi}_{j+1-k} - \alpha^{j+1}\partial_F\vec{\varphi} && \text{(V.27k)} \\[4pt]
L(\vec{\varphi}_{j+1}) &= -\sum_{k=1}^{j+1}\binom{j+1}{k}\alpha^k\partial_F\vec{\varphi}_{j+1-k} \quad\square && \text{(V.28)}
\end{aligned}
$$

We can now use this $L(\vec{\varphi})$ to remove the normal derivative terms. Proceeding with each $\vec{\varphi}_j$ in succession, we first have

$$B\partial_z\vec{\varphi} = -\partial_t\vec{\varphi} - A\partial_x\vec{\varphi} + C\vec{\varphi} + \vec{D} \ . \tag{V.29}$$

Next, we have

$$L(\vec{\varphi}_1) \equiv \partial_t\vec{\varphi}_1 + A\partial_x\vec{\varphi}_1 + B\partial_z\vec{\varphi}_1 - C\vec{\varphi}_1 = -\alpha\partial_F\vec{\varphi} \ , \tag{V.30}$$

102

which we combine with (V.29) to get

$$
\begin{aligned}
B\partial_z\vec{\varphi}_1 &= -\partial_t\vec{\varphi}_1 - A\partial_x\vec{\varphi}_1 + C\vec{\varphi}_1 - \alpha\partial_t\vec{\varphi} - \alpha u_0\partial_x\vec{\varphi} - \alpha w_0\partial_z\vec{\varphi} \\
&= \begin{cases} -\partial_t\vec{\varphi}_1 - A\partial_x\vec{\varphi}_1 + C\vec{\varphi}_1 - \alpha\left(I - w_0B^{-1}\right)\partial_t\vec{\varphi} \\ -\alpha\left(u_0I - w_0B^{-1}A\right)\partial_x\vec{\varphi} - \alpha w_0B^{-1}\left(C\vec{\varphi} + \vec{D}\right) . \end{cases}
\end{aligned} \tag{V.31}
$$

Lemma V.3

$$
B\partial_z\vec{\varphi}_j = \begin{cases} -\partial_t\vec{\varphi}_j - A\partial_x\vec{\varphi}_j + C\vec{\varphi}_j - \sum_{k=1}^{j}\binom{j}{k}\alpha^k P_k\left[\left(I - w_0B^{-1}\right)\partial_t\vec{\varphi}_{j-k}\right. \\ \left.+ \left(u_0I - w_0B^{-1}A\right)\partial_x\vec{\varphi}_{j-k} + w_0B^{-1}C\vec{\varphi}_{j-k}\right] \\ -\alpha^j P_j w_0 B^{-1}\vec{D} , \end{cases} \tag{V.32}
$$

for all $j \geq 1$, where the polynomial sequence P_j is defined recursively by

$$
P_j\left(w_0B^{-1}\right) = I - \sum_{k=1}^{j-1}\binom{j}{k}w_0B^{-1}P_k\left(w_0B^{-1}\right) . \tag{V.33}
$$

Proof. As with the preceding lemma, having demonstrated the $j = 1$ case, we proceed by induction:

$$
\begin{aligned}
L(\vec{\varphi}_{j+1}) &\equiv \partial_t\vec{\varphi}_{j+1} + A\partial_x\vec{\varphi}_{j+1} + B\partial_z\vec{\varphi}_{j+1} - C\vec{\varphi}_{j+1} \\
&= -\sum_{k=1}^{j+1}\binom{j+1}{k}\alpha^k\partial_F\vec{\varphi}_{j+1-k}
\end{aligned} \tag{V.34}
$$

$$
B\partial_z\vec{\varphi}_{j+1} = \underbrace{-\partial_t\vec{\varphi}_{j+1} - A\partial_x\vec{\varphi}_{j+1} + C\vec{\varphi}_{j+1}}_{\Phi(\vec{\varphi}_{j+1})} - \sum_{k=1}^{j+1}\binom{j+1}{k}\alpha^k\partial_F\vec{\varphi}_{j+1-k} \tag{V.35a}
$$

$$
= \Phi(\vec{\varphi}_{j+1}) - \sum_{k=1}^{j+1}\binom{j+1}{k}\alpha^k\left(\partial_t + u_0\partial_x + w_0\partial_z\right)\vec{\varphi}_{j+1-k} \tag{V.35b}
$$

$$
= \begin{cases} \Phi(\vec{\varphi}_{j+1}) - \sum_{k=1}^{j}\binom{j+1}{k}\alpha^k\left(\partial_t\vec{\varphi}_{j+1-k} + u_0\partial_x\vec{\varphi}_{j+1-k}\right. \\ +w_0B^{-1}\left\{-\partial_t\vec{\varphi}_{j+1-k} - A\partial_x\vec{\varphi}_{j+1-k} + C\vec{\varphi}_{j+1-k}\right. \\ -\sum_{l=1}^{j+1-k}\binom{j+1-k}{l}\alpha^l P_l\left[\left(I - w_0B^{-1}\right)\partial_t\vec{\varphi}_{j+1-k-l}\right. \\ \left.+ \left(u_0I - w_0B^{-1}A\right)\partial_x\vec{\varphi}_{j+1-k-l} + w_0B^{-1}C\vec{\varphi}_{j+1-k-l}\right] \\ \left.-\alpha^{j+1-k}P_{j+1-k}w_0B^{-1}\vec{D}\right\}\big) - \alpha^{j+1}\left(\partial_t\vec{\varphi} + u_0\partial_x\vec{\varphi}\right. \\ \left.+w_0B^{-1}\left(-\partial_t\vec{\varphi} - A\partial_x\vec{\varphi} + C\vec{\varphi} + \vec{D}\right)\right)\big) \end{cases} \tag{V.35c}
$$

$$
B\partial_z\vec\varphi_{j+1} \;=\;
\begin{cases}
\begin{aligned}
&\Phi(\vec\varphi_{j+1}) - \sum_{k=1}^{j}\binom{j+1}{k}\alpha^k\left[(I - w_0 B^{-1})\,\partial_t\vec\varphi_{j+1-k}\right.\\
&\left.+ (u_0 I - w_0 B^{-1}A)\,\partial_x\vec\varphi_{j+1-k} + w_0 B^{-1}C\vec\varphi_{j+1-k}\right]\\
&+ w_0 B^{-1}\sum_{k=1}^{j}\binom{j+1}{k}\alpha^k\sum_{l=1}^{j+1-k}\binom{j+1-k}{l}\alpha^l P_l\left[(I - w_0 B^{-1})\,\partial_t\vec\varphi_{j+1-k-l}\right.\\
&\left.+ (u_0 I - w_0 B^{-1}A)\,\partial_x\vec\varphi_{j+1-k-l} + w_0 B^{-1}C\vec\varphi_{j+1-k-l}\right]\\
&+ w_0 B^{-1}\sum_{k=1}^{j}\binom{j+1}{k}\alpha^{j+1}P_{j+1-k}w_0 B^{-1}\vec D - \alpha^{j+1}\left((I - w_0 B^{-1})\,\partial_t\vec\varphi\right.\\
&\left.+ (u_0 I - w_0 B^{-1}A)\,\partial_x\vec\varphi + w_0 B^{-1}\left(C\vec\varphi + \vec D\right)\right)
\end{aligned}
\end{cases}
\tag{V.35d}
$$

$$
B\partial_z\vec\varphi_{j+1} \;=\;
\begin{cases}
\begin{aligned}
&\Phi(\vec\varphi_{j+1}) - \sum_{k=1}^{j+1}\binom{j+1}{k}\alpha^k\left[(I - w_0 B^{-1})\,\partial_t\vec\varphi_{j+1-k}\right.\\
&\left.+ (u_0 I - w_0 B^{-1}A)\,\partial_x\vec\varphi_{j+1-k} + w_0 B^{-1}C\vec\varphi_{j+1-k}\right]\\
&+ w_0 B^{-1}\sum_{k=1}^{j}\sum_{l=1}^{j+1-k}\binom{j+1}{k}\binom{j+1-k}{l}\alpha^{k+l}P_l\left[(I - w_0 B^{-1})\,\partial_t\vec\varphi_{j+1-k-l}\right.\\
&\left.+ (u_0 I - w_0 B^{-1}A)\,\partial_x\vec\varphi_{j+1-k-l} + w_0 B^{-1}C\vec\varphi_{j+1-k-l}\right]\\
&- \alpha^{j+1}\left(I - \sum_{k=1}^{j}\binom{j+1}{k}w_0 B^{-1}P_{j+1-k}\right)w_0 B^{-1}\vec D\ .
\end{aligned}
\end{cases}
\tag{V.36}
$$

Since the binomial coefficients are symmetric, we can replace P_{j+1-k} with P_k in the last line of the previous equation. The terms in the final group of parentheses are thus P_{j+1} by definition. As a temporary shorthand, let

$$
\begin{aligned}
\Theta(\vec\varphi_{j+1-k-l}) &\equiv
\begin{cases}
(I - w_0 B^{-1})\,\partial_t\vec\varphi_{j+1-k-l}\\
\quad + (u_0 I - w_0 B^{-1}A)\,\partial_x\vec\varphi_{j+1-k-l} + w_0 B^{-1}C\vec\varphi_{j+1-k-l}
\end{cases}\\
\Omega &\equiv \alpha^{j+1}P_{j+1}w_0 B^{-1}\vec D\ .
\end{aligned}
$$

This gives us

$$
B\partial_z\vec\varphi_{j+1} =
\begin{cases}
\begin{aligned}
&\Phi(\vec\varphi_{j+1}) - \sum_{k=1}^{j+1}\binom{j+1}{k}\alpha^k\left[(I - w_0 B^{-1})\,\partial_t\vec\varphi_{j+1-k}\right.\\
&\left.+ (u_0 I - w_0 B^{-1}A)\,\partial_x\vec\varphi_{j+1-k} + w_0 B^{-1}C\vec\varphi_{j+1-k}\right]\\
&+ w_0 B^{-1}\sum_{k=1}^{j}\sum_{l=1}^{j+1-k}\binom{j+1}{k}\binom{j+1-k}{l}\alpha^{k+l}P_l\Theta(\vec\varphi_{j+1-k-l}) - \Omega\ .
\end{aligned}
\end{cases}
\tag{V.37}
$$

We would like to replace the double summation with one in terms of α^k rather than α^{k+l}. Let $r = k + l$. Looking at the values assumed by $k + l$ and l, and recognizing that $l < k + l$ by definition, we can rewrite this double summation as

$$
\sum_{r=1}^{j+1}\sum_{l=1}^{r-1}\binom{j+1}{r-l}\binom{j+1-(r-l)}{l}\alpha^r P_l\Theta(\vec\varphi_{j+1-r})\ .
$$

A quick check shows that, not only are the indices mapped correctly, we also have the correct number of terms in the new summation:

$$\sum_{k=1}^{j}\sum_{l=1}^{j+1-k}1=\sum_{r=1}^{j+1}\sum_{l=1}^{r-1}1=\frac{j(j+1)}{2}\;.$$

Also, we can simplify the binomial expansions by

$$\binom{j+1}{r-l}\binom{j+1-(r-l)}{l}=\binom{j+1}{r}\binom{r}{l}$$

Returning to our derivation, and reverting r back to k, we have

$$B\partial_z\vec{\varphi}_{j+1} \;=\; \begin{cases} \Phi(\vec{\varphi}_{j+1})-\sum_{k=1}^{j+1}\binom{j+1}{k}\alpha^k\left[(I-w_0B^{-1})\,\partial_t\vec{\varphi}_{j+1-k}\right.\\ +\left.(u_0I-w_0B^{-1}A)\,\partial_x\vec{\varphi}_{j+1-k}+w_0B^{-1}C\vec{\varphi}_{j+1-k}\right]\\ +w_0B^{-1}\sum_{k=1}^{j+1}\sum_{l=1}^{k-1}\binom{j+1}{k}\binom{k}{l}\alpha^kP_l\Theta(\vec{\varphi}_{j+1-k})-\Omega \end{cases} \quad\text{(V.38a)}$$

$$=\; \begin{cases} \Phi(\vec{\varphi}_{j+1})-\sum_{k=1}^{j+1}\binom{j+1}{k}\alpha^k\Theta(\vec{\varphi}_{j+1-k})\\ +w_0B^{-1}\sum_{k=1}^{j+1}\sum_{l=1}^{k-1}\binom{j+1}{k}\binom{k}{l}\alpha^kP_l\Theta(\vec{\varphi}_{j+1-k})-\Omega \end{cases} \quad\text{(V.38b)}$$

$$=\; \begin{cases} \Phi(\vec{\varphi}_{j+1})\\ -\sum_{k=1}^{j+1}\binom{j+1}{k}\alpha^k\left(I-\sum_{l=1}^{k-1}\binom{k}{l}w_0B^{-1}P_l\right)\Theta(\vec{\varphi}_{j+1-k})-\Omega \end{cases} \quad\text{(V.38c)}$$

$$=\; \Phi(\vec{\varphi}_{j+1})-\sum_{k=1}^{j+1}\binom{j+1}{k}\alpha^kP_k\Theta(\vec{\varphi}_{j+1-k})-\Omega \quad\text{(V.38d)}$$

$$B\partial_z\vec{\varphi}_{j+1} \;=\; \begin{cases} -\partial_t\vec{\varphi}_{j+1}-A\partial_x\vec{\varphi}_{j+1}+C\vec{\varphi}_{j+1}\\ -\sum_{k=1}^{j+1}\binom{j+1}{k}\alpha^kP_k\left[(I-w_0B^{-1})\,\partial_t\vec{\varphi}_{j+1-k}\right.\\ +\left.(u_0I-w_0B^{-1}A)\,\partial_x\vec{\varphi}_{j+1-k}+w_0B^{-1}C\vec{\varphi}_{j+1-k}\right]\\ -\alpha^{j+1}P_{j+1}w_0B^{-1}\vec{D}\;\square \end{cases} \quad\text{(V.39)}$$

We are now able to remove the normal derivative terms from the auxiliary variable equations. The auxiliary variable formulation for Γ_T is

$$\vec{\varphi}_{j+1} \;=\; (\partial_t+\partial_z)\,\vec{\varphi}_j \quad\text{(V.40)}$$

$$\vec{\varphi}_0 \;\equiv\; \vec{\varphi}$$

$$\vec{\varphi}_J \;\equiv\; 0\;.$$

Using our formula for $\partial_z \vec{\varphi}_j$, we have

$$\vec{\varphi}_{j+1} = \begin{cases} \partial_t \vec{\varphi}_j + B^{-1} \left\{ -\partial_t \vec{\varphi}_j - A\partial_x \vec{\varphi}_j + C\vec{\varphi}_j \right. \\[2mm] \quad - \sum_{k=1}^{j} \binom{j}{k} \alpha^k P_k \left[(I - w_0 B^{-1}) \partial_t \vec{\varphi}_{j-k} \right. \\[2mm] \quad \left. + (u_0 I - w_0 B^{-1} A) \partial_x \vec{\varphi}_{j-k} + w_0 B^{-1} C \vec{\varphi}_{j-k} \right] \\[2mm] \quad \left. - \alpha^j P_j w_0 B^{-1} \vec{D} \right\} \ . \end{cases} \tag{V.41}$$

Collecting all ∂_t terms on the left-hand side with the $\vec{\varphi}_{j+1}$ term, leaving all the other terms on the right-hand side, and left-multiplying everything by B, we have

$$\left. \begin{array}{l} \sum_{k=1}^{j} \binom{j}{k} \alpha^k P_k \left(I - w_0 B^{-1}\right) \partial_t \vec{\varphi}_{j-k} \\[2mm] \quad + (I - B) \partial_t \vec{\varphi}_j + B\vec{\varphi}_{j+1} \end{array} \right\} = \begin{cases} -A\partial_x \vec{\varphi}_j + C\vec{\varphi}_j \\[2mm] \quad - \sum_{k=1}^{j} \binom{j}{k} \alpha^k P_k \left[(u_0 I - w_0 B^{-1} A) \partial_x \vec{\varphi}_{j-k} \right. \\[2mm] \quad \left. + w_0 B^{-1} C \vec{\varphi}_{j-k} \right] - \alpha^j P_j w_0 B^{-1} \vec{D} \ . \end{cases} \tag{V.42}$$

In characteristic form, we left-multiply both sides by R^{-1} and insert RR^{-1} as needed to get

$$\left. \begin{array}{l} \sum_{k=1}^{j} \binom{j}{k} \alpha^k \tilde{P}_k \left(I - w_0 \Lambda^{-1}\right) \partial_t \vec{\xi}_{j-k} \\[2mm] \quad + (I - \Lambda) \partial_t \vec{\xi}_j + \Lambda \vec{\xi}_{j+1} \end{array} \right\} = \begin{cases} -\tilde{A}\partial_x \vec{\xi}_j + \tilde{C}\vec{\xi}_j \\[2mm] \quad - \sum_{k=1}^{j} \binom{j}{k} \alpha^k \tilde{P}_k \left[\left(u_0 I - w_0 \Lambda^{-1} \tilde{A}\right) \partial_x \vec{\xi}_{j-k} \right. \\[2mm] \quad \left. + w_0 \Lambda^{-1} \tilde{C} \vec{\xi}_{j-k} \right] - \alpha^j \tilde{P}_j w_0 \Lambda^{-1} \tilde{D} \ , \end{cases} \tag{V.43}$$

for $j \in 1, 2, \ldots, J - 1$, where

$$\Lambda = \mathrm{diag} \left(\begin{array}{cccc} w_0 + c_0 & w_0 & w_0 & w_0 - c_0 \end{array} \right)^T$$

$$R = \begin{pmatrix} \frac{\bar{\rho}}{c_0} & 1 & 1 & -\frac{\bar{\rho}}{c_0} \\[2mm] 0 & -1 & 1 & 0 \\[2mm] 1 & 0 & 0 & 1 \\[2mm] \bar{\rho}c_0 & 0 & 0 & -\bar{\rho}c_0 \end{pmatrix}$$

$$R^{-1} = \begin{pmatrix} 0 & 0 & \frac{1}{2} & \frac{1}{2\bar{\rho}c_0} \\[2mm] \frac{1}{2} & -\frac{1}{2} & 0 & -\frac{1}{2c_0^2} \\[2mm] \frac{1}{2} & \frac{1}{2} & 0 & -\frac{1}{2c_0^2} \\[2mm] 0 & 0 & \frac{1}{2} & -\frac{1}{2\bar{\rho}c_0} \end{pmatrix}$$

$$\tilde{A} = R^{-1}AR$$

$$\tilde{P}_j = R^{-1}P_j R \qquad \text{(V.44)}$$

and $\vec{\xi}_j$, $\tilde{C}$, and $\tilde{D}$ are defined as in (V.9). As with the simple case, we use natural boundary conditions for the outgoing characteristics and the truncation condition for the incoming. Hence, our auxiliary variable system is

$$\left[\partial_t\vec{\xi}_0\right] = \begin{cases} -\Lambda\partial_z\vec{\xi}_0 - \tilde{A}\partial_x\vec{\xi}_0 + \left(\Lambda(\partial_z R^{-1})R \right. \\ \left. +\tilde{C}\right)\vec{\xi}_0 + \tilde{D}\Big]_+ \end{cases}$$

$$(I - \Lambda)\partial_t\vec{\xi}_0 + \Lambda\vec{\xi}_1 = -\tilde{A}\partial_x\vec{\xi}_0 + \tilde{C}\vec{\xi}_0 + \tilde{D}$$

$$\left.\begin{array}{r}\sum_{k=1}^{j}\binom{j}{k}\alpha^k\tilde{P}_k\left(I - w_0\Lambda^{-1}\right)\partial_t\vec{\xi}_{j-k} \\ + (I - \Lambda)\partial_t\vec{\xi}_j + \Lambda\vec{\xi}_{j+1}\end{array}\right\} = \begin{cases} -\tilde{A}\partial_x\vec{\xi}_j + \tilde{C}\vec{\xi}_j \\ -\sum_{k=1}^{j}\binom{j}{k}\alpha^k\tilde{P}_k\Big[(u_0 I \\ -w_0\Lambda^{-1}\tilde{A})\partial_x\vec{\xi}_{j-k} \\ +w_0\Lambda^{-1}\tilde{C}\vec{\xi}_{j-k}\Big] - \alpha^j\tilde{P}_j w_0\Lambda^{-1}\tilde{D} \end{cases}$$

$$\left[\vec{\xi}_J = 0\right]_- , \qquad \text{(V.45)}$$

where we again use the $+$ and $-$ subscripts to denote outgoing and incoming characteristics, respectively. Note also that, in order to have the $\partial_z\vec{\xi}_0$ term in the first equation, we use the product rule and the z-dependence of R^{-1}:

$$\partial_z\vec{\xi}_0 = \partial_z\left(R^{-1}\vec{\varphi}_0\right) = R^{-1}\partial_z\vec{\varphi}_0 + \left(\partial_z R^{-1}\right)\vec{\varphi}_0 .$$

In the absence of gravity, $\alpha = 0$, and (V.45) is analogous to (V.10).

We lose some computational efficiency with this implementation. Eq. (V.10) defined a bi-diagonal matrix system, which requires $O(J)$ operations per time step with an efficient matrix solver. On the other hand, (V.45) is lower-Hessenberg and requires $O(J^2)$ operations per time step.

When we extend this derivation to the open domains defined in the previous section, we get the following system using N and T instead of A and B (compare to (V.19)):

$$\left[\partial_t\vec{\xi}\right] = \begin{cases} -\Lambda\partial_n\vec{\xi} - \tilde{T}\partial_\tau\vec{\xi} + \left(\Lambda\left(\partial_n R^{-1}\right)R \right. \\ \left. +\tilde{T}\left(\partial_\tau R^{-1}\right)R + \tilde{C}\right)\vec{\xi} + \tilde{D}\Big]_+ \end{cases}$$

$$(I - \Lambda)\, \partial_t \vec{\xi}_0 + \Lambda \vec{\xi}_1 \;=\; -\tilde{T}\left(\partial_\tau \vec{\xi}_0 - \left(\partial_\tau R^{-1}\right) R \vec{\xi}_0\right) + \tilde{C}\vec{\xi}_0 + \tilde{D}$$

$$\left.\begin{array}{c} \sum_{k=1}^{j} \binom{j}{k} \tilde{\alpha}^k \tilde{P}_k \left(I - n_0 \Lambda^{-1}\right) \partial_t \vec{\xi}_{j-k} \\[2mm] + (I - \Lambda)\, \partial_t \vec{\xi}_j + \Lambda \vec{\varphi}_{j+1} \end{array}\right\} \;=\; \left\{\begin{array}{l} -\tilde{T}\left(\partial_\tau \vec{\xi}_j - \left(\partial_\tau R^{-1}\right) R \vec{\xi}_j\right) + \tilde{C}\vec{\xi}_j \\[2mm] -\sum_{k=1}^{j} \binom{j}{k} \tilde{\alpha}^k \tilde{P}_k \big[\left(\tau_0 I\right. \\[2mm] \left. -n_0 \Lambda^{-1} \tilde{T}\right)\left(\partial_\tau \vec{\xi}_{j-k} - \left(\partial_\tau R^{-1}\right) R \vec{\xi}_{j-k}\right) \\[2mm] +n_0 \Lambda^{-1} \tilde{C}\vec{\xi}_{j-k}\big] - \tilde{\alpha}^j \tilde{P}_j n_0 \Lambda^{-1} \tilde{D} \end{array}\right.$$

$$\left[\vec{\xi}_J \;=\; 0\right]_- \,, \qquad\qquad\qquad (V.46)$$

where

$$P_k \;\equiv\; P_k\left(n_0 N^{-1}\right)$$

$$\Lambda \;=\; \mathrm{diag}\left(\begin{array}{cccc} n_0 + c_0 & n_0 & n_0 & n_0 - c_0 \end{array}\right)^T$$

$$N \;=\; R^{-1}\Lambda R$$

$$\tilde{T} \;=\; R^{-1}TR$$

$$\tilde{\alpha} \;=\; \frac{\alpha}{\sqrt{2}} \,.$$

In addition, we must replace ρ_0 in the eigenvector matrices R and R^{-1} with the z-dependent $\bar{\rho}$.

About the Polynomial Sequence. A quick literature search [2, 60, 103, 118] revealed no matches to the polynomial sequence

$$P_n(x) = 1 - \sum_{k=1}^{n-1} \binom{n}{k} x P_k(x) \,.$$

The first five polynomials of this sequence are

$$P_1 \;=\; 1$$

$$P_2 \;=\; 1 - 2x$$

$$P_3 \;=\; 1 - 6x + 6x^2$$

$$P_4 \;=\; 1 - 14x + 36x^2 - 24x^3$$

$$P_5 \;=\; 1 - 30x + 150x^2 - 240x^3 + 120x^4 \,.$$

The first three are constant multiples of the Bernoulli polynomials [103], but not the subsequent ones. We have not found any other matches to this sequence. However,

Dr. Pante Stănică at the Naval Postgraduate School observed [104] that the coefficients of P_n can be generated directly, without use of the recursion sequence, by the formula

$$P_n = \sum_{k=1}^{n} (-1)^{k+1} k! \begin{Bmatrix} n \\ k \end{Bmatrix} x^{k-1} \ , \tag{V.47}$$

where $\begin{Bmatrix} n \\ k \end{Bmatrix}$ denotes the Stirling number of the second kind [46]. Other properties of these polynomials, such as orthogonality and a generating function, may be explored in future research.

2. Numerical Examples

Let us consider a few numerical examples, using our standard simulation. First, we look briefly at the system in a semi-infinite channel, open on top (see Fig. 6), subject to gravitational forces. There is no real advection, but we define our false boundary advection $w_0 = \frac{\delta z}{4t_{max}} = 1.0417\frac{m}{s}$ to keep the matrices non-singular. Table XXII shows the error norms resulting from the cases $J \in 1\ldots10$.

J	E_ρ	E_u	E_v	E_p
1	0.073179	0.08778	0.11305	0.049617
2	0.073086	0.087435	0.11249	0.04944
3	0.07298	0.08704	0.11197	0.049261
4	0.072874	0.086646	0.11146	0.049083
5	0.07277	0.086255	0.11095	0.048907
6	0.072667	0.085866	0.11045	0.048732
7	0.072565	0.08548	0.10995	0.048558
8	0.072464	0.085096	0.10945	0.048386
9	0.072364	0.084716	0.10896	0.048215
10	0.072264	0.084337	0.10848	0.048046
Som.	0.092721	0.10278	0.22495	0.092238

Table XXII. Error norms (IV.14) for Givoli-Neta NRBCs, $J \in 1\ldots10$, gravity-influenced system (IV.31), semi-infinite vertical channel, no advection. The error norm from using a Sommerfeld boundary condition is included for comparison.

Next, we consider the open-air domain (Fig. 22). We begin first with "zero" advection (false boundary advection $u_0 = \frac{\delta x}{3t_{max}} = 1.3889\frac{m}{s}$, $w_0 = \frac{\delta z}{4t_{max}} = 1.0417\frac{m}{s}$,

chosen so that $u_0 \neq w_0$ to keep N non-singular). Fig. 39 shows the state variable p at the end of the run for $J = 10$. Table XXIII shows the error norms (IV.14) for each
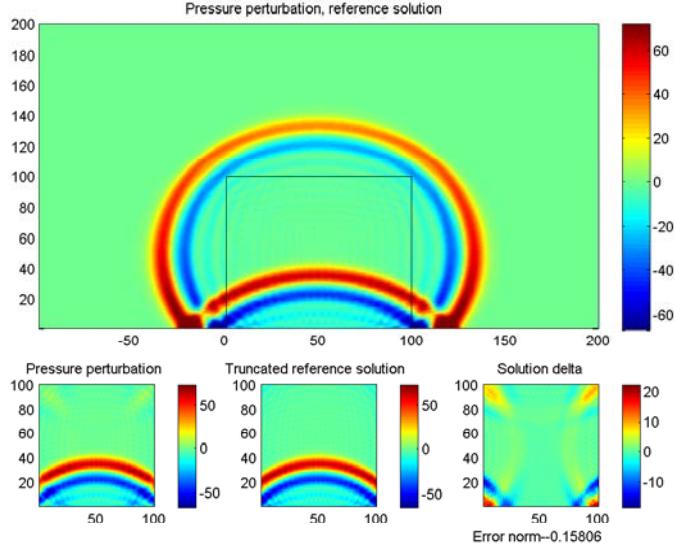
Figure 39. The solution for the pressure perturbation p using $J = 10$, Givoli-Neta NRBCs in an open half-plane subject to gravitational forces with no advection. (Top) Reference solution; the area corresponding to the computed solution is contained in the bottom-center box. (BL) Computed solution using NRBCs. (BC) Reference solution domain corresponding to NRBC solution domain. (BR) Delta between computed and reference solutions, with error norm computed by (IV.14).

state variable as J goes from 1 to 10.

For our third example, we use the non-zero mean flow $u_0 = 100\frac{\text{m}}{\text{s}}$ (maintaining the same "false" w_0 on the boundary), we get the error norms in Table XXIV.

In both cases, we observe that there is very little improvement when we increase J. This property of auxiliary variable NRBCs has been noted before in other contexts [36] and is the result of discretization errors induced by converting the normal derivative terms to tangential. Higher-order discretization schemes may improve these results [55], but for the purpose of this dissertation, it is sufficient to demonstrate how to use the auxiliary variable NRBC methods with the linearized Euler equations. Furthermore, we note by the bottom row of Tables XXII–XXIV that the

J	E_ρ	E_u	E_v	E_p
1	0.30742	0.48811	0.20486	0.21176
2	0.30615	0.48976	0.20039	0.20991
3	0.30532	0.49034	0.19818	0.2087
4	0.30472	0.49024	0.19688	0.20784
5	0.30426	0.48972	0.19598	0.20717
6	0.30387	0.48896	0.19524	0.20662
7	0.30353	0.48805	0.19459	0.20613
8	0.30321	0.48706	0.19399	0.20568
9	0.30291	0.48602	0.19342	0.20526
10	0.30261	0.48497	0.19286	0.20485
Som.	0.30224	0.85386	0.30744	0.29872

Table XXIII. Error norms (IV.14) for Givoli-Neta NRBCs, $J \in 1\ldots10$, gravity-influenced system (IV.31), open-air domain, no advection. The error norm from using a Sommerfeld boundary condition is included for comparison.

auxiliary variable method is significantly more accurate than the basic Sommerfeld (first-order Higdon) condition.

Note: Examination of our characteristic systems (V.45) and (V.19) reveals that, in a uniform domain (zero perturbations in all state variables), the presence of the non-zero $\tilde{D}$ on the right-hand side will generate non-zero results at the next time step. Physically, this should not happen; it is a consequence of replacing the normal derivatives with tangential derivatives. To avoid this problem, a check should be made at each point on the boundary prior to applying the boundary condition: If the solution at the point, its immediate neighbors, and the corresponding auxiliary variables are all zero, then the solution at the point should remain zero.

D. SUMMARY

In this chapter we have modified the Givoli-Neta auxiliary variable method for implementation in a first-order system. Although our original context is the linearized Euler equations, the linear matrix equation can be extended easily to any first-order system. The gravity-influenced derivation is specific to the linearized Euler equations,

J	E_ρ	E_u	E_v	E_p
1	0.20976	0.25767	0.24514	0.18111
2	0.20923	0.25683	0.24286	0.18049
3	0.20866	0.256	0.24061	0.17987
4	0.20813	0.25517	0.2384	0.17925
5	0.2076	0.25435	0.23623	0.17863
6	0.20703	0.25353	0.2341	0.17802
7	0.20647	0.25272	0.232	0.17741
8	0.20596	0.25191	0.22994	0.17681
9	0.20546	0.25112	0.22793	0.17621
10	0.20492	0.25036	0.22596	0.17562
Som.	0.25189	0.34105	0.27768	0.24917

Table XXIV. Error norms (IV.14) for Givoli-Neta NRBCs, $J \in 1 \ldots 10$, gravity-influenced system (IV.31), open-air domain, left-to-right advection. The error norm from using a Sommerfeld boundary condition is included for comparison.

but the rest of the implementation is fully portable to any other linear first-order system.

In the next chapter we consider a third class of NRBC, one which was recently developed in the literature, which we shall extend to our equation system.

VI.   HAGSTROM-WARBURTON NRBCS FOR THE LINEARIZED EULER EQUATIONS

A.   INITIAL IMPLEMENTATION FOR FIRST-ORDER SYSTEMS

1.   Derivation

We now consider a third class of NRBC, the Hagstrom-Warburton auxiliary variable technique, and apply it to the linearized Euler equations. We proceed similarly to Sec. 6 of [57], which documented the concept's extension to symmetric first-order systems. While our system can be made symmetric [117], it is actually not necessary to do so, and some numerical experiments have shown that the results are either the same as the following straightforward approach, worse, or unstable, depending on the domain configuration. The vector form of (III.33) is a fairly straightforward extension.

$$
\begin{aligned}
\partial_t \vec{\varphi}_1 &= a_0 \partial_t \vec{\varphi} + \partial_{\vec{n}} \vec{\varphi} \\
a_j \partial_t \vec{\varphi}_{j+1} - \partial_{\vec{n}} \vec{\varphi}_{j+1} &= a_j \partial_t \vec{\varphi}_{j+1} + \partial_{\vec{n}} \vec{\varphi}_j \\
\vec{\varphi}_{J+1} &\equiv 0
\end{aligned}
\tag{VI.1}
$$

We remove the wave speed c from the equations because the wave speeds will instead be replaced by the eigenvalues of the coefficient matrix corresponding to the normal derivative. As with the preceding chapter for the Givoli-Neta formulation, we begin with a useful lemma:

Lemma VI.1 *Let* $L(\vec{\varphi}) = \partial_t \vec{\varphi} + A \partial_x \vec{\varphi} + B \partial_y \vec{\varphi} - C \vec{\varphi}$. *The auxiliary variables* $\vec{\varphi}_j$ *satisfy*

$$
L(\vec{\varphi}_j) = 0
\tag{VI.2}
$$

for all $j \geq 1$. *The only exception is when both of the following conditions apply:*

- $\vec{n} = \pm \hat{k}$

- $g \neq 0$

Proof. Apply the differential operator L to (VI.1a), giving

$$L\left(\partial_t \vec{\varphi}_1\right) = L\left(a_0 \partial_t \vec{\varphi} + \partial_{\vec{n}} \vec{\varphi}\right)$$

$$= \left(a_0 \partial_t \left(L(\vec{D})\right) + \partial_{\vec{n}}\left(L(\vec{D})\right)\right)$$

$$\partial_t(L(\vec{\varphi}_1)) = 0 \tag{VI.3}$$

Since $\vec{\varphi}_1$ is initially zero, $L(\vec{\varphi}_1)$ is also zero, and thus it is always zero. Proceeding by induction we now apply L to (VI.1b) and get

$$L\left(a_j \partial_t \vec{\varphi}_{j+1} - \partial_{\vec{n}} \vec{\varphi}_{j+1}\right) = L\left(a_j \partial_t \vec{\varphi}_j + \partial_{\vec{n}} \vec{\varphi}_j\right)$$

$$= a_j \partial_t(L(\vec{\varphi}_j)) + \partial_{\vec{n}}(L(\vec{\varphi}_j))$$

$$= 0 \tag{VI.4}$$

We then integrate along the incoming characteristic to get $L(\vec{\varphi}_{j+1})$, which must be zero because the incoming characteristics are zero $\square$

Once again, as with Lemma V.1, the proof relies on the fact that $L\left(\partial_{\vec{n}} \vec{\varphi}\right) = \partial_{\vec{n}}\left(L\left(\vec{\varphi}\right)\right)$. On the top and bottom of a gravity-influenced domain, that is not true, because the coefficient matrices also depend on z. We will address this issue in Sec. C.

As with the Givoli-Neta formulation, we would like to get rid of the normal derivative terms in (VI.1). For definiteness, the following derivation is applied to a right-hand-side boundary, that is, $\vec{n} = \hat{i}$. Simply make the appropriate changes for the other boundaries (except a vertical boundary in the presence of gravity, as we have noted). Left-multiply (VI.1a) by A and subtract $0 = L(\vec{\varphi}) - \vec{D}$ to get

$$A \partial_t \vec{\varphi}_1 = (a_0 A - I) \partial_t \vec{\varphi} - B \partial_y \vec{\varphi} + C \vec{\varphi} + \vec{D} \tag{VI.5}$$

Similarly, left-multiply (VI.1b) by A and add $L(\vec{\varphi}_{j+1}) = -L(\vec{\varphi}_j) = 0$ to get

$$(a_j A + I) \partial_t \vec{\varphi}_{j+1} + B \partial_y \vec{\varphi}_{j+1} - C \vec{\varphi}_{j+1} = (a_j A - I) \partial_t \vec{\varphi}_j - B \partial_y \vec{\varphi}_j + C \vec{\varphi}_j \tag{VI.6}$$

Consider the eigenvalue and eigenvector matrices for the Givoli-Neta NRBCs (V.7). Left-multiply (VI.5) and (VI.6) by R^{-1} and make the substitution $\vec{\xi}_j = R^{-1} \vec{\varphi}_j$.

We get

$$\Lambda \partial_t \vec{\xi}_1 = (a_0 \Lambda - I) \partial_t \vec{\xi}_0 - \tilde{B} \partial_y \vec{\xi}_0 + \tilde{C} \vec{\xi}_0 + \tilde{D}$$

$$(a_j \Lambda + I) \partial_t \vec{\xi}_{j+1} + \tilde{B} \partial_y \vec{\xi}_{j+1} - \tilde{C} \vec{\xi}_{j+1} = (a_j \Lambda - I) \partial_t \vec{\xi}_j - \tilde{B} \partial_y \vec{\xi}_j + \tilde{C} \vec{\xi}_j , \quad \text{(VI.7)}$$

where $\tilde{B}$, $\tilde{C}$ and $\tilde{D}$ are all defined by (V.9). We also insert $R^{-1}R$ as needed to change the $\vec{\varphi}_j$ terms to $\vec{\xi}_j$'s. We have a self-contained system of equations defined solely on the boundary. Hence, with the boundary perturbations initially zero, these equations will always remain zero. So we need to incorporate interior values into our formulation in order to have something more than a rather convoluted Dirichlet condition. Following the approach in [57], we replace the four-equation truncation condition $\vec{\varphi}_{J+1} \equiv 0$ with a more characteristic-based approach. For the outgoing characteristics, we use the interior scheme

$$\left[\partial_t \vec{\xi}_0 + \Lambda \partial_x \vec{\xi}_0 + \tilde{B} \partial_y \vec{\xi}_0 = \tilde{C} \vec{\xi}_0 + \tilde{D} \right]_+ , \quad \text{(VI.8)}$$

where the $+$ subscript indicates that we only consider the resulting equations corresponding to the outgoing characteristics. This gives us one or three equations (depending on the sign of u_0) for our system of unknowns. For the remaining unknowns, we apply the truncation condition to the incoming characteristics only, i.e.,

$$\left[\vec{\xi}_{J+1} = 0 \right]_- \quad \text{(VI.9)}$$

These two equations, in conjunction with (VI.7), define a system of $4(J+2)$ equations for $4(J+2)$ unknowns $\vec{\xi}_j$. Collecting the time derivative terms onto one side gives us the explicit system:

$$\left[\partial_t \vec{\xi}_0 = -\Lambda \partial_x \vec{\xi}_0 - \tilde{B} \partial_{y|z} \vec{\xi}_0 + \left(\tilde{B} \left(\partial_z R^{-1} \right) R + \tilde{C} \right) \vec{\xi}_0 + \tilde{D} \right]_+$$

$$\Lambda \partial_t \vec{\xi}_1 + (I - a_0 \Lambda) \partial_t \vec{\xi}_0 = -\tilde{B} \partial_{y|z} \vec{\xi}_0 + \left(\tilde{B} \left(\partial_z R^{-1} \right) R + \tilde{C} \right) \vec{\xi}_0 + \tilde{D}$$

$$(I + a_j \Lambda) \partial_t \vec{\xi}_{j+1} + (I - a_j \Lambda) \partial_t \vec{\xi}_j = \begin{cases} -\tilde{B} \partial_{y|z} \vec{\xi}_{j+1} + \left(\tilde{B} \left(\partial_z R^{-1} \right) R + \tilde{C} \right) \vec{\xi}_{j+1} \\ -\tilde{B} \partial_{y|z} \vec{\xi}_j + \left(\tilde{B} \left(\partial_z R^{-1} \right) R + \tilde{C} \right) \vec{\xi}_j \end{cases}$$

$$\left[\vec{\xi}_{J+1} = 0 \right]_- , \quad \text{(VI.10)}$$

115

where the subscript $y|z$ denotes a partial derivative with respect to either y or z, depending on the domain. The $\partial_z R^{-1}$ term is non-zero only when gravity is considered.

Note that the presence of Λ on the left-hand side of (VI.10b) requires that we again have Λ (and thus A) non-singular, as with the Givoli-Neta NRBC. We solve the problem here the same way. Impose a false advection $u_0 = \epsilon \neq 0$ small enough that the system will not drift across a single grid point over the duration of the simulation; thus,

$$\|u_0\| < \frac{\delta x}{2t_{max}} \tag{VI.11}$$

where δx is the grid spacing, t_{max} is the duration of the simulation, and we include a factor of two to ensure that there will be no drift even with round-off errors.

2.   Numerical Examples

Let us consider a few numerical examples. We use our usual infinite-channel example, considering the same six cases as Sec. V.3, always with $J \in 1 \ldots 10$. Table XXV shows the state variable error norms for the basic system with no advection. Table XXVI shows the error norms for the basic system with left-to-right advection. Table XXVII shows the error norms for the Coriolis-influenced system with no advection. Table XXVIII shows the error norms for the Coriolis-influenced system with left-to-right ($u_0 = 100\frac{m}{s}$) advection. Table XXIX shows the error norms for the gravity-influenced system with no advection (recall that we can handle gravity when our open boundaries are on the left and/or right, but not on the top or bottom). Table XXX shows the error norms for the gravity-influenced system with left-to-right advection. For comparison, each table includes the error norm resulting from using a Sommerfeld condition. For the "no advection" cases we use the false advection $u_0 = 1.3889\frac{m}{s}$. In every case, we make the simplification $a_j = 1$ for all j. Hagstrom et al. [53], citing an analysis by Diaz and Joly [23], show that this choice is always adequate. We will also make this simplification in all subsequent derivations for these NRBCs. Fig. 40 shows the state variable p at the end of the run for $J = 10$

for the gravity-influenced system with left-to-right advection. Note again the strong reflections which accompany the characteristic-based implementations [72].
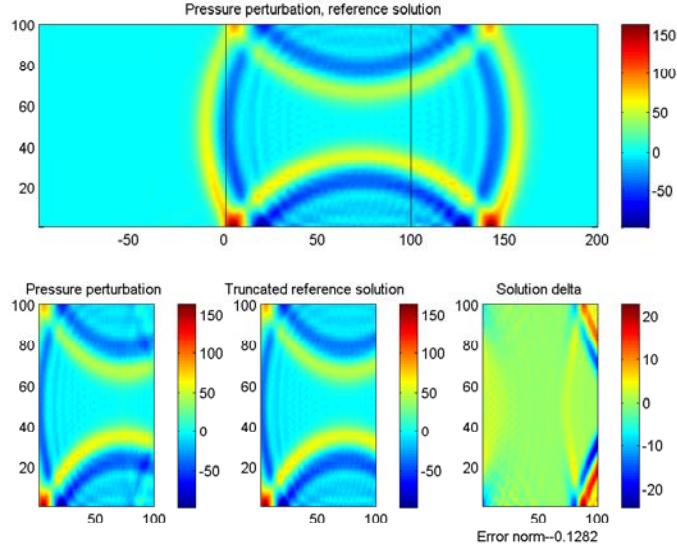
Figure 40. The solution for the pressure p using $J = 10$, Hagstrom-Warburton NRBCs, gravity-influenced system (IV.31), infinite horizontal channel, left-to-right advection. (Top) Reference solution; the area corresponding to the computed solution is contained between the vertical lines. (BL) Computed solution using NRBCs. (BC) Reference solution domain corresponding to NRBC solution domain. (BR) Delta between computed and reference solutions, with error norm computed by (IV.14).

J	E_ρ	E_u	E_v	E_p
1	0.12441	0.25176	0.10978	0.12441
2	0.12353	0.24955	0.10744	0.12353
3	0.12264	0.24735	0.10619	0.12264
4	0.12175	0.24519	0.10511	0.12175
5	0.12086	0.24305	0.10407	0.12086
6	0.11999	0.24095	0.10304	0.11999
7	0.11912	0.23887	0.10203	0.11912
8	0.11827	0.23683	0.10103	0.11827
9	0.11742	0.23482	0.10004	0.11742
10	0.11658	0.23283	0.099065	0.11658
Som.	0.21847	0.53616	0.12503	0.21847

Table XXV. Error norms (IV.14) for Hagstrom-Warburton NRBCs for basic system (IV.1) with $J \in 1 \ldots 10$ in an infinite channel with no advection. Error norms from using a Sommerfeld radiation condition are included for comparison

J	E_ρ	E_u	E_v	E_p
1	0.13788	0.2047	0.14207	0.13788
2	0.1367	0.20297	0.13915	0.1367
3	0.13553	0.20126	0.13632	0.13553
4	0.13437	0.19958	0.13358	0.13437
5	0.13322	0.19791	0.13092	0.13322
6	0.13209	0.19626	0.12835	0.13209
7	0.13096	0.19462	0.12586	0.13096
8	0.12985	0.19301	0.12344	0.12985
9	0.12874	0.19141	0.1211	0.12874
10	0.12765	0.18983	0.11884	0.12765
Som.	0.21817	0.29414	0.17727	0.21817

Table XXVI. Error norms (IV.14) for Hagstrom-Warburton NRBCs for basic system (IV.1) with $J \in 1 \ldots 10$ in an infinite channel with left-to-right advection. Error norms from using a Sommerfeld radiation condition are included for comparison

118

J	E_ρ	E_u	E_v	E_p
1	0.12441	0.25176	0.10979	0.12441
2	0.12353	0.24955	0.10745	0.12353
3	0.12264	0.24736	0.10621	0.12264
4	0.12175	0.24519	0.10513	0.12175
5	0.12086	0.24306	0.10408	0.12086
6	0.11999	0.24095	0.10306	0.11999
7	0.11912	0.23888	0.10204	0.11912
8	0.11827	0.23684	0.10104	0.11827
9	0.11742	0.23482	0.10005	0.11742
10	0.11658	0.23284	0.09908	0.11658
Som.	0.21847	0.53616	0.12503	0.21847

Table XXVII. Error norms (IV.14) for Hagstrom-Warburton NRBCs for Coriolis-influenced system (IV.15) with $J \in 1 \dots 10$ in an infinite channel with no advection. Error norms from using a Sommerfeld radiation condition are included for comparison

J	E_ρ	E_u	E_v	E_p
1	0.13855	0.31144	0.21862	0.13855
2	0.13753	0.30948	0.21789	0.13753
3	0.13654	0.3076	0.21725	0.13653
4	0.13557	0.3058	0.21668	0.13557
5	0.13464	0.30407	0.21617	0.13464
6	0.13372	0.3024	0.21573	0.13372
7	0.13284	0.3008	0.21534	0.13284
8	0.13198	0.29926	0.215	0.13197
9	0.13113	0.29777	0.21471	0.13113
10	0.13032	0.29633	0.21446	0.13032
Som.	0.1929	0.32104	0.15953	0.1929

Table XXVIII. Error norms (IV.14) for Hagstrom-Warburton NRBCs for Coriolis-influenced system (IV.15) with $J \in 1 \dots 10$ in an infinite channel with left-to-right advection. Error norms from using a Sommerfeld radiation condition are included for comparison

J	E_ρ	E_u	E_v	E_p
1	0.12896	0.25097	0.11173	0.12835
2	0.12807	0.24879	0.10934	0.12745
3	0.12714	0.24663	0.10807	0.12652
4	0.12622	0.24449	0.10697	0.1256
5	0.1253	0.24238	0.10591	0.12469
6	0.12439	0.24031	0.10487	0.12379
7	0.12349	0.23826	0.10384	0.12289
8	0.12259	0.23624	0.10283	0.12201
9	0.12171	0.23425	0.10183	0.12113
10	0.12084	0.2323	0.10084	0.12026
Som.	0.22442	0.52603	0.12775	0.22374

Table XXIX. Error norms (IV.14) for Hagstrom-Warburton NRBCs for gravity-influenced system (IV.31) with $J \in 1 \dots 10$ in an infinite channel with no advection. Error norms from using a Sommerfeld radiation condition are included for comparison

J	E_ρ	E_u	E_v	E_p
1	0.13899	0.20395	0.14268	0.13852
2	0.13779	0.20223	0.13977	0.13733
3	0.1366	0.20053	0.13696	0.13615
4	0.13543	0.19885	0.13423	0.13498
5	0.13426	0.19718	0.13158	0.13382
6	0.13311	0.19554	0.12902	0.13267
7	0.13197	0.19391	0.12654	0.13154
8	0.13084	0.1923	0.12414	0.13041
9	0.12972	0.19071	0.12181	0.1293
10	0.12861	0.18913	0.11956	0.1282
Som.	0.21869	0.28969	0.17855	0.21802

Table XXX. Error norms (IV.14) for for Hagstrom-Warburton NRBCs for gravity-influenced system (IV.31) with $J \in 1 \dots 10$ in an infinite channel with left-to-right advection. Error norms from using a Sommerfeld radiation condition are included for comparison

B. CORNER CONDITIONS
1. Derivation

We can use the same methods as in Sec. V.1 to apply these NRBCs to the corners of an open domain, *in the absence of gravity.* Using the same notation as before, our characteristic-based NRBC scheme on three open sides of a half-plane is given by

$$
\begin{aligned}
\partial_t \vec{\xi}_+ &= -\Lambda \partial_n \vec{\xi}_+ - \tilde{T} \partial_\tau \vec{\varphi}_+ \\
\Lambda \partial_t \vec{\xi}_1 + (I - \Lambda) \partial_t \vec{\xi} &= -\tilde{T} \partial_\tau \vec{\varphi} \\
(I + \Lambda) \partial_t \vec{\xi}_{j+1} + (I - \Lambda) \partial_t \vec{\xi}_j &= -\tilde{T} \partial_\tau \vec{\varphi}_{j+1} - \tilde{T} \partial_\tau \vec{\varphi}_j \\
\vec{\xi}_{J+1,-} &= 0
\end{aligned}
\tag{VI.12}
$$

where we use

$$
\text{Left} : \begin{cases} \partial_n &= -\partial_x \\ \partial_\tau &= \partial_z \\ T &= B \end{cases}
$$

$$
\text{Right} : \begin{cases} \partial_n &= \partial_x \\ \partial_\tau &= \partial_z \\ T &= B \end{cases}
$$

$$
\text{Top} : \begin{cases} \partial_n &= \partial_z \\ \partial_\tau &= \partial_x \\ T &= A \end{cases}
\tag{VI.13}
$$

$$
\text{Top-left} : \begin{cases} \partial_n &= \left(-\partial_x + \partial_z\right)/\sqrt{2} \\ \partial_\tau &= \left(\partial_x + \partial_z\right)/\sqrt{2} \\ T &= \left(A + B\right)/\sqrt{2} \end{cases}
$$

$$
\text{Top-right} : \begin{cases} \partial_n &= \left(\partial_x + \partial_z\right)/\sqrt{2} \\ \partial_\tau &= \left(\partial_x - \partial_z\right)/\sqrt{2} \\ T &= \left(A - B\right)/\sqrt{2} \end{cases}
$$

121

2. Numerical Examples

Let us now consider some examples. Since we cannot include the effects of gravity on the top of the domain, we consider only four cases: The basic system and the system influenced by Coriolis forces, with and without horizontal advection. We use the same false advection as in Sec. 2 (horizontal) and V.2 (vertical). Table XXXI shows the error norms for $J \in 1 \ldots 10$ for the basic system with no advection. Table XXXII shows the error norms for $J \in 1 \ldots 10$ for the basic system with left-to-right advection. Table XXXIII shows the error norms for $J \in 1 \ldots 10$ for the Coriolis-influenced system with no advection. Table XXXIV shows the error norms for $J \in 1 \ldots 10$ for the Coriolis-influenced system with left-to-right advection. Fig. 41 shows an example of the horizontal velocity perturbation u for the basic no-advection test. Note the reflections are stronger at the bottom corners than the top. These reflections are the result of waves reflecting off the hard wall on the bottom before impacting the left and right boundaries; thus, their incidence angles are greater than 45°. At the top corners, these waves pass through the open top with the smaller incidence angle, so there is less reflection evident. If we plot the values of Table XXXIV, we see that the error norms decrease exponentially as J increases by 2 (Fig. 42, but note that v increases with $J \geq 7$). The reason for the saw-tooth pattern is unknown, but it is only present in the Coriolis+advection case; the other cases show exponential reductions with each increase in J.
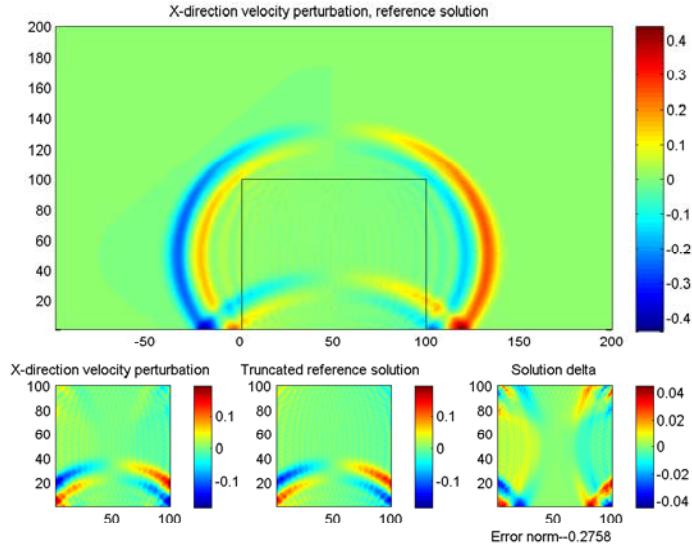
Figure 41. The solution for the horizontal velocity u using $J = 10$, Hagstrom-Warburton NRBCs, basic system (IV.1), open half-plane, no advection. (Top) Reference solution; the area corresponding to the computed solution is contained in the bottom-center box. (BL) Computed solution using NRBCs. (BC) Reference solution domain corresponding to NRBC solution domain. (BR) Delta between computed and reference solutions, with error norm computed by (IV.14).

J	E_ρ	E_u	E_v	E_p
1	0.17603	0.30011	0.13089	0.17604
2	0.17485	0.29724	0.12848	0.17485
3	0.17364	0.29438	0.12699	0.17365
4	0.17244	0.29157	0.12565	0.17245
5	0.17125	0.28881	0.12435	0.17126
6	0.17007	0.2861	0.12307	0.17007
7	0.1689	0.28345	0.12182	0.1689
8	0.16773	0.28085	0.12059	0.16774
9	0.16658	0.2783	0.11938	0.16658
10	0.16543	0.2758	0.11819	0.16543
Som.	0.33324	0.71942	0.2414	0.33325

Table XXXI. Error norms (IV.14) for Hagstrom-Warburton NRBCs for basic system (IV.1) with $J \in 1 \dots 10$ in an open half-plane with no advection. Error norms from using a Sommerfeld radiation condition are included for comparison

J	E_ρ	E_u	E_v	E_p
1	0.16823	0.20592	0.18956	0.16823
2	0.16661	0.20403	0.18543	0.16661
3	0.16501	0.20217	0.18143	0.16501
4	0.16342	0.20034	0.17755	0.16342
5	0.16186	0.19854	0.1738	0.16186
6	0.16031	0.19675	0.17016	0.16031
7	0.15878	0.19499	0.16664	0.15878
8	0.15727	0.19326	0.16323	0.15727
9	0.15577	0.19154	0.15993	0.15577
10	0.15429	0.18985	0.15673	0.1543
Som.	0.2675	0.32527	0.2411	0.2675

Table XXXII. Error norms (IV.14) for Hagstrom-Warburton NRBCs for basic system (IV.1) with $J \in 1\ldots10$ in an open half-plane with left-to-right advection. Error norms from using a Sommerfeld radiation condition are included for comparison

J	E_ρ	E_u	E_v	E_p
1	0.17604	0.30024	0.13095	0.17604
2	0.17484	0.29737	0.12852	0.17484
3	0.17364	0.29451	0.12704	0.17365
4	0.17243	0.29169	0.12569	0.17243
5	0.17125	0.28893	0.12439	0.17126
6	0.17006	0.28622	0.12311	0.17006
7	0.16889	0.28356	0.12186	0.1689
8	0.16772	0.28096	0.12063	0.16772
9	0.16657	0.2784	0.11943	0.16658
10	0.16541	0.27591	0.11824	0.16542
Som.	0.33324	0.71943	0.2414	0.33325

Table XXXIII. Error norms (IV.14) for Hagstrom-Warburton NRBCs for Coriolis-influenced system (IV.15) with $J \in 1\ldots10$ in an open half-plane with no advection. Error norms from using a Sommerfeld radiation condition are included for comparison

J	E_ρ	E_u	E_v	E_p
1	0.20445	0.35374	0.261	0.20444
2	0.20472	0.35221	0.26198	0.20471
3	0.20277	0.34939	0.26073	0.20276
4	0.20307	0.34806	0.26177	0.20306
5	0.20117	0.34542	0.26059	0.20116
6	0.20152	0.34424	0.26168	0.2015
7	0.19966	0.34175	0.26057	0.19965
8	0.20003	0.34072	0.26169	0.20002
9	0.19822	0.33836	0.26064	0.19821
10	0.19862	0.33744	0.26179	0.19861
Som.	0.26015	0.34856	0.20456	0.26014

Table XXXIV. Error norms (IV.14) for Hagstrom-Warburton NRBCs for Coriolis-influenced system (IV.15) with $J \in 1 \ldots 10$ in an open half-plane with left-to-right advection. Error norms from using a Sommerfeld radiation condition are included for comparison
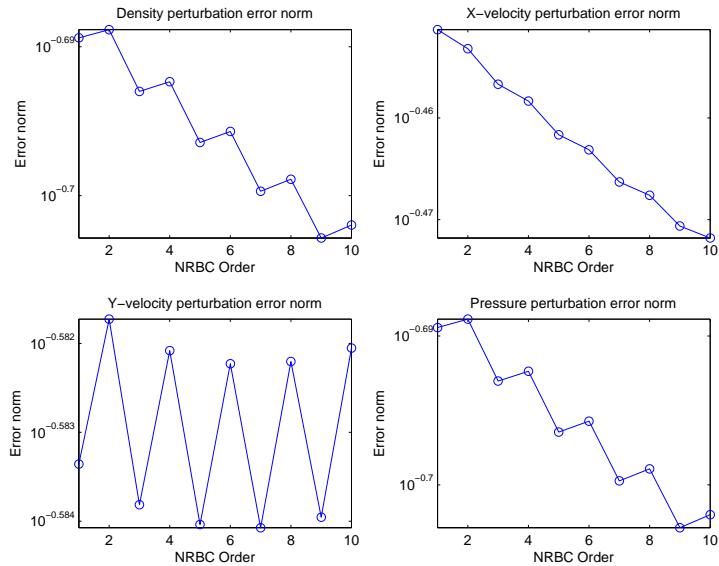
Figure 42. Logarithmic plot of error norms (IV.14) for Hagstrom-Warburton NRBC, $J \in 2 \ldots 10$, open half-plane, Coriolis, left-to-right advection. (TL) Error norm for ρ. (TR) Error norm for u. (BL) Error norm for v. (BR) Error norm for p.

C. INCOMPATIBILITY WITH GRAVITY

Problems arise, however, when we try to incorporate the effects of gravity on the top boundary. (We can include it on Γ_L and Γ_R without any difficulty.) Using the same approach as for the Givoli-Neta NRBCs, we apply the differential operator L to both sides of (VI.1a), beginning the process of removing the normal derivatives:

$$
\begin{aligned}
L\left(\partial_t \vec{\varphi}_1\right) &= L\left(a_0 \partial_t \vec{\varphi} + \partial_z \vec{\varphi}\right) \\
\partial_t\left(L\left(\vec{\varphi}_1\right)\right) &= a_0 \partial_t\left(L\left(\vec{\varphi}\right)\right) + L\left(\partial_z \vec{\varphi}\right) \\
&= a_0 \partial_t \vec{D} + \partial_{tz}\vec{\varphi} + A\partial_{xz}\vec{\varphi} + B\partial_{zz}\vec{\varphi} - C\partial_z\vec{\varphi} \\
&= \begin{cases} \partial_z\left(\partial_t\vec{\varphi} + A\partial_x\vec{\varphi} + B\partial_z\vec{\varphi} - C\vec{\varphi}\right) \\ -\left(\partial_z A\right)\vec{\varphi} - \left(\partial_z B\right)\vec{\varphi} + \left(\partial_z C\right)\vec{\varphi} \end{cases} \\
\partial_t\left(L\left(\vec{\varphi}_1\right)\right) &= \partial_z\left(L\left(\vec{\varphi}\right)\right) - \left(\partial_z A\right)\vec{\varphi} - \left(\partial_z B\right)\vec{\varphi} + \left(\partial_z C\right)\vec{\varphi} \,. \qquad \text{(VI.14)}
\end{aligned}
$$

Even with the simplifying assumption of an exponentially-decaying atmosphere, we still have

$$
\begin{aligned}
\partial_t\left(L\left(\vec{\varphi}_1\right)\right) &= \partial_z \vec{D} + \alpha A_z\vec{\varphi} + \alpha B_z\vec{\varphi} - \alpha C\vec{\varphi} \\
&= -\alpha \vec{D} + \alpha\left(L\left(\vec{\varphi}\right) - \partial_t\vec{\varphi} - u_0\partial_x\vec{\varphi} - w_0\partial_z\vec{\varphi}\right) \\
&= -\alpha \vec{D} + \alpha \vec{D} - \alpha\left(\partial_t\vec{\varphi} + u_0\partial_x\vec{\varphi} + w_0\partial_z\vec{\varphi}\right) \\
\partial_t\left(L\left(\vec{\varphi}_1\right)\right) &= -\alpha \partial_F\vec{\varphi} \,. \qquad\qquad\qquad\qquad\qquad\qquad \text{(VI.15)}
\end{aligned}
$$

To continue this derivation, we must integrate the Lagrangian flow derivative of $\vec{\varphi}$ over time. The result is then applied to find $L\left(\vec{\varphi}_2\right)$, with increasingly convoluted combinations of Lagrangian derivatives and time integrals. This approach is not satisfactory. Hence, we require a different approach if we wish to incorporate gravitational effects into the Hagstrom-Warburton NRBCs. We have not found such an approach, but future research may reveal a suitable technique.

D.   WAVE-LIKE IMPLEMENTATION
1.   Derivation

The results from this implementation are not bad, but the improvement with larger J is slight. Furthermore, the reflections downstream of the advection are troublesome. Perhaps we can do better. Looking at (VI.1), we see a hint of the problem. Although Hagstrom and Warburton do not provide a physical interpretation of their auxiliary variable formulation, inspection of (VI.1) shows that we can conceive of the second equation in the following manner: The outgoing characteristic of $\vec{\varphi}_j$ is in some sense paired with the incoming characteristic of $\vec{\varphi}_{j+1}$. However, when we use these characteristic variables for a first-order system, we contradict this interpretation of the auxiliary variables, since each variable has only one characteristic (either incoming or outgoing), not two. If we could contrive a second characteristic for each state variable, it might improve our results. Let us instead apply the NRBC to each state variable individually. Instead of Lemma VI.1, we use the following:

Lemma VI.2 *Each state variable $\varphi \in \{\rho, u, v, p\}$ has a solution which satisfies the acoustic wave equation*

$$\partial_{tt}\varphi = c_w^2 \nabla^2 \varphi ,\tag{VI.16}$$

where

$$c_w = \begin{cases} c_0 + u_0 & on\ \Gamma_E \\ c_0 - u_0 & on\ \Gamma_W \\ c_0 + v_0 & on\ \Gamma_N \\ c_0 - v_0 & on\ \Gamma_S . \end{cases}\tag{VI.17}$$

The derivation is given in Appendix C. With this fact, we can then implement the auxiliary variables exactly as given in [57], taking each state variable individually. Upon removing the normal derivatives, we are left with the following system of equations:

$$-a_0\partial_t\varphi + \partial_t\varphi_1 = c_p\partial_x\varphi$$

$$\left.\begin{array}{c} 2a_1(1-a_0^2)\partial_{tt}\varphi \\ +(1+a_1^2+2a_0a_1)\partial_{tt}\varphi_1 \\ +(1-a_1^2)\partial_{tt}\varphi_2 \end{array}\right\} = \begin{cases} c_w^2(2a_1\partial_{yy}\varphi \\ \quad +\partial_{yy}\varphi_1 + \partial_{yy}\varphi_2) \end{cases}$$

127

$$
\left.
\begin{array}{r}
a_j(1 - a_{j-1}^2)\partial_{tt}\varphi_{j-1} \\[4pt]
+(a_{j-1} + a_j)(1 + a_{j-1}a_j)\partial_{tt}\varphi_j \\[4pt]
+a_{j-1}(1 - a_j^2)\partial_{tt}\varphi_{j+1}
\end{array}
\right\}
=
\left\{
\begin{array}{l}
c_w^2(a_j\partial_{yy}\varphi_{j-1} \\[4pt]
+(a_{j-1} + a_j)\partial_{yy}\varphi_j \\[4pt]
+a_{j-1}\partial_{yy}\varphi_{j+1})
\end{array}
\right.
$$

$$
\left.
\begin{array}{r}
a_P(1 - a_{P-1}^2)\partial_{tt}\varphi_{P-1} \\[4pt]
+(a_{P-1} + a_P)(1 + a_{P-1}a_P)\partial_{tt}\varphi_P
\end{array}
\right\}
=
\left\{
\begin{array}{l}
c_w^2(a_P\partial_{yy}\varphi_{P-1} \\[4pt]
+(a_{P-1} + a_P)\partial_{yy}\varphi_P)\,,
\end{array}
\right.
\qquad \text{(VI.18)}
$$

where $c_w = c_0 + u_0$. When we make the simplification $a_j = 1$, this system reduces to

$$
-\partial_t\varphi + \partial_t\varphi_1 = c_p\partial_x\varphi
$$

$$
4\partial_{tt}\varphi_1 =
\left\{
\begin{array}{l}
c_w^2(2\partial_{yy}\varphi \\[4pt]
+\partial_{yy}\varphi_1 + \partial_{yy}\varphi_2)
\end{array}
\right.
$$

$$
4\partial_{tt}\varphi_j =
\left\{
\begin{array}{l}
c_w^2(\partial_{yy}\varphi_{j-1} \\[4pt]
+2\partial_{yy}\varphi_j \\[4pt]
+\partial_{yy}\varphi_{j+1})
\end{array}
\right.
$$

$$
4\partial_{tt}\varphi_P =
\left\{
\begin{array}{l}
c_w^2(\partial_{yy}\varphi_{P-1} \\[4pt]
+2\partial_{yy}\varphi_P)\,,
\end{array}
\right.
\qquad \text{(VI.19)}
$$

This system is the NRBC on Γ_E. On Γ_W replace $\partial_x\varphi$ in (VI.19a) with $-\partial_x\varphi$, and use $c_w = c_0 - u_0$.

2.   Numerical Examples

If we run the same infinite-channel example as in Sec. 1.2, using the wave-based auxiliary variable approach from the preceding section, we get the results illustrated in Fig. 43 with the error norms for all state variables given in Table XXXV. If we use the non-zero mean flow $u_0 = 100\frac{\text{m}}{\text{s}}$, we get the error norms in Table XXXVI. Comparing Tables XXXV and XXXVI to Tables XXV and XXVI, respectively, we see that this new version's error norms are approximately half the old version's. We note also that the new method's error norms show almost no improvement for $J \geq 5$. This "error floor" has been observed in other auxiliary variable implementations for scalar wave equations [36]. Although the old method shows continual (albeit slow) improvement, the error norms do not match those of the new method until $J \approx 500$, which runs far
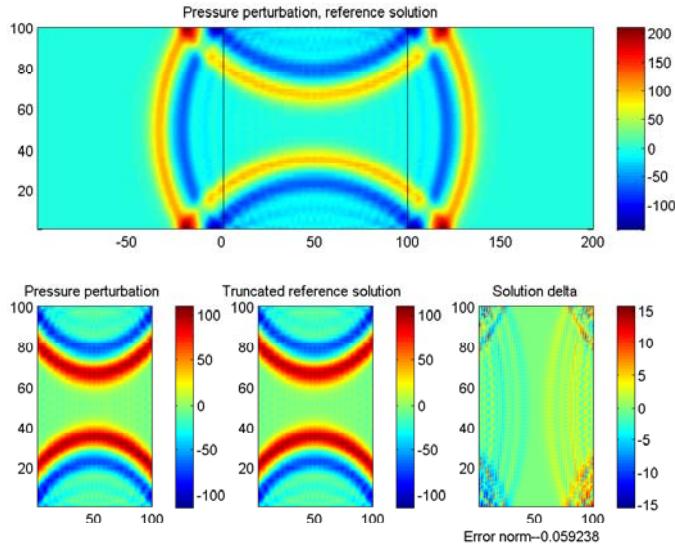
Figure 43. The solution for the pressure p using $J = 10$, wave-like Hagstrom-Warburton NRBCs in an infinite channel, basic system with no advection. (Top) Reference solution; the area corresponding to the computed solution is contained between the vertical lines. (BL) Computed solution using NRBCs. (BC) Reference solution domain corresponding to NRBC solution domain. (BR) Delta between computed and reference solutions, with error norm computed by (IV.14).

slower than the new method's $J = 5$. While this result is promising, experiments with longer integration times show that this wave-like implementation is less stable than the characteristic-based method; hence, we do not pursue its development further.

E. SUMMARY

This chapter concludes our development of NRBCs for the linearized Euler equations. For each NRBC, we have derived its implementation and demonstrated its effectiveness for short time-integrations. In the next two chapters, we will consider the question of longer time-integrations and the relative strengths and weaknesses of each method.

J	E_ρ	E_u	E_v	E_p
1	0.059866	0.16273	0.038642	0.059866
2	0.059442	0.16184	0.038079	0.059443
3	0.059306	0.16156	0.037884	0.059306
4	0.059252	0.16144	0.037804	0.059252
5	0.059236	0.16139	0.037775	0.059237
6	0.059234	0.16138	0.037765	0.059235
7	0.059235	0.16138	0.037761	0.059236
8	0.059236	0.16138	0.03776	0.059237
9	0.059237	0.16138	0.037759	0.059237
10	0.059237	0.16138	0.037759	0.059238

Table XXXV. Error norms (IV.14) for $J \in 1 \ldots 10$, wave-like Hagstrom-Warburton NRBCs, infinite channel, basic system with no advection

J	E_ρ	E_u	E_v	E_p
1	0.053965	0.078277	0.040606	0.053965
2	0.053561	0.077765	0.040013	0.053561
3	0.05347	0.077625	0.039873	0.05347
4	0.053457	0.077589	0.039842	0.053457
5	0.053456	0.077575	0.039836	0.053456
6	0.053455	0.077568	0.039835	0.053455
7	0.053454	0.077564	0.039835	0.053454
8	0.053453	0.077562	0.039835	0.053453
9	0.053453	0.077561	0.039834	0.053453
10	0.053453	0.077561	0.039834	0.053453

Table XXXVI. Error norms (IV.14) for $J \in 1 \ldots 10$, wave-like Hagstrom-Warburton NRBCs, infinite channel, basic system with left-to-right advection

VII.   LONG-TIME STABILITY

A.   OBSERVATIONS

In this chapter we address the stability of the NRBCs for long time-integrations. This issue is critical to numerical weather prediction and other applications which require time frames beyond that of a single wave's propagation through the domain.

Higdon [68] discusses the numerical stability of his NRBC formulation, using criteria developed by Kreiss [81] and Gustafsson et al. [52] (and Higdon's own characteristic-based interpretation thereof [63]). While his scheme meets the defined stability criteria, there is still concern that a scheme which is stable for the single-variable Klein-Gordon equation is also stable long-term for the equivalent linearized Euler system. Long-term stability, surprisingly, has not been much discussed or demonstrated in NRBC development. In the Givoli-Neta papers exploring the automated Higdon NRBCs and the Givoli-Neta auxiliary variable NRBCs [39, 40, 41, 42, 43, 90, 113, 114, 115, 116], only [90] discusses the long-time stability of the solution, showing that the automated Higdon NRBC of order $J = 10$ is stable for long time-integrations. In the papers exploring the Hagstrom-Warburton auxiliary variable scheme [57, 37, 53, 55], long-time stability was claimed in [57] (although the numerical example plotted showed an error norm that was increasing over time), and [55] uses an evanescent mode correction (a second set of auxiliary variables) to ensure long-time stability.

As for the papers which discuss various NRBC techniques for the linearized Euler equations, only the absorbing layer methods [1, 17, 72, 73, 88] discuss or demonstrate long-time stability. Specifically, the numerical examples in [17] are carried out for long time-integrations, and the PMLs [1, 72, 73] require additional terms to make them stable ([88] claims medium-term stability and implies stability over long time-integrations).

All three types of NRBCs presented in this dissertation suffer from some form

of long-time instability. One example may be seen in Fig. 44, which is the state variable u from the numerical example of Sec. IV.B.3, with $J = 10$, run until $t = 100$ s. As we can see, the values on the boundary have become catastrophically large, and they have polluted the domain, completely overwhelming the actual wave (faintly visible near the center of the domain). Tables XXXVII–XXXIX list the maximum order J for which the given NRBC is stable for the various domain configurations for short (24 s), medium (100 s), and long (10,000 s) time-integrations. Table entries marked "No" indicate that the configuration was unstable even for $J = 1$. The upper limit to J for the short-term stability mirrors a condition seen while producing the results given in [90]; even though the Higdon scheme is theoretically stable in the discrete case, round-off errors in the finite-precision implementation lead to instability. This same problem afflicted the examples given in Chapter IV: If the example was performed on a 50×50 grid, it was stable only up to $J = 5$; halving the grid spacings enabled the stable results up to $J = 10$.
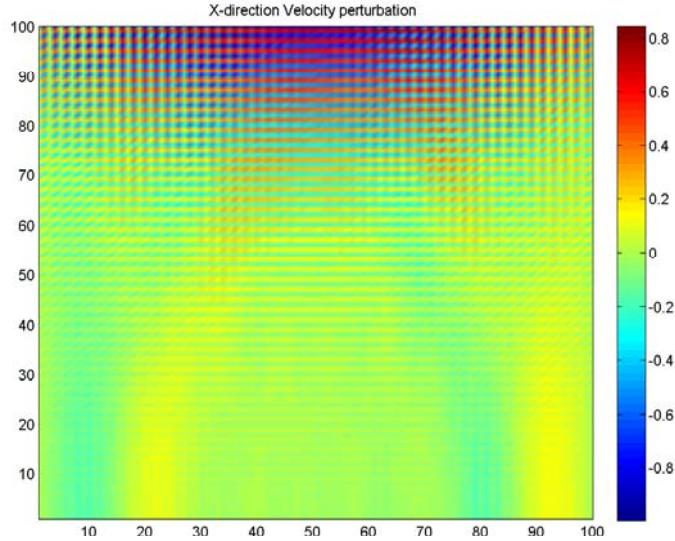
Figure 44. Plot of unstable u in basic system (IV.1) with Higdon NRBC $J = 10$ in a semi-infinite channel integrated up to $t = 100$ s. Notice the faint wave crests near the middle of the domain

Domain shape	Coriolis or gravity	Advection	Short (24 s)	Medium (100 s)	Long (10,000 s)
Bucket	None	None	10	8	4
	Coriolis	None	10	8	4
	Gravity	None	10	8	No
Channel	None	L-R	10	4	No
	Coriolis	L-R	2	2	No
	Gravity	None	10	8	4
		L-R	10	4	No
Open	None	None	10	5	2
		L-R	10	4	No
		BL-TR	10	4	No
	Coriolis	None	10	5	2
		L-R	2	No	No
		BL-TR	2	No	No
Ground	Gravity	None	10	5	No
		L-R	10	4	No

Table XXXVII. Higdon NRBCs, maximum stable order J for various domain configurations and simulation durations

For the Hagstrom-Warburton NRBCs, we found short-term stability as high as $J = 40$. While the NRBC still exhibits exponential improvement (see Fig. 45), the improvement is slight enough that the computational overhead for such high J is unjustified; hence, we did not seek an actual "maximum" stable J but simply noted that the maximum is at least $J = 40$.

Domain shape	Coriolis or gravity	Advection	Short (24 s)	Medium (100 s)	Long (10,000 s)
Bucket	None	None	15	7	No
	Coriolis	None	15	7	No
	Gravity	None	13	6	No
Channel	None	L-R	12	7	4
	Coriolis	L-R	11	7	1
	Gravity	None	15	7	No
		L-R	12	7	3
Ground	None	None	15	7	No
		L-R	12	3	No
	Coriolis	None	15	7	No
		L-R	10	3	No
	Gravity	None	13	No	No
		L-R	11	3	No

Table XXXVIII. Givoli-Neta NRBCs, maximum stable order J for various domain configurations and simulation durations

Domain shape	Coriolis or gravity	Advection	Short (24 s)	Medium (100 s)	Long (10,000 s)
Bucket	None	None	40+	40+	No
	Coriolis	None	40+	40+	No
Channel	None	L-R	40+	40+	40+
	Coriolis	L-R	40+	40+	40+
	Gravity	None	40+	40+	No
		L-R	40+	40+	5
Ground	None	None	40+	28	No
		L-R	40+	3	No
	Coriolis	None	40+	27	No
		L-R	40+	4	No

Table XXXIX. Hagstrom-Warburton NRBCs, maximum stable order J for various domain configurations and simulation durations
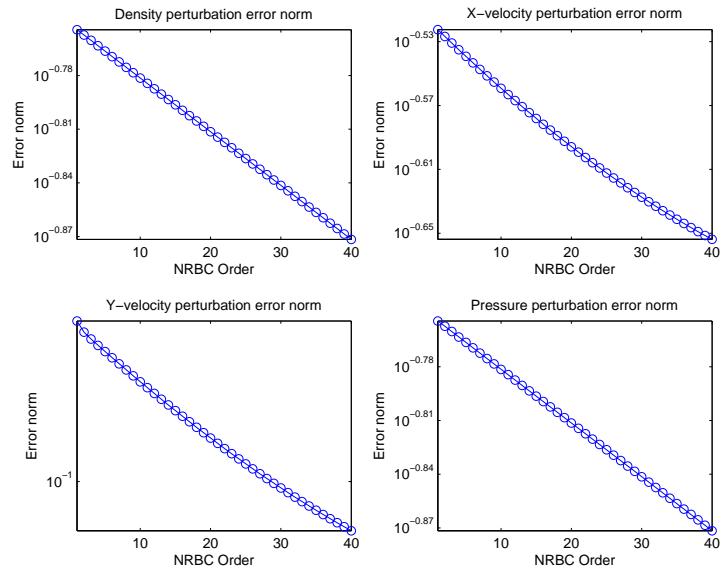
Figure 45. Logarithmic plot of error norms (IV.14) for $J \in 1 \ldots 40$, Hagstrom-Warburton NRBCs, open half-plane with Coriolis, no advection. (TL) Error norms for ρ. (TR) Error norms for u. (BL) Error norms for v. (BR) Error norms for p.

B. SPECULATIONS

Based on observations from these and other experiments during this research, we can tentatively identify several possible instability sources. These sources, though currently mere conjecture and speculation, will be explored in future research.

1. *Round-off errors.* Early tests of these NRBCs used a smaller domain, only 1 km square, and the scheme was stable up to $J \approx 8$. Increasing the domain size and grid spacing by an order of magnitude made the scheme stable up to $J = 10$.

2. *Normal derivatives reaching too far into the domain.* The first numerical examples, using the Higdon scheme, were run on a 50×50 grid. The scheme was unstable for $J > 5$. Changing the grid to 100×100 made the scheme stable up to $J = 10$. As a result, the normal derivatives of the Higdon scheme did not reach as far into the domain. Van Joolen [113] noted this same behavior for the Klein-Gordon equation.

3. *Dependency between interior and NRBC near corners.* Although no points depend on the corner values in the Higdon NRBC scheme (see Fig. 13), the interior point closest to the corner depends on two boundary points, rather than just one. It could be that this dependence creates a slight error, just enough that it grows over time and destabilizes the system.

4. *Frequency mis-match between interior and Higdon NRBC schemes.* A reviewer for [21] noted that the Higdon NRBC discretization scheme (IV.10) cannot resolve the shortest wavelengths resolvable by the interior scheme (IV.7). When a wave strikes the open boundary, the NRBC computes the value based on every other point at every other time step, as if for a wave with twice the wavelength. The skipped points of the wave are then used at the next time step to compute that next time step's boundary value. Hence, a wave striking the boundary with wavelength ν is resolved by the NRBC as a two-stage composition of two waves, each with wavelength 2ν. A stability analysis by one of the co-authors of [21] is in progress to determine the impact of this resolution discrepancy.

5. *Numerically-singular matrix computations.* For the Givoli-Neta NRBCs with gravity, in either the "bucket" or open-air domains, Matlab issued "Matrix is close to singular or badly scaled" warnings for large J and small δt. It appears the left-hand matrix used to solve the auxiliary variables is prone to numeric instability.

6. *Exponentially-growing solutions.* Although Higdon [68] proves the stability of his system by demonstrating that exponentially-growing solutions are not

permitted for the discrete system and boundary condition, it is possible that such solutions are appearing in this system. Look at Fig. 46, which shows the results of an unstable configuration run until $t = 100$s. For each unstable J, the ∞-norm of the solution grows exponentially after a certain point in time. If we were to extend these lines backward, they would intersect at approximately $t = 0$. Hence, it appears that there is an initially small, but exponentially growing, solution within the scheme. Over time, this exponentially growing solution overwhelms the other interior values and leads to the unstable system.

7. *Discrete reflection coefficient greater than unity.* Our analysis of the reflection coefficients (III.15) and (III.34) is based on the partial derivatives in the continuous case. However, we implement the system using finite differences on discrete variables. It is possible that the "reflection coefficient" in the discrete case is dependent on more factors than just the wave speed and the NRBC estimated wave speed, factors such as the grid spacing and the time step size. Some configurations may lead to $\|R\| > 1$ for some waves. See Appendix D for some initial analysis. A full analysis of this discrete reflection coefficient will be performed in future research.
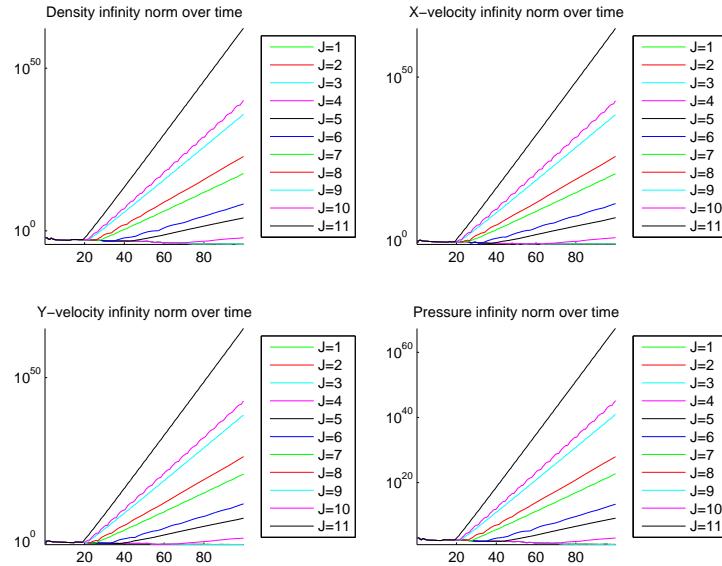
Figure 46. Logarithmic plot of state variable ∞-norms for $J \in 1 \ldots 11$, Givoli-Neta NRBCs, open half-plane, left-to-right advection, no gravity or Coriolis, run until $t = 100$s. (TL) ∞-norms for ρ. (TR) ∞-norms for u. (BL) ∞-norms for w. (BR) ∞-norms for p.

One result of the Hagstrom-Warburton table was surprising: The "bucket" configuration was always unstable long-term, but the infinite channel configuration

showed long-term stability. This result was not a programming error. Running the simulation on a horizontal semi-infinite channel showed the same instability as the vertical semi-infinite channel. The stability of the boundary condition was impacted by the type of boundary on the opposite side. Until a formal analysis is undertaken to explain this result, we offer here a tentative hypothesis. The instability comes from waves whose reflection coefficients are slightly greater than unity when striking an open boundary on one side. On an open boundary on the other side, the wave speed and NRBC wave speed combine to cause a reflection coefficient less than unity; however, if the other side is a hard wall, then its reflection coefficient is exactly unity, and so the undiminished wave is totally reflected back to the open boundary, where it is again reflected and magnified back toward the hard wall, and so forth, growing in magnitude with each pass.

VIII. SUMMARY AND COMPARISONS

Having developed three distinct NRBC methods, we now examine them side-by-side to assess their relative strengths and weaknesses. As stated in the introduction (Chapter I), there are four criteria we desire for an NRBC: speed, accuracy, stability, and ease of implementation. We consider each criterion individually and compare the three NRBC methods against each other.

Speed. We do not have speed comparisons of the implementations, as a simple "execution time" metric is dependent on the efficiency of the code and the inventiveness of the programmer. However, we can make some ballpark estimates based on the approximate operator counts required. As noted in their respective chapters, the basic Higdon scheme (as automated by the Givoli-Neta algorithm) requires $O(3^J)$ operations, but the simplification of setting all the c_j to the same value reduces the operation count to $O(J^2)$. The Givoli-Neta and Hagstrom-Warburton auxiliary variable methods each require $O(J)$ operations, except for the Givoli-Neta NRBC in the presence of gravity, which requires $O(J^2)$.

Accuracy. By using the same numerical example throughout this dissertation, we can easily compare the relative accuracy of the three implementations. The only change is that the Higdon scheme's no-advection examples used a semi-infinite channel instead of the infinite channel used for the Givoli-Neta and Hagstrom-Warburton schemes. Even if we assume the error norms for the Higdon scheme would be doubled by having two open boundaries, we still see that the Higdon NRBC error norms are approximately 80% lower than Hagstrom-Warburton NRBC error norms, which in turn are approximately 40% lower than the Givoli-Neta NRBC error norms (for the basic system, but only 10% lower for the Coriolis- and gravity-influenced systems). The only exception to this case is the Higdon scheme with advection and Coriolis. In all other cases, Hagstrom-Warburton is approximately the same or slightly better than Givoli-Neta, but Higdon is significantly better than either of them. Again,

139

this is a consequence of the characteristic-based boundary method.

Stability. When we consider stability, our comparison depends on the configuration. Comparing the Higdon scheme to the Givoli-Neta scheme, we see that Higdon is more stable when there is no advection, but Givoli-Neta is more stable in the presence of non-zero advection. In fact, the Higdon scheme is completely unstable in the non-zero advection case with Coriolis forces; however, the Givoli-Neta scheme shows some medium-term stability. The Hagstrom-Warburton scheme is the most stable, although it and the Givoli-Neta schemes are less stable in an open half-plane with non-zero advection. It also turns out that only the Hagstrom-Warburton scheme exhibited any appreciable long-term stability (specifically, in the infinite channel domain), while the other two methods failed for nearly all configurations.

Ease of implementation. All three methods are fairly straightforward and easy to implement. Since all three methods are explicit, they can be computed in a separate calculation after the interior scheme's calculations. The Higdon scheme requires a summation algorithm to automate the high-order finite-difference approximations, and the Givoli-Neta and Hagstrom-Warburton schemes require a careful consideration of characteristic and some matrix calculations. These drawbacks are not significant. However, Higdon is limited by the number of points in the domain, and it is not yet possible to implement Hagstrom-Warburton on an open top boundary in the presence of gravity. Furthermore, Higdon requires a careful choice of interior discretization schemes [39, 19], while experiments with the Hagstrom-Warburton scheme for the scalar wave equation [55] show that higher-order interior schemes can be used (an option we have not attempted to utilize here). Such high-order schemes may also be permissible for the Givoli-Neta method.

Summary. The Higdon scheme has an enormous advantage in accuracy, Hagstrom-Warburton is the most stable, Givoli-Neta and Hagstrom-Warburton are approximately equally fast, and all three are equally easy to implement.

IX. CONCLUSIONS AND AREAS FOR FURTHER RESEARCH

We have shown through the preceding chapters that high-order non-reflecting boundary conditions can be applied to the 2-D linearized Euler equations in a wide variety of configurations. The Higdon, Givoli-Neta, and Hagstrom-Warburton techniques can all be used, in channels and in open domains, with and without advection, with basic conditions or with gravity or Coriolis, excepting only the Hagstrom-Warburton method with gravity. However, despite the large amount of work contained herein, there remain many more extensions and improvements. These areas for further study include the following:

1. Application of the auxiliary variable methods (Givoli-Neta and Hagstrom-Warburton) to finite element models

2. Extension of the NRBC formulations to account for evanescent modes as well as the primary waves

3. Analysis of the stability of each scheme for long-time integrations, including an exploration of the conjectures enumerated in Chapter VII, and mitigation of identified error sources

4. Application of the NRBCs to the full three-dimensional system, including both gravity and Coriolis simultaneously

5. Incorporating the NRBCs into a nested environment

6. Finding a means to incorporate gravity into the Hagstrom-Warburton scheme

7. Application of the NRBCs to the non-linear system, in two or three dimensions

8. Extending this work to other linear first-order systems, such as Maxwell's equations or the shallow-water equations (as a first-order system, not converted to the Klein-Gordon equation as in [113] and elsewhere)

In the introduction, we stated that one motivation behind this NRBC development was to support the next generation of atmospheric modeling tools. This research has made significant progress toward that goal. With a broad-based finite-difference

implementation, the next step is to adapt the implementation for a spectral element system. In addition, the long-term stability concerns still need to be addressed. Although we have not satisfied our original purpose, we have nonetheless developed new computation tools for a broad array wave propagation models.

APPENDIX A. SIMPLIFYING THE EULER EQUATIONS

1.   INTRODUCTION

Eq. (II.55) from Sec. II.B is

$$\partial_t \rho + \partial_x(\rho u) + \partial_y(\rho v) + \partial_z(\rho w) = 0$$

$$\partial_t(\rho u) + \partial_x(\rho u^2) + \partial_y(\rho uv) + \partial_z(\rho uw) + \partial_x p = f\rho v$$

$$\partial_t(\rho v) + \partial_x(\rho uv) + \partial_y(\rho v^2) + \partial_z(\rho vw) + \partial_y p = -f\rho u \quad \text{(A.1)}$$

$$\partial_t(\rho w) + \partial_x(\rho uw) + \partial_y(\rho vw) + \partial_z(\rho w^2) + \partial_z p = -g\rho$$

$$\partial_t(\rho e) + \partial_x((\rho e + p)u) + \partial_y((\rho e + p)v) + \partial_z((\rho e + p)w) = -g\rho w$$

This form can be simplified, if we assume the fluid under consideration is an ideal gas ($p = \rho RT$). The simplified form requires fewer terms and is thus easier and faster to calculate. We will consider the mass, momentum, and energy equations separately.

2.   MASS EQUATION

We begin the simplification process with the first equation of the set:

$$\partial_t \rho + \partial_x(\rho u) + \partial_y(\rho v) + \partial_z(\rho w) = 0 \quad \text{(A.2)}$$

This equation needs no simplification. However, we will expand the three spatial derivative terms using the product rule, since that form will appear in the subsequent simplifications

$$\partial_t \rho + u\partial_x \rho + v\partial_y \rho + w\partial_z \rho + \rho\left(\partial_x u + \partial_y v + \partial_z w\right) = 0 \quad \text{(A.3)}$$

3.   MOMENTUM EQUATIONS

The next simplification can be taken with the next three equations of the set:

$$\partial_t(\rho u) + \partial_x(\rho u^2) + \partial_y(\rho uv) + \partial_z(\rho uw) + \partial_x p = f\rho v$$

$$\partial_t(\rho v) + \partial_x(\rho uv) + \partial_y(\rho v^2) + \partial_z(\rho vw) + \partial_y p = -f\rho u$$

$$\partial_t(\rho w) + \partial_x(\rho uw) + \partial_y(\rho vw) + \partial_z(\rho w^2) + \partial_z p = -g\rho \qquad (A.4)$$

We first use the product rule to separate the equations' components as follows:

$$\left. \begin{aligned} u\partial_t\rho + u\partial_x(\rho u) + u\partial_y(\rho v) + u\partial_z(\rho w) \\ +\rho\partial_t u + \rho u\partial_x u + \rho v\partial_y u + \rho w\partial_z u + \partial_x p \end{aligned} \right\} = f\rho v$$

$$\left. \begin{aligned} v\partial_t\rho + v\partial_x(\rho u) + v\partial_y(\rho v) + v\partial_z(\rho w) \\ +\rho\partial_t v + \rho u\partial_x v + \rho v\partial_y v + \rho w\partial_z v + \partial_y p \end{aligned} \right\} = -f\rho u$$

$$\left. \begin{aligned} w\partial_t\rho + w\partial_x(\rho u) + w\partial_y(\rho v) + w\partial_z(\rho w) \\ +\rho\partial_t w + \rho u\partial_x w + \rho v\partial_y w + \rho w\partial_z w + \partial_z p \end{aligned} \right\} = -g\rho \qquad (A.5)$$

We then combine terms to get

$$\left. \begin{aligned} u\left(\partial_t\rho + \partial_x(\rho u) + \partial_y(\rho v) + \partial_z(\rho w)\right) \\ +\rho\left(\partial_t u + u\partial_x u + v\partial_y u + w\partial_z u\right) + \partial_x p \end{aligned} \right\} = f\rho v$$

$$\left. \begin{aligned} v\left(\partial_t\rho + \partial_x(\rho u) + \partial_y(\rho v) + \partial_z(\rho w)\right) \\ +\rho\left(\partial_t v + u\partial_x v + v\partial_y v + w\partial_z v\right) + \partial_y p \end{aligned} \right\} = -f\rho u$$

$$\left. \begin{aligned} w\left(\partial_t\rho + \partial_x(\rho u) + \partial_y(\rho v) + \partial_z(\rho w)\right) \\ +\rho\left(\partial_t w + u\partial_x w + v\partial_y w + w\partial_z w\right) + \partial_z p \end{aligned} \right\} = -g\rho \qquad (A.6)$$

The terms in the first set of parentheses matches (A.2), so we can eliminate them. Dividing the remaining terms by ρ gives

$$\partial_t u + u\partial_x u + v\partial_y u + w\partial_z u + \frac{1}{\rho}\partial_x p = fv$$

$$\partial_t v + u\partial_x v + v\partial_y v + w\partial_z v + \frac{1}{\rho}\partial_y p = -fu$$

$$\partial_t w + u\partial_x w + v\partial_y w + w\partial_z w + \frac{1}{\rho}\partial_z p = -g \qquad (A.7)$$

4.   ENERGY EQUATION

Now the simplification process gets more complicated, using the final equation of the set:

$$\partial_t(\rho e) + \partial_x((\rho e + p)u) + \partial_y((\rho e + p)v) + \partial_z((\rho e + p)w) = -g\rho w \qquad (A.8)$$

144

We begin with our state equation and our definition of energy

$$p = \rho R T \tag{A.9}$$

$$e = c_v T + \frac{1}{2}(u^2 + v^2 + w^2) \tag{A.10}$$

$$R = c_p - c_v \tag{A.11}$$

Combining these terms, we have

$$\rho e = p\frac{c_v}{R} + \frac{\rho u^2 + \rho v^2 + \rho w^2}{2} \tag{A.12}$$

Substituting this value into (A.8) gives

$$\left. \begin{aligned}
&\partial_t \left(p\frac{c_v}{R} + \frac{\rho u^2 + \rho v^2 + \rho w^2}{2} \right) \\
&+\partial_x \left(\left(p\frac{c_v}{R} + \frac{\rho u^2 + \rho v^2 + \rho w^2}{2} \right) u + pu \right) \\
&+\partial_y \left(\left(p\frac{c_v}{R} + \frac{\rho u^2 + \rho v^2 + \rho w^2}{2} \right) v + pv \right) \\
&+\partial_z \left(\left(p\frac{c_v}{R} + \frac{\rho u^2 + \rho v^2 + \rho w^2}{2} \right) w + pw \right)
\end{aligned} \right\} = -g\rho w \tag{A.13}$$

Separating the sums and using the product rule gives the expansion

$$\left. \begin{aligned}
&\frac{c_v}{R}\partial_t p + \rho u \partial_t u + \rho v \partial_t v + \rho w \partial_t w + \frac{u^2+v^2+w^2}{2}\partial_t \rho \\
&+\frac{c_v}{R}\partial_x(pu) + \frac{1}{2}\partial_x\left(\rho u\left(u^2+v^2+w^2\right)\right) + \partial_x(pu) \\
&+\frac{c_v}{R}\partial_y(pv) + \frac{1}{2}\partial_y\left(\rho v\left(u^2+v^2+w^2\right)\right) + \partial_y(pv) \\
&+\frac{c_v}{R}\partial_z(pw) + \frac{1}{2}\partial_z\left(\rho w\left(u^2+v^2+w^2\right)\right) + \partial_z(pw)
\end{aligned} \right\} = -g\rho w \tag{A.14}$$

Combining the $\frac{c_v}{R}$ terms and expanding more pieces with the product rule gives

$$\left. \begin{aligned}
\frac{c_v}{R}\left(\partial_t p + u\partial_x p + v\partial_y p + w\partial_z p + p\left(\partial_x u + \partial_y v + \partial_z w\right)\right) \\
+\rho u \partial_t u + \rho v \partial_t v + \rho w \partial_t w \\
+\frac{u^2+v^2+w^2}{2}\left(\partial_t \rho + \partial_x(\rho u) + \partial_y(\rho v) + \partial_z(\rho w)\right) \\
+(\rho u)\left(u\partial_x u + v\partial_x v + w\partial_x w\right) \\
+(\rho v)\left(u\partial_y u + v\partial_y v + w\partial_y w\right) \\
+(\rho w)\left(u\partial_z u + v\partial_z v + w\partial_z w\right) \\
+u\partial_x p + v\partial_y p + w\partial_z p + p\left(\partial_x u + \partial_y v + \partial_z w\right)
\end{aligned} \right\} = -g\rho w \tag{A.15}$$

145

The parenthetical term in the third line matches (A.2), so we can eliminate it entirely. In addition, if we combine the ρu, ρv, and ρw terms together, we get

$$
\left.\begin{aligned}
\tfrac{c_v}{R}\left(\partial_t p + u\partial_x p + v\partial_y p + w\partial_z p + p\left(\partial_x u + \partial_y v + \partial_z w\right)\right) & \\
+(\rho u)\left(\partial_t u + u\partial_x u + v\partial_x v + w\partial_x w\right) & \\
+(\rho v)\left(\partial_t v + u\partial_y u + v\partial_y v + w\partial_y w\right) & \\
+(\rho w)\left(\partial_t w + u\partial_z u + v\partial_z v + w\partial_z w\right) & \\
+u\partial_x p + v\partial_y p + w\partial_z p + p\left(\partial_x u + \partial_y v + \partial_z w\right) &
\end{aligned}\right\} = -g\rho w \qquad \text{(A.16)}
$$

Based on the simplified results in (A.7), we can replace the third, fourth, and fifth lines of the above equation, resulting in the following

$$
\left.\begin{aligned}
\tfrac{c_v}{R}\left(\partial_t p + u\partial_x p + v\partial_y p + w\partial_z p + p\left(\partial_x u + \partial_y v + \partial_z w\right)\right) & \\
+(\rho u)\left(-\tfrac{1}{\rho}\partial_x p + fv\right) & \\
+(\rho v)\left(-\tfrac{1}{\rho}\partial_y p - fu\right) & \\
+(\rho w)\left(-\tfrac{1}{\rho}\partial_z p - g\right) & \\
+u\partial_x p + v\partial_y p + w\partial_z p + p\left(\partial_x u + \partial_y v + \partial_z w\right) &
\end{aligned}\right\} = -g\rho w, \qquad \text{(A.17)}
$$

which we can expand into

$$
\left.\begin{aligned}
\tfrac{c_v}{R}\left(\partial_t p + u\partial_x p + v\partial_y p + w\partial_z p + p\left(\partial_x u + \partial_y v + \partial_z w\right)\right) & \\
-u\partial_x p + f\rho uv - v\partial_y p - f\rho uv - w\partial_z p - g\rho w & \\
+u\partial_x p + v\partial_y p + w\partial_z p + p\left(\partial_x u + \partial_y v + \partial_z w\right) &
\end{aligned}\right\} = -g\rho w, \qquad \text{(A.18)}
$$

Canceling terms reduces this equation to

$$
\frac{c_v}{R}\left(\partial_t p + u\partial_x p + v\partial_y p + w\partial_z p + p\left(\partial_x u + \partial_y v + \partial_z w\right)\right) + p\left(\partial_x u + \partial_y v + \partial_z w\right) = 0,
$$
$$\text{(A.19)}$$

which we can also write as

$$
\frac{c_v}{R}\left(\partial_t p + u\partial_x p + v\partial_y p + w\partial_z p\right) + \left(\frac{c_v}{R} + 1\right) p\left(\partial_x u + \partial_y v + \partial_z w\right) = 0, \qquad \text{(A.20)}
$$

From our definition of R we have

$$
\frac{c_v}{R} + 1 = \frac{c_v + R}{R} = \frac{c_v + (c_p - c_v)}{R} = \frac{c_p}{R}, \qquad \text{(A.21)}
$$

146

so that multiplying the above equation by $\frac{R}{c_v}$ gives the simplified equation

$$\partial_t p + u\partial_x p + v\partial_y p + w\partial_z p + \gamma p \left(\partial_x u + \partial_y v + \partial_z w\right) = 0, \qquad \text{(A.22)}$$

where $\gamma = \frac{c_p}{c_v}$, and we have replaced our energy variable with the primitive state variable for pressure.

THIS PAGE INTENTIONALLY LEFT BLANK

APPENDIX B. THE FINITE DIFFERENCE INTERIOR SCHEME

Let us briefly analyze the interior scheme used in Chapters IV–VI. We claim that this discretization scheme is $O(\delta x^2 + \delta y^2 + \delta t^2)$. Is that claim true? To test this scheme, we contrive an analytic solution of sines and cosines

$$
\begin{aligned}
\rho &= \rho_0 \cos(k_x x) \cos(k_y y) \cos(\omega t) \\
u &= u_0 \sin(k_x x) \cos(k_y y) \cos(\omega t) \\
v &= v_0 \cos(k_x x) \sin(k_y y) \cos(\omega t) \\
p &= p_0 \cos(k_x x) \cos(k_y y) \cos(\omega t)
\end{aligned}
\tag{B.1}
$$

with $k_x = k_y = \frac{\pi}{4}$ and $\omega = \sqrt{\frac{\gamma p_0}{\rho_0}} \cdot \sqrt{k_x^2 + k_y^2}$. On a 40×40 m domain, these values match a hard wall boundary condition on all four sides. We apply the differential operators of (IV.1) to this equation, and set the results as the right-hand-side values of (IV.1). These terms will then act to force the solution to remain equal to (B.1) within the limits of the discretization error. So that all four state variables are approximately the same order of magnitude, we set $\rho_0 = 1$, $\gamma = 1$, $p_0 = 1$, and $u_0 = v_0 = 0.25$.

Since the leap-frog method requires two prior time steps, we use the analytic solution to set the values for the first two time steps. We then use the discretization scheme to compute the next time step, which we compare to the analytic solution at that same time step. We compute the average absolute error at each interior point for each state variable by

$$
E_\varphi = \frac{\sum_{i=2}^{N_x-1} \sum_{j=2}^{N_y-1} |\hat{\varphi}_{i,j} - \varphi_{i,j}|}{(N_x - 2)(N_y - 2)}
\tag{B.2}
$$

where $\hat{\varphi}$ is our computed state variable, and φ is the analytic solution state variable.

For the first test, we begin with $\delta x = 0.8$, and we halve it with each iteration. We set $\delta y = 0.00625$ for all iterations, so that the discretization error in y does not overwhelm the x-discretization error we wish to measure, and we set $\delta t = 2^{-6}$, which

δx	δy	δt	E_ρ, E_p	E_u	E_v
0.8	0.00625	0.015625	2.7983×10^{-4}	8.0102×10^{-4}	4.9978×10^{-5}
0.4	0.00625	0.015625	7.1×10^{-5}	2.0223×10^{-4}	1.2617×10^{-5}
0.2	0.00625	0.015625	1.7814×10^{-5}	5.062×10^{-5}	3.1584×10^{-6}
0.1	0.00625	0.015625	4.4562×10^{-6}	1.2654×10^{-5}	7.91×10^{-7}

Table XL. Discretization errors for different grid spacings δx

δx	δy	δt	E_ρ, E_p	E_u	E_v
0.00625	0.8	0.015625	2.7983×10^{-4}	4.9978×10^{-5}	8.0102×10^{-4}
0.00625	0.4	0.015625	7.1×10^{-5}	1.2617×10^{-5}	2.0223×10^{-4}
0.00625	0.2	0.015625	1.7814×10^{-5}	3.1584×10^{-6}	5.062×10^{-5}
0.00625	0.1	0.015625	4.4562×10^{-6}	7.91×10^{-7}	1.2654×10^{-5}

Table XLI. Discretization errors for different grid spacings δy

is well below the CFL limit for these conditions. Table XL shows the discretization errors for each state variable with each halving of δx. The error norms decrease by a factor of almost four with each halving of δx, exacly as expected for a second-order method. The only exception to this decrease is the error norm for v. We note, however, that the equation for v contains two ∂_y terms and only one ∂_x term, so it is not surprising that reducing the error for ∂_x *without simultaneously reducing the error for ∂_y* would have only a small impact.

For our second test, we set $\delta x = 0.00625$, and we begin with $\delta y = 0.8$, halving it with each iteration. Keeping δt the same as before, we get the results shown in Table XLI. Note that these errors are almost identical to those for the δx test, with the error norms for u and v reversed. Hence we conclude that the method is also second-order in the y direction.

As a third test, we start with $\delta x = \delta y = 0.8$ and halve both grid spacings at each iteration. Using a larger $\delta t = 2^{-5}$, we get the results shown in Table XLII, and we see second-order results in all four state variables.

Finally, we test δt. This time, we set $\delta x = \delta y = 0.4$, and we begin with

δx	δy	δt	E_ρ, E_p	E_u	E_v
0.8	0.8	0.03125	9.5561×10^{-4}	1.5883×10^{-3}	1.5883×10^{-3}
0.4	0.4	0.03125	2.4401×10^{-4}	4.031×10^{-4}	4.031×10^{-4}
0.2	0.2	0.03125	6.1292×10^{-5}	1.012×10^{-4}	1.012×10^{-4}
0.1	0.1	0.03125	1.5216×10^{-5}	2.5368×10^{-5}	2.5368×10^{-5}

Table XLII. Discretization errors for different grid spacings δx and δy

δx	δy	δt	E_ρ, E_p	E_u	E_v
0.8	0.8	0.25	0.0066075	0.012469	0.012469
0.8	0.8	0.125	0.0037399	0.0063109	0.0063109
0.8	0.8	0.0625	0.0019051	0.0031717	0.0031717
0.8	0.8	0.03125	0.00095561	0.0015883	0.0015883

Table XLIII. Discretization errors for different time steps δt

$\delta t = 0.25$, halving it with each iteration. The results are somewhat surprising. As shown in Table XLIII, the error norms only decrease by a factor of two with each halving of δt, which implies a first-order method rather than second-order. The discretization scheme is the same. How can a scheme which is second-order in space be only first-order in time? Perhaps the difference comes from how the discretization scheme is used. For the spatial derivative approximations, we use the known node values to approximate the derivative, that is,

$$\partial_x u \approx \frac{u_{i+1}^n - u_{i-1}^n}{2\delta x} \,, \tag{B.3}$$

which is a second-order approximation, easily demonstrated via Taylor series expansion. For the time derivative, we approximate it using the equation system, and then use that approximation and the earlier node value to compute the new node value:

$$\partial_t u = \mathrm{RHS}(\vec{\varphi}) \tag{B.4}$$

$$\frac{u_i^{n+1} - u_i^{n-1}}{2\delta t} \approx \partial_t u \tag{B.5}$$

$$u_i^{n+1} \approx u_i^{n-1} + 2\delta t \partial_t u \tag{B.6}$$

151

If we rewrite the superscript for the u_i^{n-1} term, we see that this method is in fact Euler's method over $2\delta t$:

$$u_i^{n+1} \approx u_i^{(n+1)-2} + 2\delta t \partial_t u \tag{B.7}$$

Since Euler's method is only a first-order approximation, our time marching method is only first-order, even though it is defined using the same discretization scheme for our second-order spatial derivative approximations. Thus, it appears that our discretization scheme is in fact $O(\delta x^2 + \delta y^2 + \delta t)$.

This analysis "feels" wrong, and it caused some strenuous debates with the dissertation supervisors. However, it fits the observations. Furthermore, other experiments designed to test the leap-frog scheme's performance also showed similarly inexplicable results. Testing it as an ODE solver resulted in $O(\delta x^3)$ performance for a single-step and a global $O(\delta x^2)$ convergence. Contrariwise, a test using an analytic solution to the heat equation

$$\partial_t u = \partial_{xx} u + \partial_{yy} u$$

initially showed $O(\delta x^{5/2})$ single-step convergence, but as the time step became smaller, the improvement shrank to $O(\delta x)$ and remained there. The cause of this performance is under investigation.

APPENDIX C. WAVE-LIKE SOLUTIONS OF THE LINEARIZED EULER EQUATIONS

We now derive the wave-like solution used in Lemma VI.2. The derivation is similar to Hu's [71], where he uses a non-dimensionalized system and split variables to derive the PML equations. We first assume the existence of a wave-like solution, then we derive the amplitude of each state variable. By avoiding contradictions, we prove that such a wave-like solution exists. This wave-like solution has the form

$$\vec{\varphi} = \vec{\varphi}^* e^{ikx+ily-i\omega t} \ , \tag{C.1}$$

where $\vec{\varphi}$ denotes our state variables, and $\vec{\varphi}^*$ denotes the amplitudes of each component. If we apply (C.1) to (IV.1) and cancel out the common exponential term, we get

$$
\begin{aligned}
-i\omega\rho^* + iku_0\rho^* + ilv_0\rho^* + ik\rho_0 u^* + il\rho_0 v^* &= 0 \\
-i\omega u^* + iku_0 u^* + ilv_0 u^* + \tfrac{ik}{\rho_0}p^* &= 0 \\
-i\omega v^* + iku_0 v^* + ilv_0 v^* + \tfrac{il}{\rho_0}p^* &= 0 \\
-i\omega p^* + iku_0 p^* + ilv_0 p^* + ik\gamma p_0 u^* + il\gamma p_) v^* &= 0 \ .
\end{aligned}
\tag{C.2}
$$

Combining terms, we get

$$
\begin{aligned}
\left(ku_0 + lv_0 - \omega\right)\rho^* + k\rho_0 u^* + l\rho_0 v^* &= 0 \\
\left(ku_0 + lv_0 - \omega\right)u^* + \tfrac{k}{\rho_0}p^* &= 0 \\
\left(ku_0 + lv_0 - \omega\right)v^* + \tfrac{l}{\rho_0}p^* &= 0 \\
k\gamma p_0 u^* + l\gamma p_0 v^* + \left(ku_0 + lv_0 - \omega\right)p^* &= 0 \ .
\end{aligned}
\tag{C.3}
$$

For acoustic waves, $ku_0 + lv_0 - \omega \neq 0$. ($ku_0 + lv_0 - \omega = 0$ for entropy and vorticity waves; see [71]). We can easily solve for ρ^* and p^* in terms of u^* and v^*:

$$
\begin{aligned}
\rho^* &= \frac{\rho_0\left(ku_0^* + lv^*\right)}{\omega - ku_0 - lv_0} \\
p^* &= \frac{\gamma p_0\left(ku_0^* + lv^*\right)}{\omega - ku_0 - lv_0} \ .
\end{aligned}
\tag{C.4}
$$

From (C.3b,c) we have

$$\frac{ku_0 + lv_0 - \omega}{k}u^* = \frac{ku_0 + lv_0 - \omega}{l}v^* \ , \tag{C.5}$$

which leads directly to

$$\frac{u^*}{v^*} = \frac{k}{l} \ . \tag{C.6}$$

If we insert our solution for p^* into (C.3b,c), we get

$$
\begin{aligned}
u^* &= \frac{kp^*}{\rho_0\left(\omega - ku_0 - lv_0\right)} \\
&= \frac{k\gamma p_0\left(ku^* + lv^*\right)}{\rho_0\left(\omega - ku_0 - lv_0\right)^2} \\
&= \frac{\gamma p_0}{\rho_0}\frac{k^2 u^* + klv^*}{\left(\omega - ku_0 - lv_0\right)^2}
\end{aligned}
\tag{C.7}
$$

$$
\begin{aligned}
v^* &= \frac{lp^*}{\rho_0\left(\omega - ku_0 - lv_0\right)} \\
&= \frac{l\gamma p_0\left(ku^* + lv^*\right)}{\rho_0\left(\omega - ku_0 - lv_0\right)^2} \\
&= \frac{\gamma p_0}{\rho_0}\frac{klu^* + l^2 v^*}{\left(\omega - ku_0 - lv_0\right)^2}
\end{aligned}
\tag{C.8}
$$

If we use (C.6) to remove l from the numerator of (C.7a) and k from the numerator of (C.7b), we get

$$
\begin{aligned}
u^* &= \frac{\gamma p_0}{\rho_0}\frac{k^2\frac{u^{*2}}{v^*} + k^2 v^*}{\left(\omega - ku_0 - lv_0\right)^2} \\
v^* &= \frac{\gamma p_0}{\rho_0}\frac{l^2 u^* + l^2\frac{v^{*2}}{u^*}}{\left(\omega - ku_0 - lv_0\right)^2} \ ,
\end{aligned}
\tag{C.9}
$$

which, after a little algebra, can be reformulated as

$$
\begin{aligned}
k &= \pm\frac{\omega - ku_0 - lv_0}{c_0}\frac{u^*}{\sqrt{u^{*2} + v^{*2}}} \\
l &= \pm\frac{\omega - ku_0 - lv_0}{c_0}\frac{v^*}{\sqrt{u^{*2} + v^{*2}}} \\
c_0 &= \sqrt{\frac{\gamma p_0}{\rho_0}}
\end{aligned}
\tag{C.10}
$$

Now, let $u^* = U \cos \theta$, $v^* = U \sin \theta$, for some $U \in \mathcal{C}$ and $\theta \in [0, 2\pi]$ measured counterclockwise from the positive x axis. After some manipulation, we can explicitly solve for k and l:

$$
\begin{aligned}
k &= \frac{\omega \cos \theta}{c_0 + u_0 \cos \theta + v_0 \sin \theta} \\
l &= \frac{\omega \sin \theta}{c_0 + u_0 \cos \theta + v_0 \sin \theta} ,
\end{aligned} \tag{C.11}
$$

where we choose the positive for each $\pm$ in (C.10), denoting propagation in the positive x and y directions. We then insert these values of k and l into the equations for $\vec{\varphi}^*$ and simplify, yielding

$$
\begin{aligned}
\rho^* &= U \frac{\rho_0}{c_0} \\
u^* &= U \cos \theta \\
v^* &= U \sin \theta \\
p^* &= U \frac{\gamma p_0}{c_0}
\end{aligned} \tag{C.12}
$$

Thus our wave solution becomes

$$
\vec{\varphi} = \vec{\varphi}^* \exp\left(i\omega \left(\frac{\cos x + \sin y}{c_0 + u_0 \cos \theta + v_0 \sin \theta} - t \right) \right) , \tag{C.13}
$$

with $\vec{\varphi}^*$ defined by (C.12). A little tedious algebra shows that this solution satisfies (IV.1). If we insert this solution into (VI.16), we get the wave speed

$$
c_w^2 = (c_0 + u_0 \cos \theta + v_0 \sin \theta)^2 . \tag{C.14}
$$

Similarly, when we consider the opposite-sign terms of (C.10), we again get a wave-like solution, this time with

$$
c_w^2 = (u_0 \cos \theta + v_0 \sin \theta - c_0)^2 . \tag{C.15}
$$

Since we do not know in advance the propagation angle of these plane waves, for the purpose of defining the NRBC wave speed, we assume the angle is normal to the boundary. With this assumption, and the requirement that $c_w \geq 0$, we have the

following:

$$\begin{aligned}
\Gamma_E &: c_w = c_0 + u_0 \\
\Gamma_N &: c_w = c_0 + v_0 \\
\Gamma_W &: c_w = c_0 - u_0 \\
\Gamma_S &: c_w = c_0 - v_0
\end{aligned} \tag{C.16}$$

APPENDIX D. DISCRETE REFLECTION COEFFICIENT—A PRELIMINARY ANALYSIS

Let us briefly look at this idea of quantifying the reflection coefficient for the discrete case (see Chapter VII). This analysis differs from Sec. 8.1.5 of [24] in that we consider the physical waves, not merely the high-frequency non-physical computational waves generated by the finite-difference scheme. For our initial analysis, we consider a Sommerfeld (first-order Higdon) boundary condition in a 1-D domain. A full analysis is outside the scope of this dissertation. We begin the work here to show its potential for future research.

1.   DERIVATION

As with the analysis of the reflection coefficient for the continuous equation (Sec. III.B.1.a), we begin by considering a wave of the form

$$u(x,t) = e^{i(x-c_x t)} \tag{D.1}$$

traveling left to right at unknown speed c_x. (For a two-dimensional wave, we consider only the portion of the wave traveling parallel to the x axis.) If we use a Sommerfeld condition $(\partial_t + c_0 \partial_x) u = 0$, then the computed solution for u will include a reflected wave of the correct magnitude to satisfy the boundary condition. Thus,

$$u(x,t) = e^{i(x-c_x t)} + R e^{i(x+c_x t)} \tag{D.2}$$

Discretizing the Sommerfeld condition with a backward difference in x and t, we have

$$\frac{u_N^n - u_N^{n-1}}{k} + c_0 \frac{u_N^n - u_{N-1}^n}{h} = 0 \ , \tag{D.3}$$

where the subscripts N and $N-1$ denote the point on the right boundary and the point immediately to its left, respectively; the superscripts n and $n-1$ denote the current and previous time steps, respectively; k denotes the time step size; and h

denotes the spatial step size. Thus, at the right boundary at time step n, we have $x = Nh$ and $t = nk$. Applying this discretization to our wave (D.2) at this point, we have

$$\left.\begin{aligned} e^{i(Nh-c_x nk)} + Re^{i(Nh+c_x nk)} - e^{i(Nh-c_x(n-1)k)} - Re^{i(Nh+c_x(n-1)k)} \\ +\lambda\left(e^{i(Nh-c_x nk)} + Re^{i(Nh+c_x nk)} - e^{i((N-1)h-c_x nk)} - Re^{i((N-1)h-c_x nk)}\right) \end{aligned}\right\} = 0 , \quad \text{(D.4)}$$

where $\lambda = \frac{c_0 k}{h}$. After we cancel and combine terms, we solve for R and get

$$R = -\frac{1 - e^{ic_x k} + \lambda\left(1 - e^{-ih}\right)}{e^{2ic_x nk}\left(1 - e^{-ic_x k} + \lambda\left(1 - e^{-ih}\right)\right)} \quad \text{(D.5)}$$

We are interested in the magnitude of R more than its actual value. Solving for this magnitude, we have

$$\begin{aligned} \|R\| &= \left\|\frac{1 - e^{ic_x k} + \lambda\left(1 - e^{-ih}\right)}{1 - e^{-ic_x k} + \lambda\left(1 - e^{-ih}\right)}\right\| \\ &= \left\|1 - \frac{\sin(c_x k)}{2i\left(1 - e^{-ic_x k} + \lambda\left(1 - e^{-ih}\right)\right)}\right\| \\ \|R\| &= \left\|1 - \frac{\sin(c_x k)}{e^{\frac{-ic_x k}{2}}\sin\left(\frac{c_x k}{2}\right) + \lambda e^{\frac{-ih}{2}}\sin\left(\frac{h}{2}\right)}\right\| . \end{aligned} \quad \text{(D.6)}$$

2. IMPLICATIONS AND SPECULATION

Looking at (D.6), we see that certain combinations of $c_x k$ and h could make the fractional term negative, resulting in a reflection coefficient R with magnitude greater than one. In fact, if we use the following constants,

$$\begin{aligned} c_0 &= 343\frac{\text{m}}{\text{s}} \\ h &= 100 \text{ m} \\ k &= 0.18 \text{ s} , \end{aligned}$$

which are close to those used in our numerical examples in this dissertation, we get several large reflection coefficients as c_x varies from 1 up to c_0. The top half of Fig. 47 shows these reflection coefficients. Each value of R larger than one represents a potentially unstable wave mode.
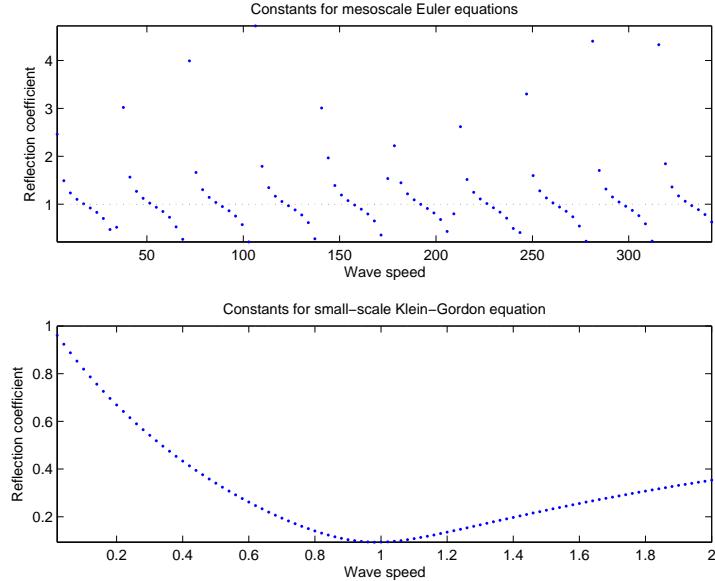
Figure 47. Discrete reflection coefficients for varying wave speeds c_x. The x-axis is the wave speed c_x; the y-axis is the magnitude of the reflection coefficient R computed by (D.6). (Top) Discrete reflection coefficients using constants approximately equal to those in this dissertation's numerical examples for a mesoscale model. (Bottom) Discrete reflection coefficients using the same constants as the numerical example of [90] for the Klein-Gordon equation in a small-scale model.

On the other hand, if we use the values from the numerical example in [90],

$$c_0 = 1\frac{\text{m}}{\text{s}}$$

$$h = 0.25 \text{ m}$$

$$k = 0.125 \text{ s},$$

then our discrete reflection coefficients are all less than one, even if c_x is twice as large as c_0. These coefficients are plotted in the bottom half of Fig. 47. These plots imply the stability of the example in [90] and the instability of our examples.

The problem appears to be the scale of the domain. Perhaps the introduction of a scaling factor can improve the stability. Future research will expand this analysis, to determine the general formula for the Higdon NRBC of order J, and also to consider the Givoli-Neta and Hagstrom-Warburton NRBCs, *after* converting the normal derivatives to tangential. Ideally, this analysis will uncover the choice (or combina-

tion of choices) of c_j to choose to keep $\|R\| < 1$ for all possible c_x. In the meantime, this quick test has uncovered a possible reason for the instabilities exhibited by these NRBCs.

LIST OF REFERENCES

[1] Abarbanel, S., D. Gottlieb, and J. Hesthaven, "Well-Posed Perfectly Matched Layers for Advective Acoustics," *Journal of Computational Physics* 154, pp.266–283, 1999.

[2] Abramowitz, M., and I. Stegun, eds., *Handbook of Mathematical Functions with Formulas, Graphs, and Mathematical Tables*, Dover, New York, 1965.

[3] Acheson, D.J., *Elementary Fluid Dynamics*, Clarendon Press, Oxford, 1990.

[4] Alpert, B., L. Greengard, and T. Hagstrom, "Rapid Evaluation of Nonreflecting Boundary Kernels for Time-Domain Wave Propagation," *SIAM Journal on Numerical Analysis* 37, pp.1138–1164, 2000.

[5] Alpert, B., L. Greengard, and T. Hagstrom, "Nonreflecting Boundary Conditions for the Time-Dependent Wave Equation," *Journal of Computational Physics* 180, pp.270–296, 2002.

[6] Appelö, D., T. Hagstrom, and G. Kreiss, "Perfectly Matched Layers for Hyperbolic Systems: General Formulation, Well-Posedness, and Stability," *SIAM Journal on Applied Mathematics* 67, pp.1–23, 2006.

[7] Appelö, D., and G. Kreiss, "Application of a Perfectly Matched Layer to the Nonlinear Wave Equation," *Wave Motion* 44, pp.531–548, 2007.

[8] Atassi, O., and J. Galán, "Implementation of Nonreflecting Boundary Conditions for the Nonlinear Euler Equations," *Journal of Computational Physics* 227, pp.1643–1662, 2008.

[9] Bayliss, A., and E. Turkel, "Radiation Boundary Condition for Wave-Like Equations," *Communications on Pure and Applied Mathematics* 33, pp.707–725, 1980.

[10] Bayliss, A., and E. Turkel, "Far Field Boundary Conditions for Compressible Flows," *Journal of Computational Physics* 48, pp.182–199, 1982.

[11] Bérenger, J., "A Perfectly Matched Layer for the Absorption of Electromagnetic Waves," *Journal of Computational Physics* 114, pp.185–200, 1994.

[12] Bermúdez, A., L. Hervella-Nieto, A. Prieto, and R. Rodríguez, "An Optimal Perfectly Matched Layer with Unbounded Absorbing Function for Time-Harmonic Acoustic Scattering Problems," *Journal of Computational Physics* 223, pp.469–488, 2007.

[13] Blayo, E., and L. Debreu, "Revisiting Open Boundary Conditions from the Point of View of Characteristic Variables," *Ocean Modelling* 9, pp.231–252, 2005.

[14] Chang, S.-C., A. Himansu, C.-Y. Loh, X.-Y. Wang, and S.-T.J. Yu, *Robust and Simple Non-Reflecting Boundary Conditions for the Euler Equations—A New Approach Based on the Space-Time CE/SE Method*, NASA/TM—2003-212495/REV1, 2005.

[15] Collino, F., "High Order Absorbing Boundary Conditions for Wave Propagation Models: Straight Line Boundary and Corner Cases," in Kleinman et. al. (eds.), *Proceedings of the Second International Conference on Mathematical and Numerical Aspects of Wave Propagation*, SIAM, Delaware, pp.161–171, 1993.

[16] Colonius, T., and H. Ran, "A Super-Grid-Scale Model for Simulating Compressible Flow on Unbounded Domains," *Journal of Computational Physics* 182, pp.191–212, 2002.

[17] Davies, H., "A Lateral Boundary Formulation for Multi-Level Prediction Models," *Quarterly Journal of the Royal Meteorological Society* 102, pp.405–418, 1976.

[18] Davies, H., "Limitations of Some Common Lateral Boundary Schemes Used in Regional NWP Models," *Monthly Weather Review* 111, pp.1002–1012, 1983.

[19] Dea, J., F.X. Giraldo, and B. Neta, *High-Order Higdon Non-Reflecting Boundary Conditions for the Linearized Euler Equations*, NPS-MA-07-001, Naval Postgraduate School, Monterey, CA, 2007.

[20] Dea, J., F.X. Giraldo, and B. Neta, "Gravity, Open Domains and Givoli-Neta Non-Reflecting Boundary Conditions for the Linearized Euler Equations," submitted to *Journal of Computational Physics*, 2008.

[21] Dea, J., F.X. Giraldo, and B. Neta, "High-Order Non-Reflecting Boundary Conditions for the Linearized 2-D Euler Equations: No Mean Flow Case," submitted to *Wave Motion*, 2008.

[22] Dea, J., F.X. Giraldo, and B. Neta, "Hagstrom-Warburton Non-Reflecting Boundary Conditions for the 2-D Linearized Euler Equations," under revision.

[23] Diaz, J., and P. Joly, "An Analysis of Higher Order Boundary Conditions for the Wave Equation," *SIAM Journal on Applied Mathematics* 65, pp.1547–1575, 2005.

[24] Durran, D., *Numerical Methods for Wave Equations in Geophysical Fluid Dynamics*, Springer, New York, 1999.

162

[25] Engquist, B., and A. Majda, "Absorbing Boundary Conditions for the Numerical Simulation of Waves," *Mathematics of Computation* 31, pp.629–651, 1977.

[26] Engquist, B., and A. Majda, "Radiation Boundary Conditions for Acoustic and Elastic Wave Calculations," *Communications on Pure and Applied Mathematics* 32, pp.313–357, 1979.

[27] Ferm, L., and B. Gustafsson, "A Down-Stream Boundary Procedure for the Euler Equations," *Computers & Fluids* 10, pp.261–276, 1982.

[28] Gabersek, S., private communication.

[29] Gerald, C., and P. Wheatley, *Applied Numerical Analysis, Seventh Edition*, Pearson, Boston, 2004.

[30] Giles, M., "Nonreflecting Boundary Conditions for Euler Equation Calculations," *AIAA Journal* 28, pp.2050–2058, 1990.

[31] Giraldo, F.X., private communication.

[32] Giraldo, F.X., and M. Restelli, "A Study of Spectral Element and Discontinuous Galerkin Methods for the Navier-Stokes Equations in Nonhydrostatic Mesoscale Atmospheric Modeling: Equation Sets and Test Cases," *Journal of Computational Physics* 227, pp.3849–3877, 2008.

[33] Givoli, D., "Non-Reflecting Boundary Conditions," *Journal of Computational Physics* 94, pp.1–29, 1991.

[34] Givoli, D., "High-Order Nonreflecting Boundary Conditions without High-Order Derivatives," *Journal of Computational Physics* 170, pp.849–870, 2001.

[35] Givoli, D., "High-Order Local Non-Reflecting Boundary Conditions: A Review," *Wave Motion* 39, pp.319–326, 2004.

[36] Givoli, D., private communication.

[37] Givoli, D., T. Hagstrom, and I. Patlashenko, "Finite Element Formulation with High-Order Absorbing Boundary Conditions for Time-Dependent Waves," *Computer Methods in Applied Mechanics and Engineering* 195, pp.3666–3690, 2006.

[38] Givoli, D., and J. Keller, "A Finite Element Method for Large Domains," *Computer Methods in Applied Mechanics and Engineering* 76, pp.41–66, 1989.

[39] Givoli, D., and B. Neta, *High-Order Higdon Non-Reflecting Boundary Conditions for the Shallow Water Equations*, NPS-MA-02-001, Naval Postgraduate School, Monterey, CA, 2002.

[40] Givoli, D., and B. Neta, "High-Order Non-Reflecting Boundary Conditions for Dispersive Waves," *Wave Motion* 37, pp.257–271, 2003.

[41] Givoli, D., and B. Neta, "High-Order Non-Reflecting Boundary Conditions for the Dispersive Shallow Water Equations, *Journal of Computational and Applied Mathematics* 158, pp.49–60, 2003.

[42] Givoli, D., and B. Neta, "High-Order Non-Reflecting Boundary Scheme for Time-Dependent Waves," *Journal of Computational Physics* 186, pp.24–26, 2003.

[43] Givoli, D., B. Neta, and I. Patlashenko, "Finite Element Analysis of Time-Dependent Semi-Infinite Wave-Guides with High-Order Boundary Treatment," *International Journal for Numerical Methods in Engineering* 58, pp.1955–1983, 2003.

[44] Givoli, D., and I. Patlashenko, "An Arbitrarily High Order Local Non-Reflecting Boundary Scheme," *European Congress on Computational Methods in Applied Sciences and Engineering (ECCOMAS) 2000*, Barcelona, 11-14 September 2000.

[45] Goodrich, J., and T. Hagstrom, "A Comparison of Two Accurate Boundary Treatments for Computational Aeroacoustics," AIAA Paper 97-1585, 1997.

[46] Graham, R., D. Knuth, and O. Patashnik, *Concrete Mathematics: A Foundation for Computer Science, Second Edition*, Addison-Wesley, Boston, 1994.

[47] Grote, M., and J. Keller, "Exact Nonreflecting Boundary Conditions for the Time Dependent Wave Equation," *SIAM Journal on Applied Mathematics* 55, pp.280–297, 1995.

[48] Grote, M., and J. Keller, "On Nonreflecting Boundary Conditions," *Journal of Computational Physics* 122, pp.231–243, 1995.

[49] Grote, M., and J. Keller, "Nonreflecting Boundary Conditions for Time-Dependent Scattering," *Journal of Computational Physics* 127, pp.52–65, 1996.

[50] Grote, M., and J. Keller, "Exact Nonreflecting Boundary Condition for Elastic Waves," *SIAM Journal on Applied Mathematics* 60, pp.803–819, 2000.

[51] Guddati, M., and K.-W. Lim, "Continued Fraction Absorbing Boundary Conditions for Convex Polygonal Domains," *International Journal for Numerical Methods in Engineering* 66, pp.949–977, 2006.

[52] Gustafsson, B., H.-O. Kreiss, and A. Sundström, "Stability Theory of Difference Approximations for Mixed Initial Boundary Value Problems II," *Mathematics of Computation* 26, pp.649–686, 1972.

[53] Hagstrom, T., M. de Castro, D. Givoli, and D. Tzemach, "Local High-Order Absorbing Boundary Conditions for Time-Dependent Waves in Guides," *Journal of Computational Acoustics* 15, pp.1–22, 2007.

[54] Hagstrom, T., and S. Hariharan, "A Formulation of Asymptotic and Exact Boundary Conditions Using Local Operators," *Applied Numerical Mathematics* 27, pp.403–416, 1998.

[55] Hagstrom, T., A. Mar-Or, and D. Givoli, "High-Order Local Absorbing Boundary Conditions for the Wave Equation: Extensions and Improvements," *Journal of Computational Physics* 227, pp.3322–3357, 2008.

[56] Hagstrom, T., and J. Nordström, "Analysis of Extrapolation Boundary Conditions for the Linearized Euler Equations," *Applied Numerical Mathematics* 44, pp.95–108, 2003.

[57] Hagstrom, T., and T. Warburton, "A New Auxiliary Variable Formulation of High-Order Local Radiation Boundary Conditions: Corner Compatibility Conditions and Extension to First-Order Systems," *Wave Motion* 39, pp.327–338, 2004.

[58] Halliday, D., and R. Resnick, *Fundamentals of Physics, Third Edition Extended*, John Wiley and Sons, New York, 1988.

[59] Han, H., and Z. Zhang, "Split Local Absorbing Conditions for One-Dimensional Nonlinear Klein-Gordon Equation on Unbounded Domain," *Journal of Computational Physics* , in press, DOI: 10.1016/j.jcp.2008.07.006, 2008.

[60] Harris, J., and H. Stocker, eds., *Handbook of Mathematics and Computational Science*, Springer-Verlag, New York, 1998.

[61] Henrici, P., *Discrete Variable Methods in Ordinary Differential Equations*, John Wiley and Sons, New York, 1962.

[62] Higdon, R., "Absorbing Boundary Conditions for Difference Approximations to the Multi-Dimensional Wave Equation," *Mathematics of Computation* 47, pp.437–459, 1986.

[63] Higdon, R., "Initial-Boundary Value Problems for Linear Hyperbolic Systems," *SIAM Review* 28, pp.177–217, 1986.

[64] Higdon, R., "Numerical Absorbing Boundary Conditions for the Wave Equation," *Mathematics of Computation* 49, pp.65–90, 1987.

[65] Higdon, R., "Radiation Boundary Conditions for Elastic Wave Propagation," *SIAM Journal on Numerical Analysis* 27, pp.831–869, 1990.

[66] Higdon, R., "Absorbing Boundary Conditions for Elastic Waves," *Geophysics* 56, pp.231–241, 1991.

[67] Higdon, R., "Absorbing Boundary Conditions for Acoustic and Elastic Waves in Stratified Media," *Journal of Computational Physics* 101, pp.386–418, 1992.

[68] Higdon, R., "Radiation Boundary Conditions for Dispersive Waves," *SIAM Journal on Numerical Analysis* 31, pp.64–100, 1994.

[69] Hobson, G., private communication.

[70] Holton, J., *An Introduction to Dynamic Meteorology, Third Edition*, Academic Press, San Diego, 1992.

[71] Hu, F., "On Absorbing Boundary Conditions for Linearized Euler Equations by a Perfectly Matched Layer," *Journal of Computational Physics* 129, pp.201–219, 1996.

[72] Hu, F., "A Stable, Perfectly Matched Layer for Linearized Euler Equations in Unsplit Physical Variables," *Journal of Computational Physics* 173, pp.455–480, 2001.

[73] Hu, F., "A Perfectly Matched Layer Absorbing Boundary Condition for Linearized Euler Equations with a Non-Uniform Mean Flow," *Journal of Computational Physics* 208, pp.469–492, 2005.

[74] Hu, F., X. Li, and D. Lin, "Absorbing Boundary Conditions for Nonlinear Euler and Navier-Stokes Equations Based on the Perfectly Matched Layer Technique," *Journal of Computational Physics* 227, pp.4398–4424, 2008.

[75] Huan, R., and L. Thompson, "Accurate Radiation Boundary Conditions for the Time-Dependent Wave Equation on Unbounded Domains," *International Journal for Numerical Methods in Engineering* 47, pp.1569–1603, 2000.

[76] Huebner, K., E. Thornton, and T. Byrom, *The Finite Element Method for Engineers, Third Edition*, John Wiley and Sons, New York, 1995.

[77] Jensen, T., "Open Boundary Conditions in Stratified Ocean Models," *Journal of Marine Systems* 16, pp.297–322, 1998.

[78] Keller, J., and D. Givoli, "Exact Non-Reflecting Boundary Conditions," *Journal of Computational Physics* 82, pp.172–192, 1989.

[79] Klemp, J., and D. Durran, "An Upper Boundary Condition Permitting Internal Gravity Wave Radiation in Numerical Mesoscale Models," *Monthly Weather Review* 111, pp.430–444, 1983.

[80] Kreiss, G., "The Dependence on the Outflow Boundary Condition of the Solution of Steady, Incompressible Euler Equations," *SIAM Journal on Numerical Analysis* 28, pp.1242–1264, 1991.

[81] Kreiss, H.-O., "Initial Boundary Value Problems for Hyperbolic Systems," *Communications on Pure and Applied Mathematics* 23, pp.277–298, 1970.

[82] Kröner, D., "Absorbing Boundary Conditions for the Linearized Euler Equations in 2-D," *Mathematics of Computation* 57, pp.153–167, 1991.

[83] Lie, I., "Well-Posed Transparent Boundary Conditions for the Shallow Water Equations," *Applied Numerical Mathematics* 38, pp.445–474, 2001.

[84] Mar-Or, A., and D. Givoli, "High-Order Global-Regional Model Interaction: Extension of Carpenter's Scheme," *International Journal for Numerical Methods in Engineering*, in press, DOI: 10.1002/nme.2405, 2008.

[85] McDonald, A., "A Step toward Transparent Boundary Conditions for Meteorlogical Models," *Monthly Weather Review* 130, pp.140–151, 2002.

[86] McDonald, A., "Transparent Boundary Conditions for the Shallow-Water Equations: Testing in a Nested Environment," *Monthly Weather Review* 131, pp.698–705, 2003.

[87] Miller, M., and A. Thorpe, "Radiation Conditions for the Lateral Boundaries of Limited-Area Numerical Models," *Quarterly Journal of the Royal Meteorological Society* 107, pp.615–628, 1981.

[88] Nataf, F., "A New Approach to Perfectly Matched Layers for the Linearized Euler System," *Journal of Computational Physics* 214, pp.757–772, 2006.

[89] Navon, I., B. Neta, and M. Hussaini, "A Perfectly Matched Layer Approach to the Linearized Shallow Water Equations Models," *Monthly Weather Review* 132, pp.1369–1378, 2004.

[90] Neta, B., V. van Joolen, J. Dea, and D. Givoli, "Application of High-Order Higdon Non-Reflecting Boundary Conditions to Linear Shallow Water Models," *Communications in Numerical Methods in Engineering*, in press, DOI: 10.1002/cnm.1044, 2007.

[91] Oliveira, F., "Improvement on Open Boundaries on a Time Dependent Numerical Model of Wave Propagation," *Ocean Engineering* 28, pp.95–115, 2000.

[92] Orlanski, I., "A Simple Boundary Condition for Unbounded Hyperbolic Flows," *Journal of Computational Physics* 21, pp.251–269, 1976.

[93] Pearson, R., "Consistent Boundary Conditions for Numerical Models of Systems That Admit Dispersive Waves," *Journal of the Atmospheric Sciences* 31, pp.1481–1489, 1974.

[94] Pedlosky, J., *Geophysical Fluid Dynamics, Second Edition*, Springer, New York, 1987.

[95] Raymond, W., and H. Kuo, "A Radiation Boundary Condition for Multi-Dimensional Flows," *Quarterly Journal of the Royal Meteorological Society* 110, pp.535–551, 1984.

[96] Ren, X., K.-H. Wang, and K.-R. Jin, "Open Boundary Conditions for Obliquely Propagating Nonlinear Shallow-Water Waves in a Wave Channel," *Computers & Fluids* 26, pp.269–278, 1997.

[97] Rowley, C., and T. Colonius, "Discretely Nonreflecting Boundary Conditions for Linear Hyperbolic Systems," *Journal of Computational Physics* 157, pp.500–538, 2000.

[98] Safjan, A., "Highly Accurate Non-Reflecting Boundary Conditions for Finite Element Simulations of Transient Acoustics Problems," *Computer Methods in Applied Mechanics and Engineering* 152, pp.175–193, 1998.

[99] Sjögreen, B., and N. Petersson, "Perfectly Matched Layers for Maxwell's Equations in Second Order Formulation," *Journal of Computational Physics* 209, pp.19–46, 2005.

[100] Skelton, E., S. Adams, and R. Craster, "Guided Elastic Waves and Perfectly Matched Layers," *Wave Motion* 44, pp.573–592, 2007.

[101] Smith, W., "A Nonreflecting Plane Boundary for Wave Propagation Problems," *Journal of Computational Physics* 15, pp.492–503, 1974.

[102] Song, C., and M. Bazyar, "A Boundary Condition in Padé Series for Frequency-Domain Solution of Wave Propagation in Unbounded Domains," *International Journal for Numerical Methods in Engineering* 69, pp.2330–2358, 2007.

[103] Spanier, J., and K. Oldham, eds., *An Atlas of Functions* Hemisphere, New York, 1987.

[104] Stănică, P., private communication.

[105] Strauss, W., *Partial Differential Equations: An Introduction*, John Wiley and Sons, New York, 1992.

[106] Tam, C., and J. Webb, "Dispersion-Relation-Preserving Finite Difference Schemes for Computational Acoustics," *Journal of Computational Physics* 107, pp.262–281, 1993.

[107] Tannehihll, J., D. Anderson, and R. Pletcher, *Computational Fluid Mechanics and Heat Transfer, Second Edition*, Taylor & Francis, Washington, DC, 1997.

[108] Thomas, J., *Numerical Partial Differential Equations: Finite Difference Methods*, Springer, New York, 1995.

[109] Thompson, L., and R. Huan, "Finite Element Formulation of Exact Non-Reflecting Boundary Conditions for the Time-Dependent Wave Equation," *International Journal for Numerical Methods in Engineering* 45, pp.1607–1630, 1999.

[110] Ting, L., and M. Miksis, "Exact Boundary Conditions for Scattering Problems," *Journal of the Acoustical Society of America* 80, pp.1825–1827, 1986.

[111] Trefethen, L., and L. Halpern, "Well-Posedness of One-Way Wave Equations and Absorbing Boundary Conditions," *Mathematics of Computation* 47, pp.421–435, 1986.

[112] Vallado, D., *Fundamentals of Astrodynamics and Applications, Second Edition*, Microcosm Press, El Segundo, CA, 2001.

[113] Van Joolen, V., *Application of Higdon Non-Reflecting Boundary Conditions to Shallow Water Models*, PhD Dissertation, Naval Postgraduate School, Monterey, CA, 2003.

[114] Van Joolen, V., D. Givoli, and B. Neta, "High-Order Non-Reflecting Boundary Conditions for Dispersive Waves in Cartesian, Cylindrical and Spherical Coordinate Systems," *International Journal of Computational Fluid Dynamics* 17, pp.263–274, 2003.

[115] Van Joolen, V., B. Neta, and D. Givoli, "A Stratified Dispersive Wave Model with High-Order Non-Reflecting Boundary Conditions," *Computers and Mathematics with Applications* 48, pp.1167–1180, 2004.

[116] Van Joolen, V., B. Neta, and D. Givoli, "High-Order Higdon-Like Boundary Conditions for Exterior Transient Wave Problems," *International Journal for Numerical Methods in Engineering* 63, pp.1041–1068, 2005.

[117] Warming, R., R. Beam, and B. Hyett, "Diagonalization and Simultaneous Symmetrization of the Gas-Dynamic Matrices," *Mathematics of Computation* 29, pp.1037–1045, 1975.

[118] Wikipedia, "Polynomial Sequence – Wikipedia, the Free Encyclopedia," http://en.wikipedia.org/wiki/Polynomial_sequence, and links on that page to Abel, Bell, Bernoulli, Chebyshev, Fibonacci, Hermite, Legendre, Laguerre, Spread, Touchard, Rook, Orthogonal, Secondary, Sheffer sequence, Sturm sequence, and Generalized Appell Polynomials, accessed on 16 May 2008.

[119] Wurtele, M., J. Paegle, and A. Sielecki, "The Use of Open Boundary Conditions with the Storm-Surge Equations," *Monthly Weather Review* 99, pp.537–544, 1971.

[120] Zahid, M., and M. Guddati, "Padded Continued Fraction Absorbing Boundary Conditions for Dispersive Waves," *Computer Methods in Applied Mechanics and Engineering* 195, pp.3797–3819, 2006.

[121] Zienkiewicz, O., and R. Newton, "Coupled Vibrations of a Structure Submerged in a Compressible Fluid," presented at the *International Symposium on Finite Element Techniques*, Stuttgart, West Germany, 1969.

INITIAL DISTRIBUTION LIST

1. Defense Technical Information Center
   Fort Belvoir, Virginia

2. Dudley Knox Library
   Naval Postgraduate School
   Monterey, California

3. Beny Neta
   Naval Postgraduate School
   Monterey, California

4. Francis X. Giraldo
   Naval Postgraduate School
   Monterey, California

5. Clyde Scandrett
   Naval Postgraduate School
   Monterey, California

6. Garth Hobson
   Naval Postgraduate School
   Monterey, California

7. Saša Gaberšek
   Naval Research Laboratory
   Monterey, California

8. Carlos Borges, Chairman
   Naval Postgraduate School
   Monterey, California

9. Alan Lair, Chairman
   Air Force Institute of Technology
   Wright-Patterson Air Force Base, Ohio

10. Maj. John R. Dea
    Air Force Institute of Technology
    Wright-Patterson Air Force Base, Ohio